PORTLAND CEMENT CONCRETE PAVEMENT THICKNESS AND SHEAR WAVE VELOCITY VARIATION VERSUS OBSERVED PAVEMENT DISTRESSES

A THESIS
SUBMITTED TO THE FACULTY OF
UNIVERSITY OF MINNESOTA
BY

Ryan Joseph Conway

IN PARTIAL FULFILLMENT OF THE REQUIREMENTS
FOR THE DEGREE OF
MASTER OF SCIENCE

Randal Barnes
Lev Khazanovich

February 2017

Acknowledgements

First, I would like to thank my advisors Dr. Randal Barnes and Dr. Lev Khazanovich. Without their guidance, this study and research could not have occurred.

Next, I would like to thank the Minnesota Department of Transportation for funding and coordinating this project.

I would like to thank Kyle Hoegh, Lucio Salles, Flavia Campos Macedo Britto, and Deividi Pereira for their work in data collection and analysis and MnDOT for allowing the data collection.

Finally, I would like to thank Dr. Randal Barnes, Dr. Lev Khazanovich and Dr. Justin Revenaugh for reviewing this thesis and agreeing to be on my committee.

Abstract

Concrete slab thickness is the key design characteristic of a concrete pavement. It is the most important design parameter and the major focus of control and inspection during construction. It is widely accepted that thickness deficiencies can reduce performance. In order to investigate possible correlations between Portland cement concrete (PCC) thickness with observed surface distresses, a combination of non-destructive ultrasonic thickness tests and distress surveys were performed on three existing highways prior to their rehabilitation. In addition to concrete thickness, concrete shear wave velocity was also measured in ultrasonic tests. Statistical and visual analysis were performed in order to investigate possible correlations between thickness and velocity variation and observed distress. The results of these analyses were inconclusive for thickness variation, but showed highly significant correlation for shear wave velocity. Investigation of the design documents for the some of the survey areas showed that the shear wave velocity survey was able to identify design changes which have significant impact on pavement performance. A methodology for the implementation of a shear wave velocity survey for identification of design changes which may influence pavement performance is presented.

Table of Contents

List of Tables

List of Figures

1. INTRODUCTION

Concrete slab thickness is the key design characteristic of Portland cement concrete (PCC) pavement. It is the most important design parameter and the major focus of control and inspection during and after construction. It is widely accepted that thickness deficiencies can reduce performance, an assumption which has lead most road agencies, including the Minnesota Department of Transportation (MnDOT) to adopt contractor compensation deductions for thickness deficiencies (MnDOT, 2005). Consequently, contractors have a tendency to build slabs slightly thicker than design procedures recommend (Stubstad, Tayabji and Lukanen, 2002; Jiang, Selezneva, Mladenovic, Aref, and Darter, 2003; Kim, McCullough, 2002), Although it is commonly believed that an excess in concrete thickness increases pavement longevity, there is only anecdotal evidence to support this claim.

The lack in field validation of the performance-thickness relationship results primarily from the QA/QC methodology used to determine PCC thickness. Traditionally, PCC thickness is determined using coring, a destructive practice which is time consuming, expensive, and often creates surface or subsurface damage. These drawbacks make complete and thorough thickness characterization via coring unrealistic and result in measurements which are widely spaced and generally only taken in the middle of the slab (Vancura, 2013). For example, MnDOT QA/QC calls for exploratory cores to be drilled initially every 1000ft and at smaller spacings only if a deficiency is encountered (MnDOT, 2005). These coring practices result in widely spaced longitudinal data which gives little insight to the small scale longitudinal thickness variation and no information about transverse thickness variation and their potential impacts on performance. This limited data also impacts the type of research analysis which can be performed.

Recent advances in nondestructive testing, such as the introduction of the MIRA ultrasonic tomographer, allow for large-scale, rapid collection of reliable pavement thickness measurements (Hoegh, 2013; Vancura, 2013). Several past studies showed that MIRA measurements were able to accurately and reliably predict the thickness determined by coring (Hoegh, 2013; Vancura, 2013). A study conducted by Vancura, found that a comparison of 27 MIRA and hand measurements produced a R^2 of .997 and a slope of 0.983, suggesting MIRA is highly precise and

may contain only an insignificant negative bias (Vancura, 2013). Additionally, 60 repeat measurements conducted as part of the same study found that repeat measurements had an average discrepancy of 0.1in, suggesting a high degree of repeatability (Vancura, 2013).

In addition to thickness, MIRA is also capable of in-situ determination of shear wave velocity (SWV) at the slab surface, an important indicator of material properties. SWV is analytically related to Young's modulus, Poisson's ratio, and material density. Multiple studies have found strong correlations between compressive and flexural strength and SWV for similar concrete mixes (Heisey, Stokoe and Meyer, 1982; An, Nam, Kwon, and Joh, 2009; Freeseman, Hoegh, and Khazanovich, 2016). Though lab studies have been performed, large scale field studies of pavement SWV variation, or pavement SWV as an indicator of pavement quality, have not yet been conducted.

The research described in this paper had the main goal of investigating the variation of PCC thickness and velocity and investigating potential correlation between distresses with thickness or SWV variation. Thickness/SWV data were obtained through ultrasonic measurements while surface distresses were visually recorded. Construction records were also reviewed. Statistical and visual analysis were performed in order to investigate possible correlations between thickness and velocity variation and observed distress. The results of these analyses were inconclusive for thickness variation, but showed highly significant correlation for shear wave velocity. Investigation of the design documents for the some of the survey areas showed that the shear wave velocity survey was able to identify design changes which have significant impact on pavement performance. These results were used to develop a methodology for the implementation of a shear wave velocity survey for identification of design changes which may influence pavement performance.

2. LITERATURE REVIEW

A review of the current literature related to PCC thickness and velocity variation, pavement distress and the application and foundations of ultrasonic tomography for pavements is presented.

2.1 PCC thickness variations

After construction, PCC thickness is often measured as a key QA/QC measure. This is generally done by taking exploratory core samples every 500-1000ft. This study was conducted in Minnesota, and therefore Minnesota Department of Transportation (MnDOT) prescribed practices will be used throughout the report. MnDOT calls for borings to be taken every 1000ft. If the initial exploratory boring is found to show a deficiency of greater than ½ in, additional cores are drilled at 10ft on either side of the initial core (MnDOT, 2005). Additional exploratory cores will be drilled in both directions at 10 – 25ft intervals until cores are found to be of sufficient thickness (MnDOT, 2005). Though accurate, the method of coring is time consuming, destructive, expensive and does not provide data on small scale thickness variation. In general, cores are taken in the center of the slab to avoid damaging high stress areas such as the slab edge and the wheel path (MnDOT, 2005). This results in sparse data for critical locations of the slab such as edges and corners.

Other states have similar practices as those of MnDOT. This results widely spaced longitudinal data which gives little insight to the small scale longitudinal variation and little information about potential transverse variation (Vancura, 2013). A thickness variation study was conducted by the Federal Highway Administration (FHWA) (Selezneva, Jiang, and Mladenovic, 2002). This study consisted of more than 4000 pavement layer thickness measurements taken from all 50 states, Canada, and the District of Columbia. The main findings of the study were that pavement thickness in general followed a normal distribution, as did the deviations from design thickness based on a skewness and kurtosis analysis. According to the FHWA study (Selezneva, Jiang, and Mladenovic, 2002) , the mean deviation from design for PCC pavements ranged from from .8 in. to -0.03 in depending on pavement design. In general, pavements were over-built with thinner pavements being the most overbuilt. Only the thickest pavement had an average thickness less than the design thickness (Selezneva, Jiang, and Mladenovic, 2002).

2.2 PCC velocity variations

No literature on the field-scale variation of PCC shear wave velocity as an indicator pavement strength was found in the literature. A recent study conducted at the University of Minnesota used pavement shear wave velocity to determine optimal time to trafficking for newly constructed PCC pavements. The study determined that a significant correlation between flexural strength and maturity and shear wave velocity (Freeseman, Hoegh, and Khazanovich 2016b). Another study (Cho, Joh, Kwon, and Kang, 2007) determined pavement shear wave velocity in an in-situ field setting and the verified the results using cores. The study determined that in-field determined shear wave velocity was, on average, 3.6% greater than velocities determined within the laboratory. The study also investigated the velocity-strength relationship of the cores. A highly significant geometric relationship was determined between shear wave velocity and compressive strength. No studies considering shear wave variability and its effect on long term pavement performance were found in the literature review.

2.3 Pavement performance predictions

The current literature on various models for pavement performance is presented. The primary models of focus are the design prediction models developed under the mechanistic empirical pavement design guide (MEPDG) and a model developed by AASHTO using the Long Term Pavement Performance Database (LTPP)

2.3.1 FHWA Logistic Regression Analysis

Pavement performance prediction is commonly used to design new pavements and rehabilitate existing pavements. PCC thickness is a key design aspect and the main input in many predicative models. The main predicative model used in pavement design and rehabilitation is the Mechanistic-Empirical Pavement Design Guide (MEPDG) (AASHTO, 2008). Another predictive model that will be discussed was developed by Federal Highway Administration (FHWA) as part of the Long Term Pavement Performance (LTPP) study (Carvalho, R., et al., 2012). Both the MEPDG and FHWA model used the LTPP databases to relate pavement characteristics to pavement performance. However, the prediction models developed for the MEPGD and FHWA models use

different methods. The MEPDG used empirical curve fitting relationships while the FHWA used logistic regression which included tests for statistical significance.

The FHWA logistic model will be reviewed first (Carvalho, R., et al., 2012). A probabilistic failure model was developed by the FHWA during a 2012 study titled “Simplified Techniques for Evaluation and Interpretation of Pavement Deflections for Network-Level Analysis”. This model was designed to determine the likelihood of premature failure using load deflection techniques on rigid and flexible pavements. This deflection-based model was designed to be sensitive to structural pavement performance. The purpose of the model was not to create a predictive design model, rather to use regression as simplified procedure to identify critical sections with a high likelihood of developing premature distress. A key component of this model was the potential for model calibration based on local network characteristics.

A logistic regression model was used to identify variables which were significant predictors of premature pavement failure. The dichotomous dependent response variable of the regression was “acceptable” and “not acceptable” based on several distress types. Pavement sections which prematurely exceed threshold values of roughness, joint faulting, or transverse cracking were denoted as "not acceptable”. Pavements which did not prematurely exceed distress thresholds were deemed “acceptable”. Premature exceedance was defined as exceeding the distress thresholds within 20 years for rigid pavement (Carvalho, R., et al., 2012).

Many predictors were investigated within this study. The main goal of this investigation was to develop techniques for the evaluation of deflection data, so input data was divided into two categories; pavement deflection data and other data. The latter category included design characteristics, traffic levels, and environmental conditions. Deflection data was typically collected at a longitudinal spacing of 500ft (Carvalho, R., et al., 2012).

Forward and backward stepwise regression were performed for all deflection predictors resulting in one model per deflection predictor. After this was completed, highly correlated predictor variables and unreasonable trends were removed. Goodness of fit was used to selected the best regression models using the Receiver Operating Characteristic (ROC) Curve. The results of the logistic analysis found significant correlations between deflection and roughness, joint faulting and

transverse cracking. It should be noted that significance was claimed for many of the variable at a p-value above 0.05, which is commonly accepted as a cutoff for the limiting of type two error (Carvalho, R., et al., 2012). Though thickness was found to be significant in several models, the p-values associated with thickness were often above 0.05. The fact that this study was primarily performed on widely spaced data may play a role in the lack of significance found for thickness. It is possible that the widely spaced QA data used in this study missed the local relationships that would be expected between thickness and performance.

2.3.2 MEPDG

The main predicative model used in pavement design and rehabilitation is the MEPDG (AASHTO, 2008). The MEPDG uses pavement performance prediction models to design pavements. The method involves empirical prediction of distress based on design inputs. The models used to calculate distress are empirically fit and generally non-linear. The data used in the prediction models was taken from the Long Term Pavement performance data base. Designs are evaluated iteratively by comparing predicted distress to acceptable distress levels. For rigid pavements, the MEPDG can be used to predict cracking and fatigue damage. However, like the data used in the FHWA study, data used to create the MEPDG models does not include high-density measurements of thickness variability or PCC shear wave velocity (AASHTO, 2008).

2.4 MIRA Ultrasonic Tomography

Ultrasonic testing works by producing shear waves with a transmitter and then receiving the signal after it has traveled through the material. The shear waves are reflected at acoustic impedance interfaces. Acoustic impedance is defined as the product of the density and velocity. Ultrasonic tomography has long been employed in the medical field. However, the use of ultrasonic tomography in nondestructive testing of PCC is relatively new development (Hoegh, Khazanovich, Yu, 2011).

Early methods of ultrasonic tomography relied on time consuming-liquid coupling of the sensor to the material. Additionally, the heterogeneity inherent in PCC caused rapid attenuation which severely limited the penetration depth. These difficulties impeded the adoption of the ultrasonic

tomography as a nondestructive pavement analysis method (Hoegh, Khazanovich, Yu, 2011). The issues of penetration depth and ease-of-use were addressed by the development of the dry point contact transducer. The dry point contact transducer is also referred to as a "touch and go" transducer because it does not require liquid coupling. This method also addressed penetration depth by transmitting a lower frequency (55 kHz).

2.4.1 MIRA System Description

The introduction of the dry point contact transducer allowed for the development of MIRA. MIRA is an ultrasonic tomography device specifically designed for evaluation of concrete structures. Borrowing principals from the medical field, MIRA uses an array of transmitting and receiving seismic transducers to create 45 measurement pairs (Figure 1, (Hoegh, Khazanovich, Yu, 2011)).

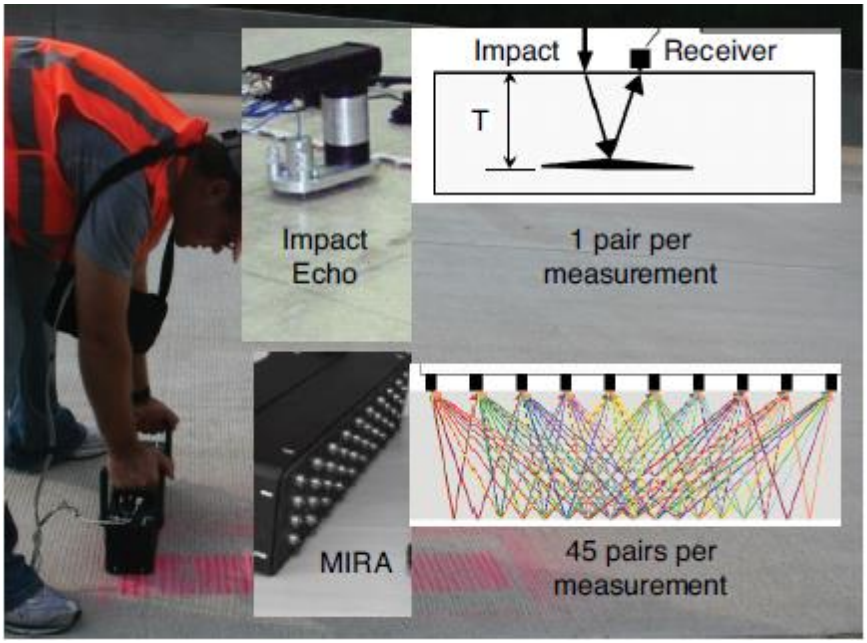

Figure 1. MIRA System (Hoegh, Khazanovich, Yu, 2011).

The large number of pairs allows the device to address heterogeneity by providing many redundant checks of results. A scan takes approximately 3 seconds and results in 2D cross section beneath the device. With this method, analysis is possible at depths of 3ft (Hoegh, Khazanovich, Yu, 2011).

2.4.2 MIRA Data Processing and Visualization

Various transducer configurations are possible. MIRA, the ultrasonic tomography device employed in this study, uses a firmly fixed array of 40 transducers arranged in ten channels of four transducers (Figure 1). The transducers operate at a default frequency of 55kHz. The array is arranged in a rectangular scanning aperture 50mm by 400mm. The device measures the time of surface wave propagation between fixed transducers to compute material shear wave velocity. This velocity is used in the synthetic aperture focusing technique (SAFT) to reconstruct the medium below the device by analyzing shear wave reflection arrival times (Hoegh, Khazanovich, Yu, 2011). The results of the reconstruction give a 2D cross section of echo intensity versus depth along the length of the aperture. Differences in acoustic impedance could result from an inclusion, a layer interface, or damage to the concrete (Hoegh, Khazanovich, Yu, 2011).

2.4.3 Accuracy and Precision of MIRA

Hoegh, Khazanovich and Yu (2011) made several test of the accuracy of MIRA when applied to PCC pavements. First, the thickness of the concrete cover at several locations was determined both with MIRA and coring. A regression of MIRA derived thickness VS cored thickness produced a slope of $y = 0.972$ and an $R^2 = 0.991$, suggesting that MIRA measurements are both unbiased and precise (Figure 2 (Hoegh, Khazanovich, Yu, 2011)).

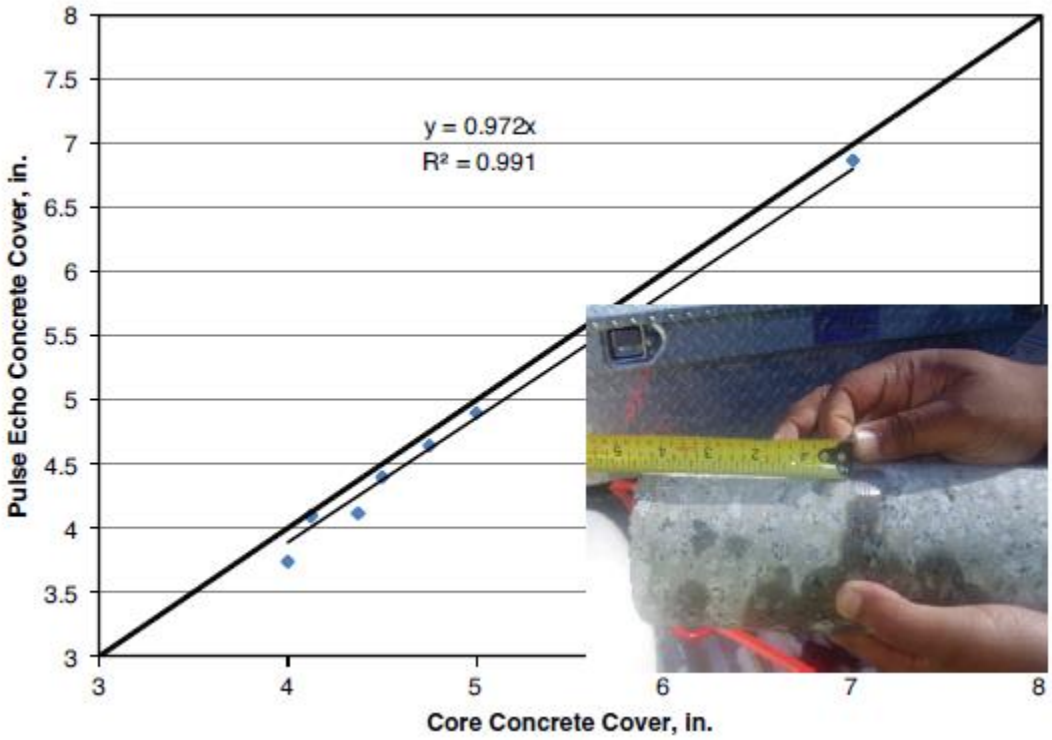

Figure 2: MIRA thickness VS Core thickness (Hoegh, Khazanovich, Yu, 2011)

A similar regression was performed between MIRA measurements taken over a continuously reinforced concrete pavement (CRCP), producing a slope of y = 0.971 and an R^2 = 0.967, again suggesting that MIRA measurements are both unbiased and precise (Figure 3 (Hoegh, Khazanovich, Yu, 2011)). Further refinement of the data which accounted for errors produced by the dowel reinforcements produced a slope of y = 0.982 and an R^2 = 0.997 (Figure 4 (Hoegh, Khazanovich, Yu, 2011)).

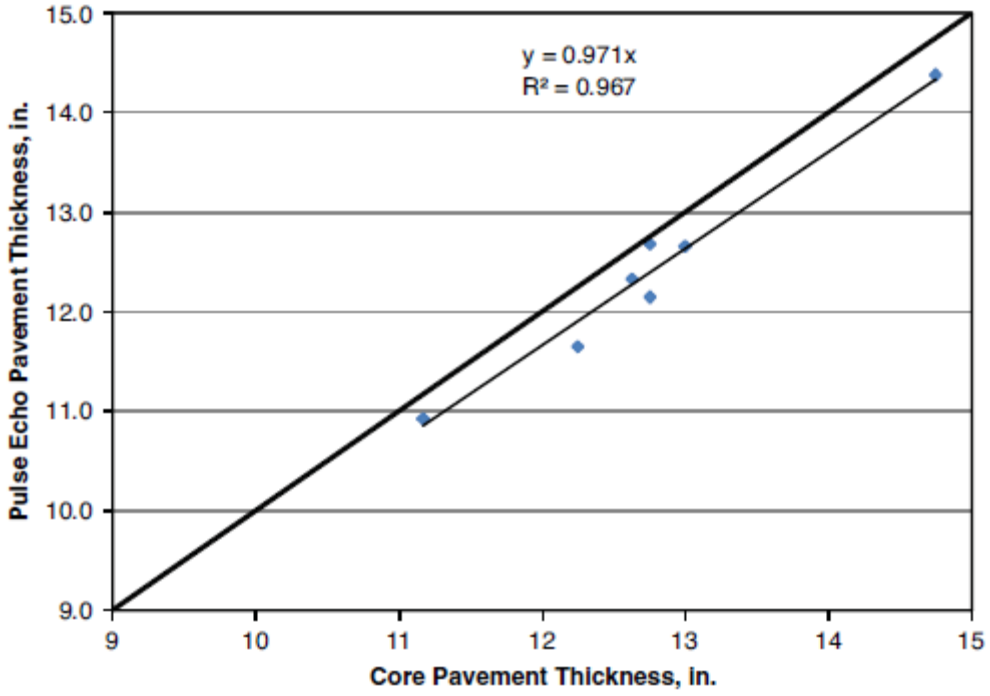

Figure 3: MIRA thickness VS CRCP core thickness

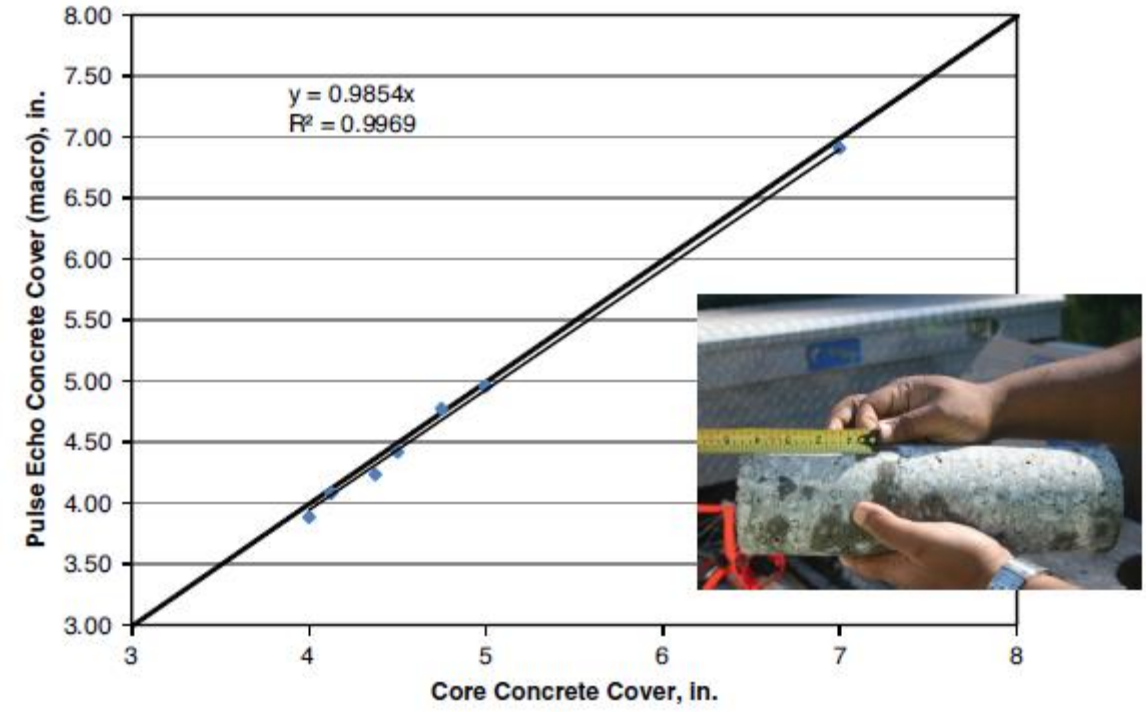

Figure 4: MIRA thickness VS CRCP core thickness

Another verification of MIRA was performed in 2013 (Vancura, 2013). To test the repeatability of the results, Vancura conducted an experiment in which 2 MIRA measurements were taken in 60 locations. The device was left on the ground and not moved between the measurements. Of the 60 locations, only four had discrepancies greater than 0 in, and the maximum discrepancy recorded was 0.092 in

To test the accuracy of the results 27 measurements were taken at core locations across several states. Comparison of core data to the MIRA data resulted in a high accuracy and good agreement (R^2 = 0.997, slope = 0.9834) (Figure 5).

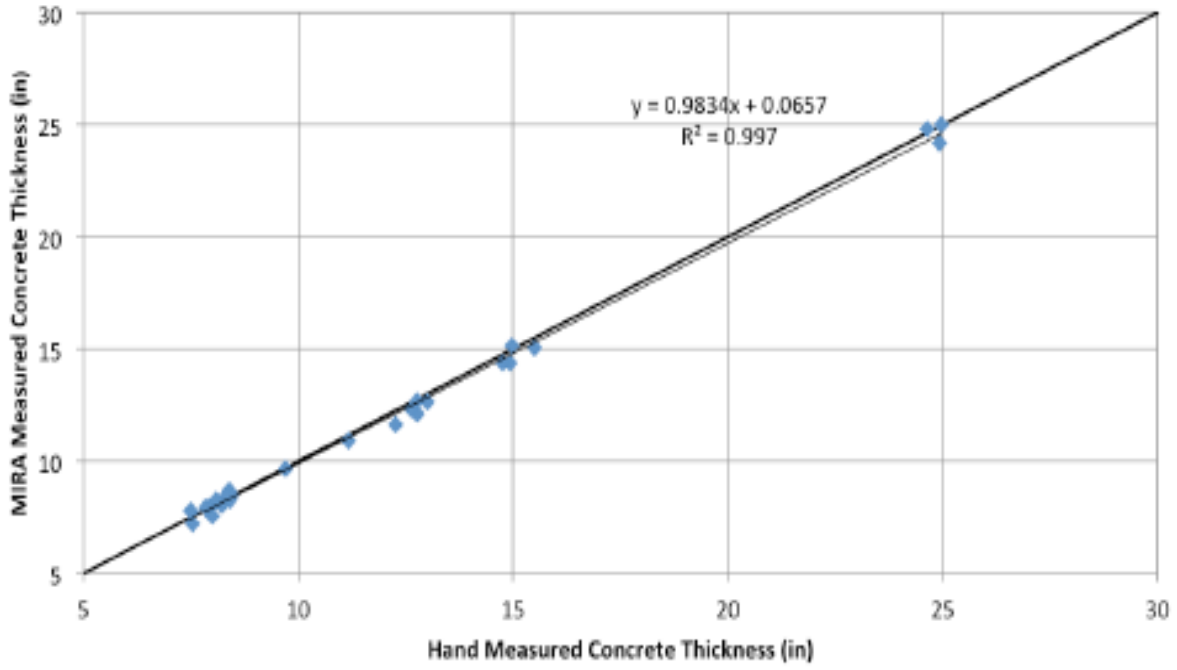

Figure 5: MIRA thickness VS CRCP core thickness (Vancura, 2013)

2.4.4 Applications and Field Implementation of MIRA

Though MIRA has yet to be applied by applied by state DOT agencies, several significant field studies have been conducted. The first large scale field application of MIRA occurred in 2009 on a continually reinforced concrete pavement on I-85 near Atlanta, Georgia. The results of the survey showed that MIRA was able to reliably determine the depth of the concrete cover. (Hoegh, Khazanovich, Yu, 2011). Additionally, it was found that all discrepancies in MIRA measurements were within the uncertainty of the core measurements (0.125 in) (Hoegh, Khazanovich, Yu, 2011). These results prompted large scale measurements at the I-85 project location. The large scale survey involved measurements taken 18in from the fog line every 50ft along 3 miles of pavement. A limited number of cores were taken as well to provide verification. The survey results showed that 67% of concrete cover thickness was outside of tolerance levels and 40% of slab thickness was outside of tolerance levels (Figure 6 (Hoegh, Khazanovich, Yu, 2011)).

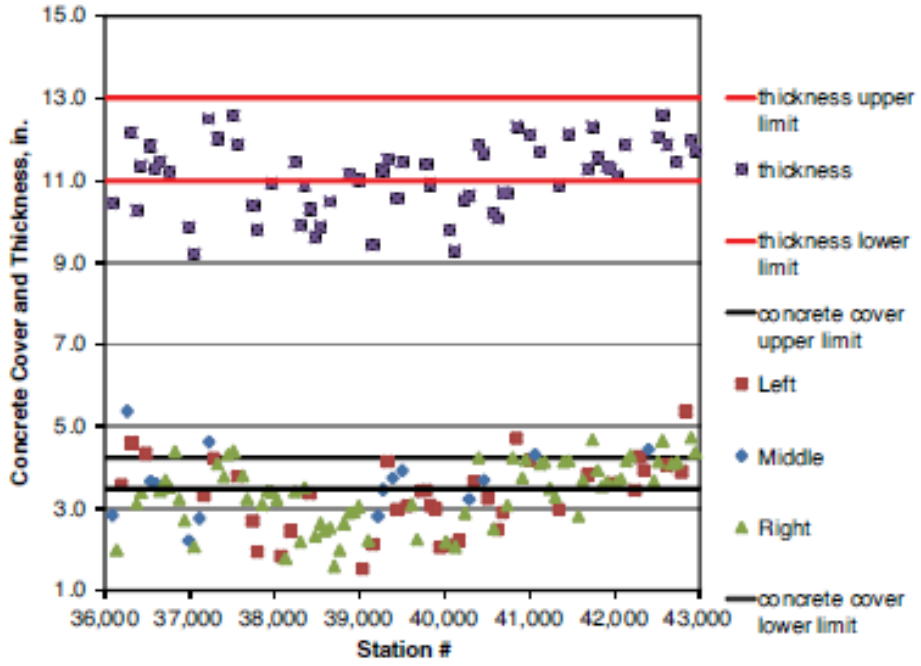

Figure 6: MIRA survey of I-85 (Hoegh, Khazanovich, Yu, 2011)

MIRA was also used to test partial bond depth repairs conducted on I_94 in Minnesota (Hoegh, 2013). Chaining (a nondestructive testing method which uses acoustics created by dragging chains over pavement) was carried out by experienced MnDOT personal to identify regions with potential debonding (Hoegh, 2013). Many MIRA measurements were taken over partial depth repair locations Figure 7 (Hoegh, 2013). The MIRA measurements taken over the partial depth repair produced backwall reflections of varying strength. The results are presented in Figure 7 (Hoegh, 2013), where a strong backwall reflection is represented by warm colors (red, yellow) and a weak reflection is represented by cool colors (blue, green). It was hypothesized that strong backwall reflections were indicative of a strong bond, while weak backwall reflections suggested poor bonding. Cores were conducted to test this hypothesis. It was found that a core taken near position 1 and position 6 was well bonded, as suggested by the strong backwall reflection and a core taken near position 9 and position 10 was poorly bonded as suggested by the weak backwall reflection (Figure 8 (Hoegh, 2013)). The results of the analysis suggest that MIRA is promising tool for nondestructive testing of partial depth bond repairs.

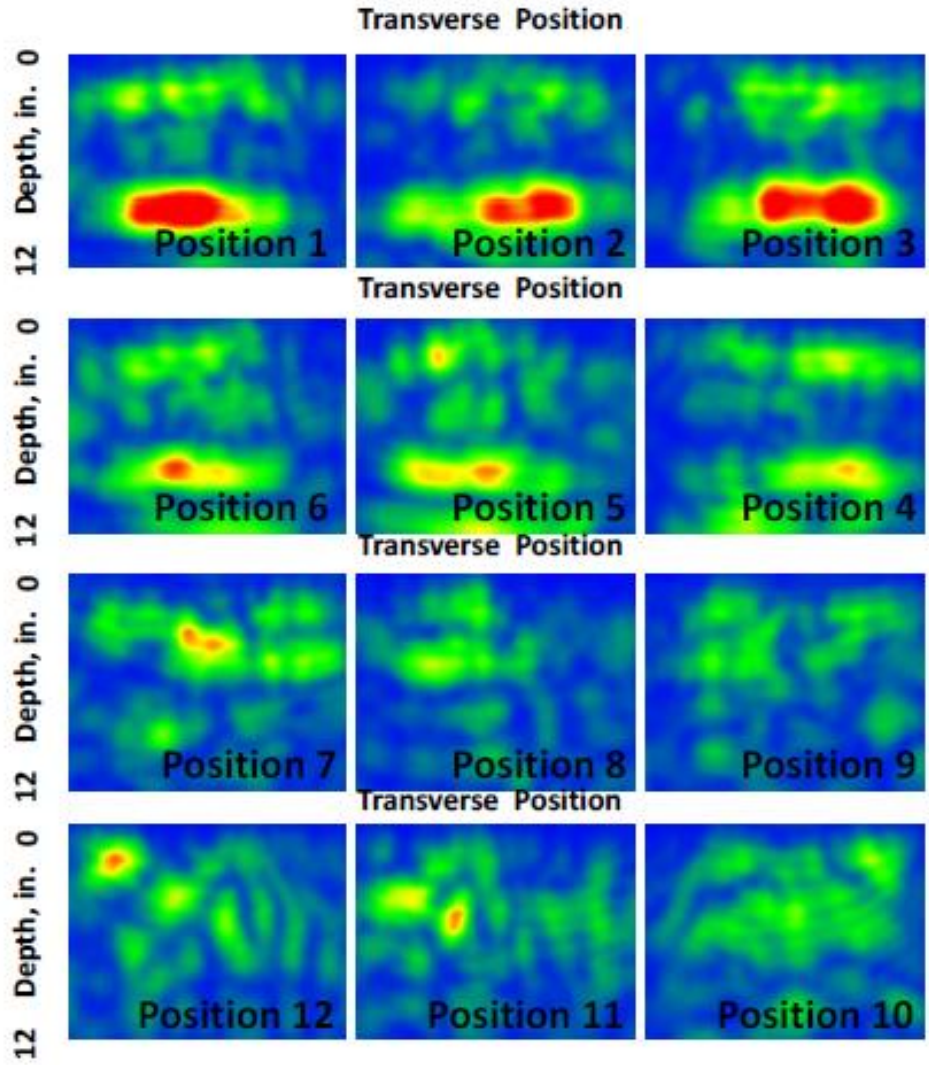

Figure 7: MIRA Scans of Partial Depth Repair (Hoegh, 2013)

Figure 8: Bonding Verification Cores

MIRA has also shown promise as a tool detecting delamination in asphalt pavements (Hoegh, Khazanovich, Maser, and Tran, 2012). The nondestructive testing of delamination in hot mix asphalts is of particular interest to road agencies, as delamination can lead to multiple types of distress and cannot be detected by visual inspection of the surface (Hoegh, Khazanovich, Maser, and Tran, 2012). MIRA was tested as nondestructive method for identifying delamination. MIRA tests were conducted on ten test sections of asphalt constructed with varying types and qualities of bond (Hoegh, Khazanovich, Maser, and Tran, 2012). The results of the test showed that MIRA could be used to detect delamination between new AC and old AC (Figure 9, (Hoegh, Khazanovich, Maser, and Tran, 2012)) as well as delamination between individual lifts within new AC (Figure 10, (Hoegh, Khazanovich, Maser, and Tran, 2012)). Delamination was indicted by high backwall reflection at the interface between new and old pavement or between individual lifts within new pavement.

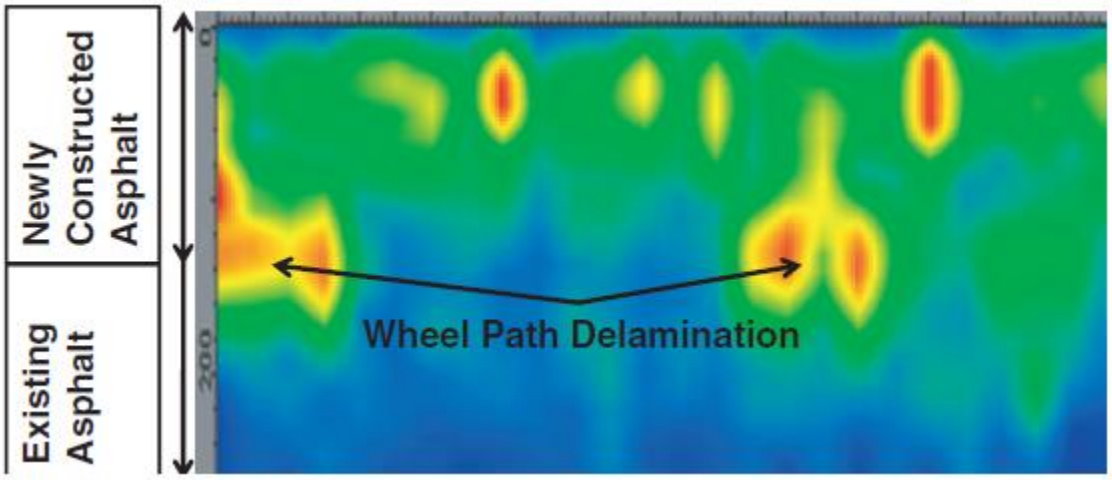

Figure 9: MIRA Detection of Delamination Between Old and New AC (Hoegh, Khazanovich, Maser, and Tran, 2012)

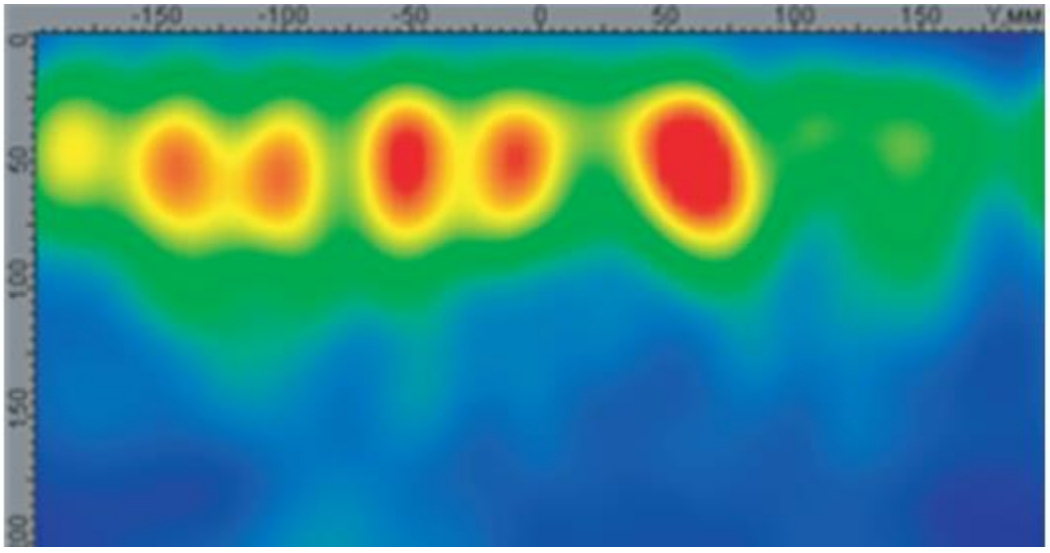

Figure 10: MIRA Detection of Delamination Between Old and New AC (Hoegh, Khazanovich, Maser, and Tran, 2012)

MIRA has also shown promise as a tool for joint assessment (Hoegh, Khazanovich, and Yu, 2012). Though damage to longitudinal can be visually determined, the damage is often severe by the time it is noticed and requires costly repairs. A method capable of detecting in-situ joint damage was of interest. Though MIRA had previously been used to detect interfaces between various aggregate materials, it was shown that interfaces with metal materials, such as dowels, could also be detected

(Hoegh, Khazanovich, and Yu, 2012. Figure 11 shows reflections associated with both the back wall reflection associated with the concrete base layers as well as the reflections associated with the dowels (Hoegh, Khazanovich, and Yu, 2012. An undamaged joint, as shown in Figure 11 was signified by circular reflections at the depth of the dowels and a strong planar reflection and depth of the concrete base layer. A MIRA joint analysis field test was implemented along a section I-94 in Minnesota. Multiple MIRA scans were taken along traverse joints. The survey produced scans indicative of both undamaged (Figure 12a (Hoegh, Khazanovich, and Yu, 2012)) and damaged joint (Figure 12b (Hoegh, Khazanovich, and Yu, 2012).). Several MIRA scans taken along joints showed regions where strong reflections were present in locations which could not be associated with dowels or the pavement base layer (Figure 12b). To verify the results of the MIRA analysis, a section of the transverse joint was cut. Visual inspection of the transverse joint revealed significant deterioration corresponding with the shallow backwall reflection seen in the MIRA scans (Figure 13) (Hoegh, Khazanovich, and Yu, 2012).

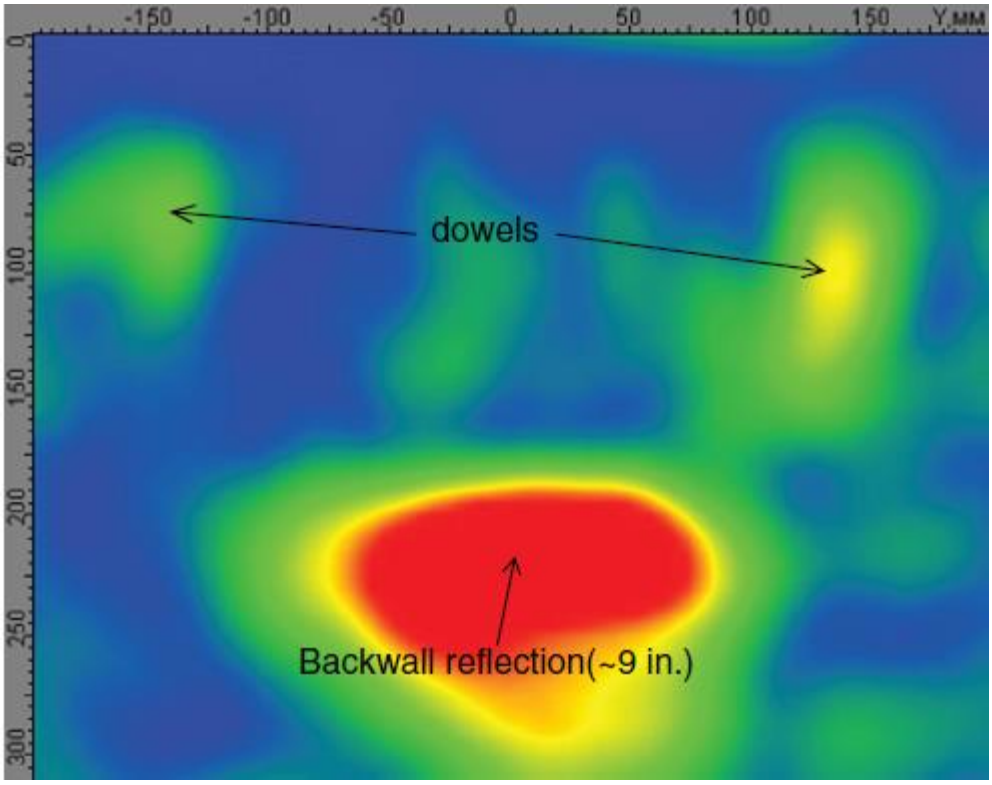

Figure 11: Backwall and Dowel Reflection in MIRA Scan (Hoegh, Khazanovich, and Yu, 2012)

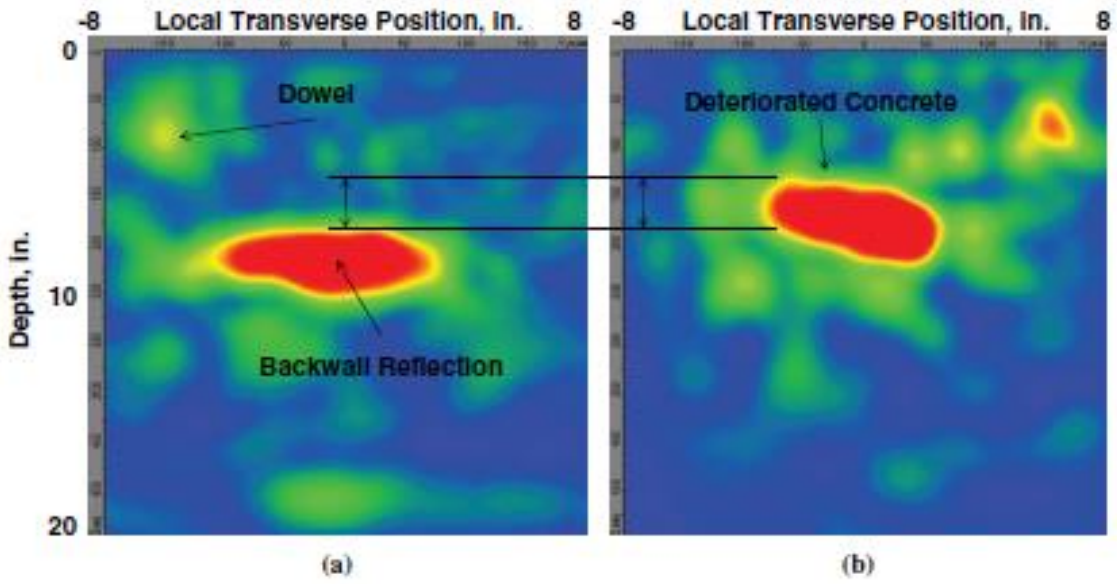

Figure 12: (a) Undamaged Joint and (b) Deteriorated Joint (Hoegh, Khazanovich, and Yu, 2012)

Figure 13: Damaged Joint Detected by MIRA (Hoegh, Khazanovich, and Yu, 2012)

The largest MIRA field study conducted to date was performed by Vancura. All discussion of the work performed by Vancura was taken from (Vancura, 2013). In addition to the accuracy and precision verification discussed in section 2.4.3, Vancura also performed a large scale field study of the PCC thickness variation. During this study, Vancura surveyed three Minnesota highways (referred to as "HWY 1", "HWY 2", and "HWY 3") covering nearly 30000ft of pavement and performing 2862 measurements. The MIRA results for HWY1 and HWY2 were validated with the collection of cores, however cores were not available for HWY3.

Two different survey surveys protocols were used in the investigation. Protocol 1 consisted of a single measure taken within each panel of the truck lane. This protocol was primarily designed to determine large scale longitudinal variation. The measurement was taken approximately 3ft from the fog line and 2ft from the joint in the direction of traffic (Figure 14 (Vancura, 2013)). This survey was continued as long as feasible. Protocol 2 consisted of a total of 12 measurements taken per panel. Six equally spaced measurement (approximately 2ft) were taken near the edge (2ft from fog line) and center of the lane (11ft from fog line). Measurements were taken between 2ft from the starting joint and 3ft from the ending joint. Protocol 2 was conducted on the both edge of panel and center of the panel (Figure 15 (Vancura, 2013)). Protocol 2 was designed to give more insight into small scale longitudinal variation and transverse variation. This survey was conducted for 500 feet. Protocol 1 and 2 were collected on three different Minnesota highways.

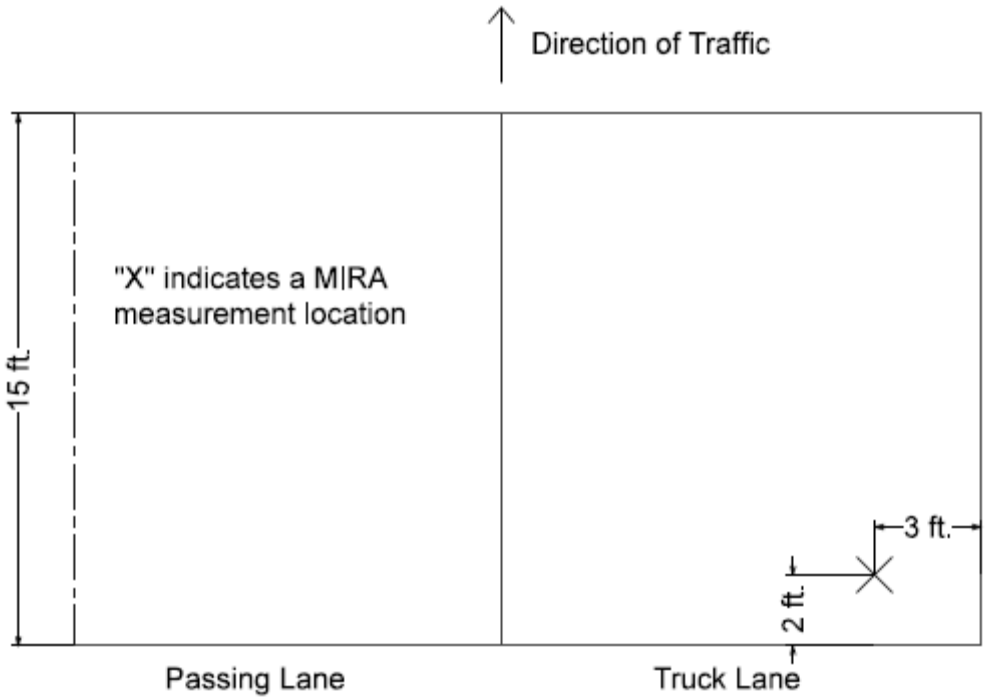

Figure 14: Vancura's Survey Protocol 1(Vancura, 2013)

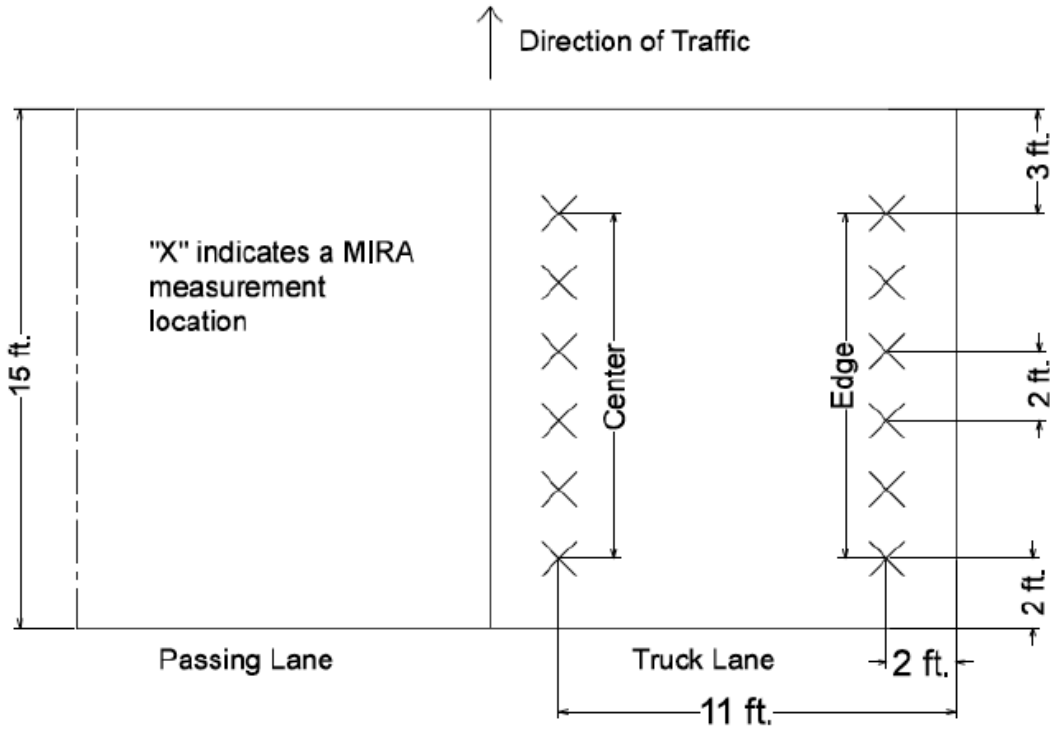

Figure 15:Vancura's Survey Protocol 2 (Vancura, 2013)

The surveys conducted on the three Minnesota highways produced several interesting results (Table 1 (Vancura, 2013)). First, statistical analysis showed that MIRA measurements were able to predict the average thickness determined by coring. Additionally, MIRA measurements were better able find maximum and minimum thickness values than could be achieved from coring (Table 1 (Vancura, 2013)). The data collected using sample protocol 1 showed a surprising degree of thickness variation in the longitudinal direction. A sample profile taken on HWY 1 is presented in the longitudinal direction (Figure 16 (Vancura, 2013)). Data collected using protocol 2 showed interesting transverse variation in pavement thickness. Data collected using sample protocol 2 showed pavement tended to be thicker in the middle and thinner near the edge (Figure 17 (Vancura, 2013)). An example of this trend is presented in Figure 17(Vancura, 2013). In some locations this discrepancy was as high 1.5 in.

Statistical analysis of the data collected using protocol 1 and protocol 2 produced similar results (Table 1 (Vancura, 2013)). However, the standard deviation and thickness range were less for protocol 2 than for protocol 1 (Table 1 (Vancura, 2013)). This suggests that the difference in longitudinal measurement frequency does not affect the measurement range of concrete thickness, but the total length of the survey does. As can be seen in Figure 18 (Vancura, 2013) the thickness data appears to be normally distributed. The finding of normality agrees with the results of the variability analysis conducted by the FHWA (Jiang, Selezneva, Mladenovic, Aref, and Darter, 2003).

Table 1: Vancura's Results of Large Scale Field Survey (Vancura, 2013)

	HWY 1				HWY 2				HWY 3			
		SP 2				SP 2				SP 2		
	SP 1	Edge	Center	Cores	SP1	Edge	Center	Cores	SP 1	Edge	Center	Cores
Length Evaluated (ft.)	6645	500	500	6551	15985	500	500	15045	3000	500	500	NA
Number of data points	444	204	204	7	1032	204	196	16	201	183	194	NA
Design Thickness (in.)	9				8				8			
Mean Thickness (in.)	9.15	8.12	9.02	9.24	8.27	8.19	8.25	8.39	7.75	7.84	7.83	NA
Thickness Stand. Dev. (in.)	0.45	0.31	0.21	0.43	0.34	0.16	0.16	0.29	0.17	0.14	0.16	NA
Max Thickness (in.)	11	9.38	9.45	9.88	9.42	8.59	8.68	9	8.16	8.22	8.16	NA
Min Thickness (in.)	8.01	8.01	8.44	8.69	7.34	7.83	7.89	8	7.24	7.52	7.58	NA
Thickness Range (in.)	3	1.38	1.01	1.19	2.08	0.76	0.79	1	0.83	0.7	0.58	NA

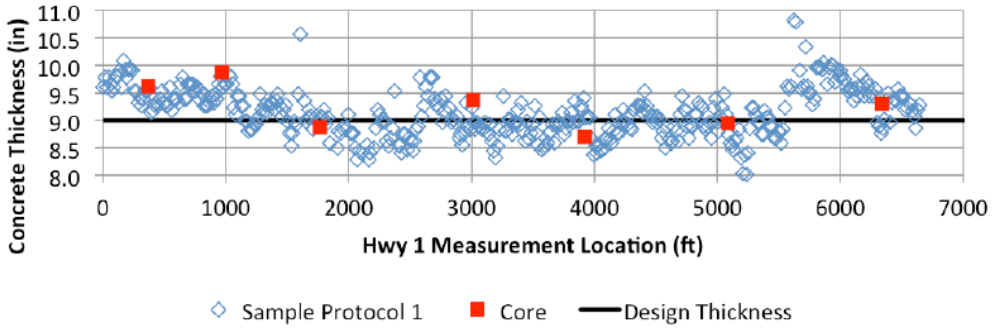

Figure 16: Protocol 1 Thickness Profile (Vancura, 2013)

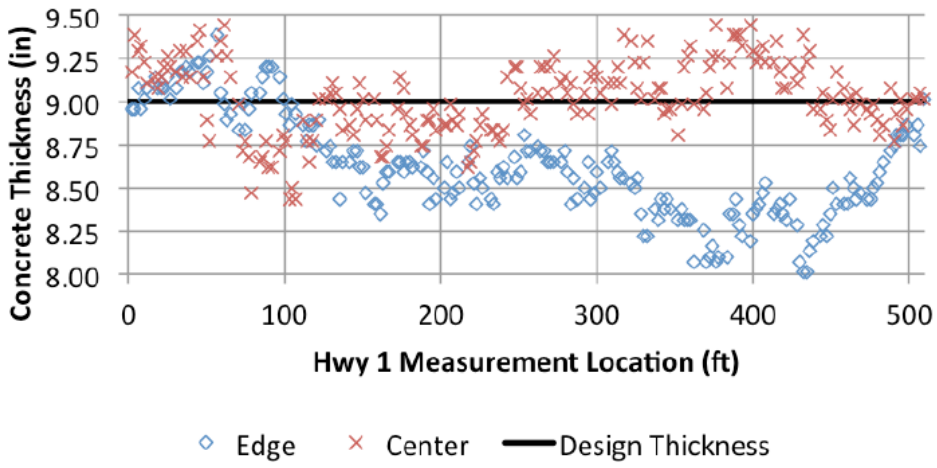

Figure 17: Protocol 2 Thickness Profile (Vancura, 2013)

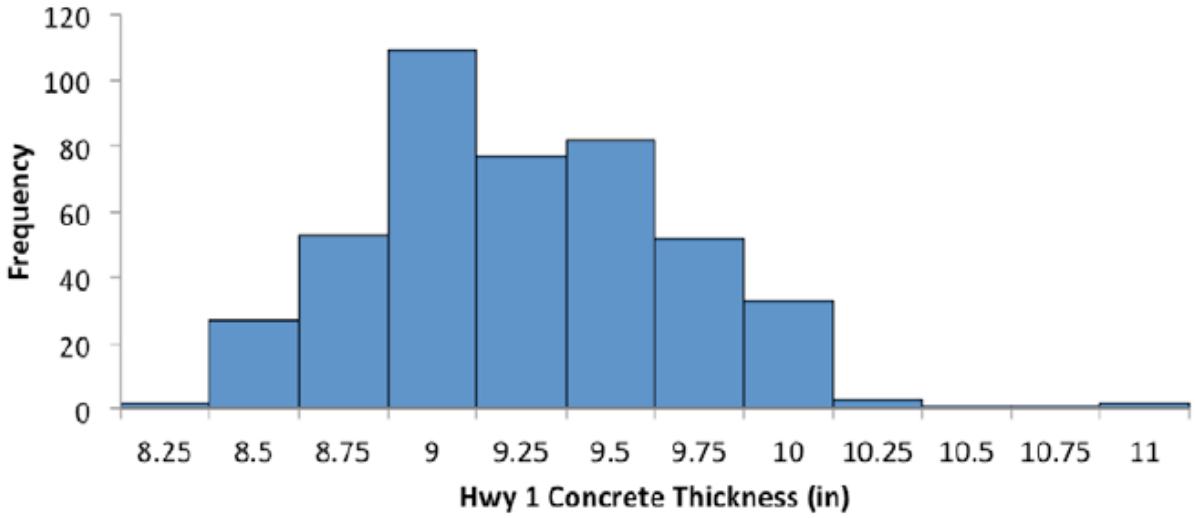

Figure 18: Histogram of Pavement Thickness (Vancura, 2013)

The results of the large scale surveys were used in an attempt to determine the optimum spacing of measurements. The optimum spacing was defined as the measurement spacing that produced an accepted probability of missing a thickness deficiency. Semi variograms and the autocorrelation function were used in attempt to determine the distance at which measurements were no longer spatially correlated and thus a new measurement would be justified. The results of the variogram analysis were produced data collected using protocol 1 produced correlation lengths from 250ft to 1750ft (Table 2 (Vancura, 2013)). The wide discrepancy in correlation length is more than could be accounted for by pavement thickness variation alone, and indicates that the variogram analysis

was inconclusive for protocol 1 data. The variogram analysis of protocol 2 data produced much more reasonable correlation lengths from 35ft to 165ft (Table 3 (Vancura, 2013)). Periodicity was observed in the protocol 2 data collected on HWY 3. Variogram analysis is only appropriate for which exhibits monotonically increasing variance with distance and cannot be used to model periodicity. A fast Fourier transform model unsuccessfully applied to the data. A better model of HWY 3 data was produced using a first order autoregressive function (Vancura, 2013).

Table 2: Results of Semivariogram Analysis for Protocol 1 (Vancura, 2013)

JPCP Hwy	Sample Protocol 1 Semi-variogram	Approximate Nugget (in^2)	Approximate Sill (in^2)	95% of Approximate Sill (in^2)	Range (ft)
1	Figure 5.4	0.05	0.183	0.174	575
2	Figure 5.5	0.026	0.076	0.072	1750
3	Figure 5.6	0.009	0.0252	0.024	250

Table 3: Results of Semivariogram Analysis for Protocol 2 (Vancura, 2013)

JPCP Hwy	Sample Protocol 2 Semi-variogram	Location	Approximate Nugget (in^2)	Approximate Sill (in^2)	95% of Approximate Sill (in^2)	Range (ft)
1	Figures 5.7 and 5.8	Center	0.009	0.048	0.046	72
		Edge	0	0.081	0.077	165
2	Figures 5.9 and 5.10	Center	0.007	0.032	0.03	70
		Edge	0.002	0.028	0.027	35
3	Figures 5.11 and 5.12	Center	periodicity			
		Edge	periodicity			

The results of the variogram and autoregressive analysis were used to create a model for estimating optimal concrete thickness sample spacing. The model incorporated the thickness variation statistical parameters of mean thickness, standard deviation, and autocorrelation length. This model output the probability of missing varying magnitudes of thickness excursions based on sampling length. The results of this model vary by survey location and sampling protocol, but general conclusions were drawn. First, the 1000ft spacing mandated by MnDOT has a 100% chance of missing an excursion; generally, so does the 500ft length. Additionally, a there is not a statistically significant decrease in the probability of missing a thickness excursion until sample spacing enters the 15ft range (Vancura, 2013).

Calculation of HTI

In addition to thickness and distress, MIRA ultrasonic tomography data can also be used to compute the Hilbert Transform Indicator (HTI) (Freeseman, Hoegh, and Khazanovich, 2016). MIRA data was originally used to compute the HTI in a study of freeze-thaw affected pavements. It was noted in the study that the measurements taken over pavements known to be freeze-thaw affected resulted in a different signal impulse magnitude and shape than those taken over pavements known to be clean (Figure 19). The difference in impulse can be quantified with the HTI Figure 20. Fundamentally, the HTI sums and normalizes the absolute instantaneous amplitudes of the raw signal. The increased magnitude and variation of signal pulse associated with damaged pavement will result in a higher HTI value than for clean pavement. In the study performed on freeze-thaw affected pavement (Freeseman, Hoegh, and Khazanovich, 2016), damaged pavement was found to have an average HTI value of 133 while clean pavement was found to have an average HTI of 61. The dramatic change increase in HTI associated with damaged pavements suggests is may be a powerful predictor of distress.

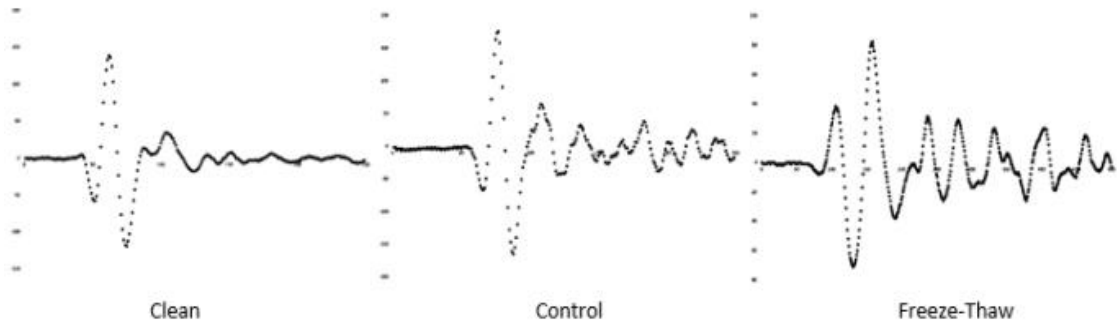

Figure 19: Signal Pulse of Clean, Control and Freeze-That Damaged Pavement (Freeseman, Hoegh, and Khazanovich, 2016)

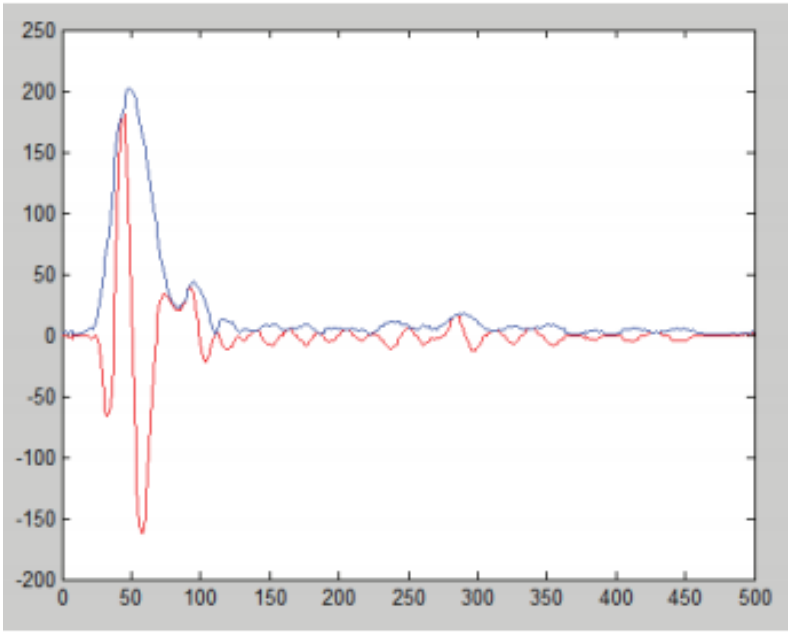

Figure 20: HTI From Signal Pulse (Freeseman, Hoegh, and Khazanovich, 2016)

	Clean	Control	Freeze-Thaw
Sample Size	45	11	11
Minimum	34.47	46.34	86.12
Maximum	57.56	79.22	166.22
Average	48.89	61.13	133.25

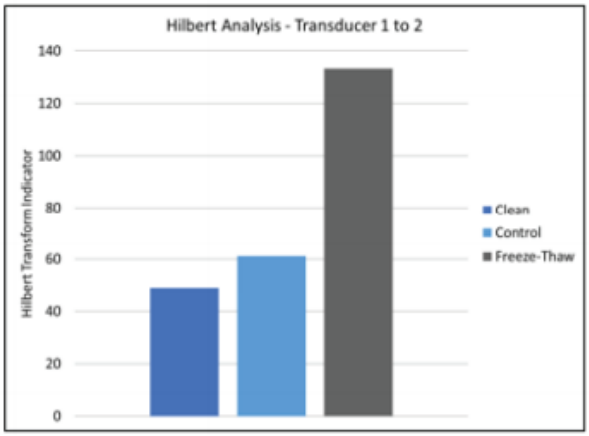

Figure 21: HTI of Clean, Control and Freeze-Thaw Damaged Pavements (Freeseman, Hoegh, and Khazanovich, 2016)

2.4.5 Other Non-destructive Testing Methods

It is important to compare ultrasonic tomography with other NDT methods such as GPR and MIT-Scan T2. The main advantage of GPR is that it can be employed at road speed, and therefore does not require road closures (Hoegh, 2013). However, GPR does not provide as high of resolution as MIRA, is highly sensitive to water and requires occasional coring to calibrate the dielectric constant. MIRA could be used compliment a GPR survey by providing better resolution where required and eliminating the need for coring by providing nondestructive determination of the dielectric constant (Hoegh, 2013). The MIT-Scan-T2 is an electromagnetic method which has been shown to be highly accurate of locating dowels. The MIT-Scan-T2 can also be used to for fast and accurate dowel detection and concrete thickness measurements, but only if a metal reflector is placed in the pavement during construction. It is suggested that MIRA be used to compliment a MIT-Scan-T2 survey to provide further information on pavement thickness and condition (Hoegh, 2013).

3. STUDY METHODOLOGY

The survey methodology used in this and process with which it was developed study will be presented. Protocols outlined MIRA surveying and distress surveying are described.

3.1 PCC Thickness and Velocity Data Collection

PCC thickness and velocity surveying was conducted on Minnesota roadways using MIRA ultrasonic tomographer. The methodology presented below was developed specifically for this study.

3.1.1 Introduction to MIRA and Distress Data Collection

In order to build a database of thickness and velocity data and associated distress, field data was needed. There are no accepted survey protocols for MIRA surveys of pavement, so an effective survey protocol had to be determined. Various MIRA survey protocols were considered. These protocols explored differences in longitudinal and transverse measurement spacing. The various protocol patterns are listed in Table 4. The key considerations in final protocol selection were scale of longitudinal and transverse variation and the time to implement the survey. The survey which was able to best capture the transverse and longitudinal thickness variation would be selected for field implementation. If multiple protocols were found capture the thickness variation, the most efficient protocol would be selected. As discussed in the literature review, a variogram analysis conducted by Vancura suggested longitudinal spacing on the order of tens to hundreds of feet while

statistical modeling suggested that spacing of 15ft provided a statistically significant chance of detecting deviations from design thickness. The Vancura study also showed interesting variation of up to 1.5in. in the transverse direction across a single lane.

Table 4: Trial Test Protocol Conducted on MnROAD

Trial Protocol	Transverse Measurement Description	Longitudinal Measurement Description
Protocol 1	Perform five pairs of coupled transverse measurements (10 total) starting 1ft from center of fog line. Perform 2 coupled measurements 0.5ft apart every 1.5ft.	Perform transverse measurement every 100ft in the longitudinal direction
Protocol 2	Perform two coupled transverse measurements spaced 0.5ft apart 2.5ft from the center of the fog line	Perform transverse measurement every 5ft in the longitudinal direction
Protocol 3	Perform three pairs of coupled transverse measurements (6 total) 2.5-3ft, 6-6.5ft, 9.5-10ft from the center of the fog line	Perform transverse measurement every 20ft in the longitudinal direction
Protocol 4	Perform five pairs of coupled transverse measurements (10 total) starting 1ft from center of fog line. Perform 2 coupled measurements 0.5ft apart every 1.5ft.	Perform transverse measurement every 10ft in the longitudinal direction

3.1.2 Protocol Trial Survey of MnROAD Low Volume Loop

A trial survey was performed on the MnROAD Low Volume Loop to test the protocols described above. The MnROAD Low Volume Loop is an experimental pavement laboratory with many pavement sections of different construction (Figure 22). Surveys were conducted on various cells using all four protocols above. A total of 15 separate surveys were conducted on 15 distinct cells. The result of the surveys showed significant longitudinal and transverse variation, similar to that described by Vancura, 2013. Though no quantitative statistical assessment was made of the variation, visual examination of the results and the results of Vancura (2013) suggested that transverse variability was significant and either protocol 1 or protocol 4 should be implemented, as both provided dense transverse measurements. Additionally, visual analysis of longitudinal thickness variation and findings by (Vancura, 2013) suggested that the 100ft longitudinal sampling was too large and would miss significant thickness excursions. Therefore, protocol 4, which consists of 10 transverse measurement taken every 10 feet longitudinally, was chosen as the final field survey protocol.

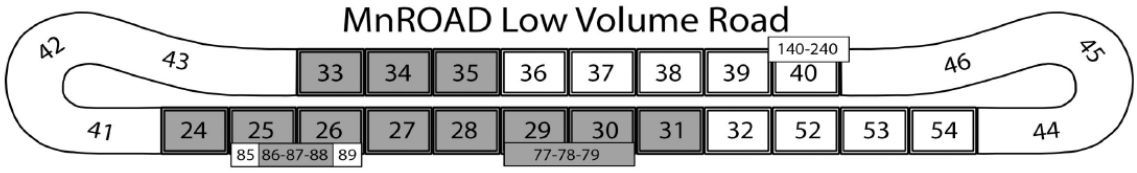

	West Loop			North Side Cells									East Loop		
	ASR Concrete Testing (West Loop)			Acid Modified			Original PCC			Pervious Overlay	Unbonded Concrete Overlay		ASR Concrete Testing (East Loop)		
	41	42	43	33	34	35	36	37	38	39	140	240	46	45	44
	12" Trans Tined 12x15 1" Dowels	12" Trans Tined 12x15 1" Dowels	12" Trans Tined 12x15 1" Dowels	4" 58-34 PPA	4" 58-34 SBS+PPA	4" 58-34 SBS	6" Trans Tined 15x12 1" dowel	6" Trans Tined 12x12	6" Trans Tined 15x12 1" dowel	4" Perv Overlay	3" UBOL* thin fabric	3" UBOL* std fabric	12" Trans Tined 12x15 1" Dowels	12" Trans Tined 12x15 1" Dowels	12" Trans Tined 12x15 1" Dowels
				12" Class 6	12" Class 6	12" Class 6	5" Class S	5" Class S	5" Class S	6" 20x12 1" dowel	5.5"-7.0" Trans Tined 15x12	5.5"-7.0" Trans Tined 15x12			
	Clay	Clay	Clay	Clay	Clay	Clay	Sand	Sand	Clay	5" Class S	5" Class S	5" Class S	Clay	Clay	Clay
								2007 PCC Grind Strips		Clay	Clay	Clay			
											6x6 panels Fiber PCC Long Tined	6x6 panels Fiber PCC Long Tined			
	Jul 93	Jul 93	Jul 93	Sep 07	Sep 07	Sep 07	Jul 93	Jul-93	Jul 93	Oct 08	Jul 13	Jul 13	Jul 93	Jul 93	Jul 93
Inside Cell (ft)	491	490	508	500	499	499	480	504	480	440	225	234	508	489	442
Inside Gap 179	97	147	175	71	54	132	41	42	67	67	0	108	98	146	0
Outside Gap 179	102	152	175									108	102	153	0
Outside Cell (ft)	510	510	494										493	511	463

Figure 22: MnROAD Low Volume Loop

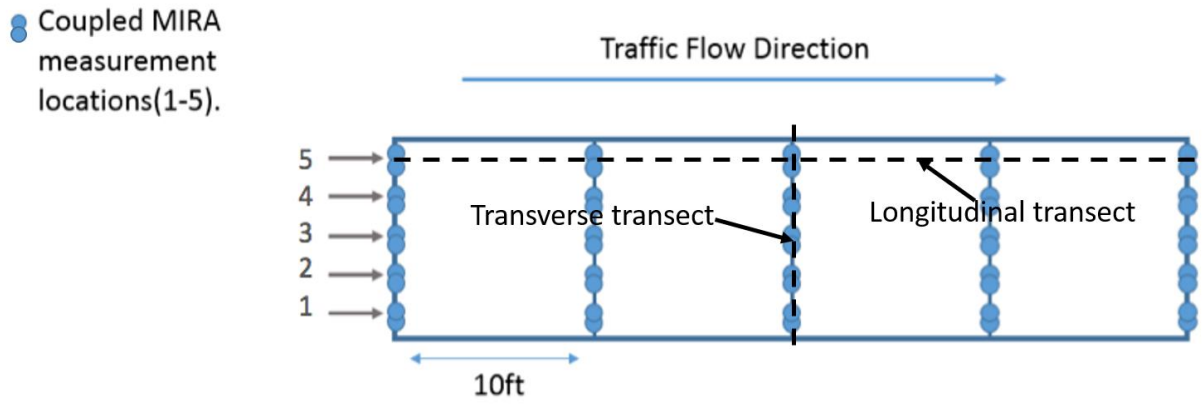

Figure 23: Protocol 4 (Field Survey Method)

3.1.2 MIRA Survey Geometry

As discussed above, a survey pattern consisting of 10 coupled transverse measurements taken every 10ft longitudinally was chosen as final field method. In addition to honoring the findings reported by Vancura, 2013 and providing dense data, this geometry was chosen in an attempt to remain consistent with transverse spacing outlined by the FHWA (Miller and Bellinger, 2003) for distress location identification. The FHWA calls for recording distress in five traverse locations defined as left of left wheel path, left wheel path, center, right wheel path, and right of right wheel path. The distresses can be recorded at any longitudinal spacing. The traverse measurements outlined in the FHWA protocol were adopted for the MIRA survey. When converted to distances on a typical 12 ft lane, these locations corresponded the locations outline in Table 5

Also, Readings were not taken within approximately 6 in. of joints or observable distress, as this was shown to cause issues with data quality. If a distress or joint was found at a measurement location, MIRA was offset to closest acceptable location.

The field protocol also included performing all MIRA measurements as two closely spaced MIRA readings as a form measurement verification. These measurements, referred to as a couple, were taken approximately 6 inches apart in the transverse direction and were to be taken centered on the locations defined by the FHWA. In later analysis, these coupled readings would be compared. If the difference between the readings was greater than a certain tolerance, the couple was deemed an error and neither measurement was used in further analysis. For measurements within the error

tolerance, the measurements were averaged and final value was used in continued analysis. A field data sheet was created to ease the collection of MIRA data (Appendix A).

Table 5: Transverse Survey Locations

location #	approximate area	distance from center of fog line (ft)
location 5	left edge	11.4
location 4	left wheel	9.5
location 3	center	6.0
location 2	right wheel	2.5
location 1	right edge	0.6

3.1.3 MIRA Field Surveying Method

To ensure data quality and consistency, a MIRA field survey methodology was developed. A general outline of the survey method is described below. A procedural guide can be found in Appendix A. The first step in MIRA data collection was determining a valid data collection site. The characteristics of a valid site are outlined in section 3.2. Before going out to a site location, general checks of equipment and battery charge were performed. To initiate surveying, the starting location was accurately recorded including roadway name, stationing, GPS and other identifying characteristics. The starting location was marked and photographed. Ten transverse measurements were recorded as outlined in section 3.1.2. A survey measuring wheel was used to advance 10ft and transverse measurements were repeated. To protect from data loss, the ten measurements recorded for each transverse were saved within a unique folder. The ten transverse measurements recorded were referred to as a transverse transect and measurements in the same transverse location was referred to as a longitudinal transect. Survey data sheets were created for recording data (Appendix A).

3.2 Observable Distress Surveying Method

A method of recording distresses also needed to be determined. The goals of project required a method of distress surveying that recorded the type, severity, and the exact transverse and longitudinal location of distress features. The methods outlined by MnDOT and the FHWA were both investigated. The MnDOT method was preferred, as the study is being conducted on Minnesota roads. Therefore, the distresses outlined by MnDOT were chosen as the distress type classification to be used in the study. However, the MnDOT method does not outline the recording of exact location or severity of distress. Rather, the MnDOT method calls for recording the percent of panels distressed within a certain distance interval (usually 500ft) (MnDOT, 2003). Additionally, the MnDOT method only records distress for transverse and longitudinal joint spalling. Therefore, augmentation of the method was required. The additional location and severity recording methodology were taken from distress recording method outlined by the Federal Highway Administration (FHWA).

The FHWA distress survey protocol does outline procedures for recording the exact location and severity of distress. In the FHWA method, distress longitudinal location is recording in stationing and the transverse location can be categorized into one of the five locations outlined in ase the collection of MIRA data (Appendix A).

Table 5).

Additionally, the FHWA method provided thorough document on recording of severity for most distress types. Therefore, the distress location and severity recording protocol outlined by the FHWA were applied to the distress types outlined by MnDOT. It is important to note that the MnDOT and FHWA distress type definitions were not exactly the same. Therefore, some generalizations had to be made when applying distress severity definitions from FHWA to MnDOT distress types. The final set of distresses and associated severity measurements are outlined in Table 6.

Table 6: Survey Distress Types

MnDOT #	MnDOT Distress Description
1	Transverse Joint Spalling
2	Longitudinal Joint Spalling
3	Faulted Joints
4	Cracked Panels
5	Broken Panels
6	Faulted Panels
7	Overlaid Panels
8	Patched Panels
9	Durability Cracking (D-Cracking)

Distress Surveys were initially conducted with intent to use images recorded with the application Pathview II. This is a pavement management system which takes georeferenced photographs of road surfaces. These images are then stored in a database and can be used to inform pavement management decisions. However, issues were encountered with the georeferencing in the application. The location of a single distress was often found to change when the application was shut down and restarted. It was determined that the application did not provide the desired resolution and another method would be required.

As a result of the issues encountered in the Pathveiw II software, it was determined the most accurate and verifiable method would be to manually conduct the distress survey while the MIRA survey was being conducted. This would allow for both surveys to use the same measurement scale and initial location. Additionally, the images provided in the Pathview II software are not real time and may not represent the current state of distress at the time of the survey. A field data sheet was created to ease the collection of the distress data (Appendix A).

3.3 Selection of Field Sites and Data Collection

3.3.1 Preferred Field Site Criteria

Several factors were considered when looking for field survey locations. First, only PCC locations were investigated. Secondly, for safety reasons only sites which were closed to traffic were considered. Third, locations which exhibited distress were preferred, but not exclusively so. Finally, though sites could have construction being performed, sites surveyed should contain sections greater than 1000ft which can be surveyed without interfering with construction practices. Timeliness was also an important issue. A survey could cover approximately 1 mile in 4 - 5 hours, and set-up and take down was found to take about 1 hour. Therefore, any site chosen must be available for several hours.

3.3.2 Field Sites Selected and Data Collection

MIRA and pavement distress data were collected at a total of four locations within Minnesota. These locations included Minnesota State Highway 60 (HWY 60), Minnesota State Highway 100 (HWY 100), Interstate 394 (I 394) and Interstate 494 (I 494). Surveys performed on HWY 60 and HWY 494 were taken in East and West directions. This results in a total of six data sets, each data set containing spatial measurements of pavement thickness and velocity as well as distress. The construction data of survey locations is provided in Table 7. I-494 is not included, as the survey location was not properly recorded and the data proved be highly corrupted. A listing of the general survey parameters can be seen in Table 8.

A. Minnesota State Highway 100

The survey for East HWY 100 was performed on 31 May, 2015 southwest of Minneapolis. The 1520ft investigation section was taken from approximately MP 3.39 to MP 4.64. The survey was conducted in the right most lane in the direction of traffic. A total of 1530 measurements were performed. A continuous visual distress survey was conducted along the entirety of the investigation section.

The slab design thickness at the Highway 100 survey location is 9.00 inches. Traverse joints are spaced at 27ft. Dowels are 1 in diameter and 18in in length and spaced 12in apart. Full design details including jointing, reinforcing, concrete mixing, and base and subgrade material, see appendix C.

The survey of HWY 100 included a bridge approach region. This change in construction caused errors in the MIRA data. Therefore, only data excluded the bridge sections was used in the full analysis.

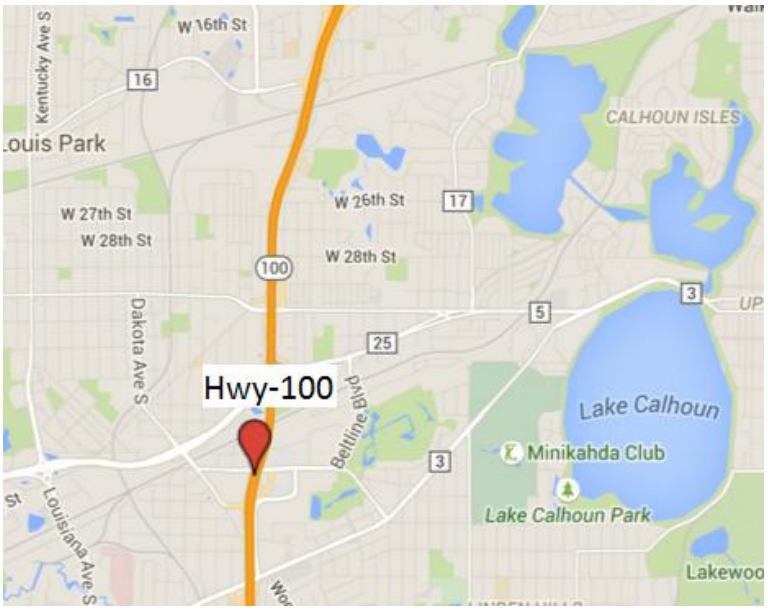

Figure 24: HWY 100 Survey Location (Google, 2016)

B. Minnesota State Highway 60

The survey for HWY 60W was performed on 9 June, 2015. The 2990ft investigation sections was located from approximately MP49.91 to MP53.27. The survey was conducted in the right most lane. A total of 3000 measurements were performed. A continuous visual distress survey was conducted along the entity of the investigation section.

The survey for East HWY 60 was performed on 19 June, 2015. The 1990ft investigation sections was located from MP53.27 to MP 54.17. A total of 2000 measurements were performed. A continuous visual distress survey was conducted along the entity of the investigation section.

The slab design thickness at over the survey area over Highway 60W and 60E is 8.00 inches. Traverse joints are spaced at 27ft. Dowels are 1 in diameter and 18in in length and spaced 12in apart. Full construction details including jointing, reinforcing, concrete mixing, and base and subgrade material, see appendix C.

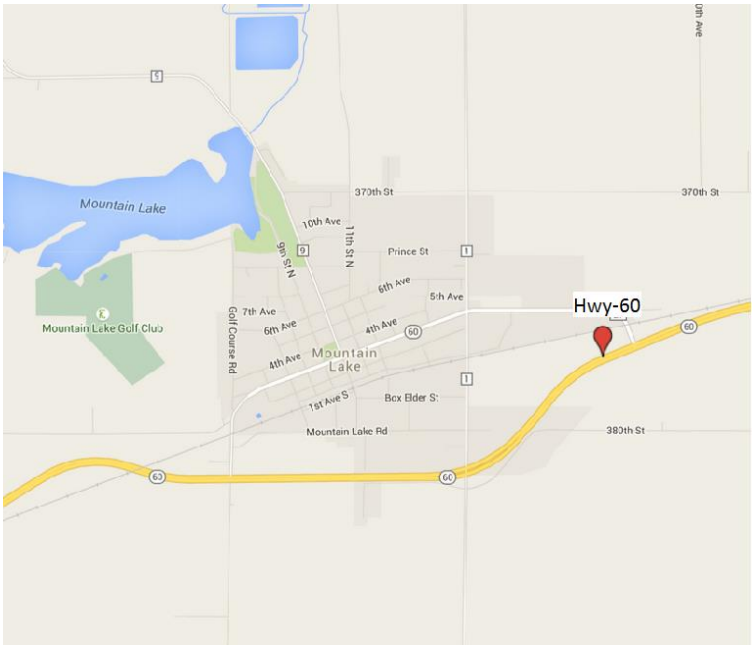

Figure 25: HWY 60 Survey Location (Google, 2016)

Figure 26: HWY 60E and HWY 60E locations (Google, 2016)

C. Interstate 494

Two surveys were conducted on I-494. The first survey of I-494 was performed on 1 July, 2015. The first survey consisted of 800 measurements and covered 790ft. The survey was conducted in the right most lane in the direction of traffic. The second survey on I-494 was performed on 1 July, 2015. The second survey consisted of 1300 measurements and covered 1290 ft. A continuous visual distress survey was conducted along the entity of both MIRA surveys. Location data is unavailable for the survey taken on I-494 therefore construction data cannot be provided. I-494 survey was performed on PCC pavement exposed during the removal of an asphalt overlay. Therefore, the PCC is highly distressed and contains extensive asphalt overlays. For this reason, this data is suspect and is not recommended for further analysis.

D. Interstate 394

The survey for I-394 was performed on 9 July, 2015. The 1990ft investigation sections was located approximately from MP6.52 to MP7.64. The survey was conducted in the right most lane. A total of 2000 measurements were performed. The measurements were taken in the reversible high occupancy lane. A continuous visual distress survey was conducted along the entity of the investigation section.

The slab design thickness over the survey area over Highway 394 is 10.00 inches. Traverse joints are spaced at 27ft. Dowels are 1.25in diameter and 15in in length and spaced 12in apart. Full construction details including jointing, reinforcing, concrete mixing, and base and subgrade material, see appendix C.

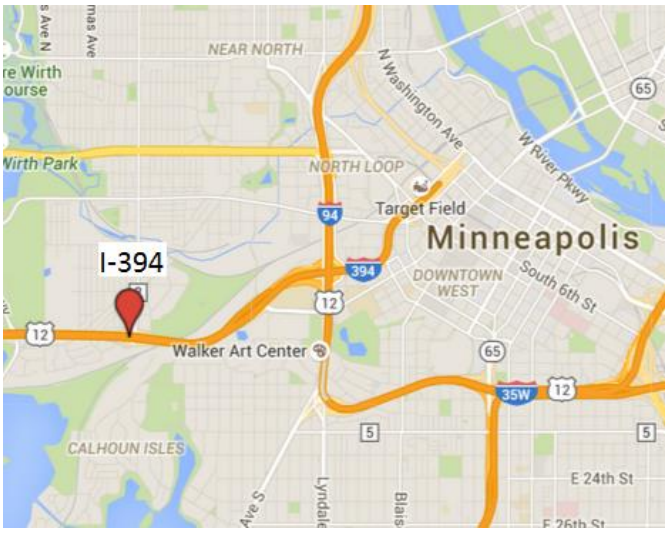

Figure 27: I-394 Survey Location (Google, 2016)

Table 7: Site Survey and Construction Data

Section	**Beginning - Ending MP (mi.)**	**Design Thick. mm (in.)**	**Date Completed**	**Base Layer**	**Base Thick. mm (in.)**	**Drainage**
HWY 100	3.39 - 4.64	228.6 (9)	10/1/1973	Crushed Gravel	330.2 (13)	Long. Drains
HWY 60 (1)	49.91 – 53.27	203.2 (8)	10/1/1988	NA	NA	Long. Drains
HWY 60 (2)	53.27 – 54.17	203.2 (8)	6/1/1987	Crushed Gravel	76.2 (3)	No subsurface drainage
I 394	6.52 - 7.64	254 (10)	10/1/1990	Gravel	NA	Long. Drains

NA = data not available

Table 8: MIRA Survey Parameters

Section	**HWY 60E**	**HWY 60W**	**HWY 100**	**I 394**
# Measurements	2000	3000	1530	2000
# Couple	1000	1500	765	1000
# Trans. Transects	200	300	153	200
Distance [ft]	2000	3000	1530	2000

3.4 Preprocessing of MIRA Data

After MIRA surveys were completed, data preprocessing was required. The end goal of data preprocessing was to convert the MIRA data into a format which would allow for spatial relationship of thickness and velocity data to observed distress. Once the data was related, a statistical analysis could be performed. MATLAB was chosen to perform the spatial relation and statistical analysis.

First, the thickness and velocity measurements were extracted from the data. This is done application of an algorithm used by Hoegh, Khazanovich and Yu (2011). The algorithm is applied by a program referred to as 'ThicknessEngine'. ThicknessEngine takes the .lbv data files output by MIRA and processes them into a .csv file with measurement thickness, velocity, and delay time. Once the .csv file has been produced, the input thickness file for the MATLAB spatial combination could be created. This input file is .xlsx spreadsheet which contains important survey information which will be used in the data processing. The input file contains survey data including starting point, distance between longitudinal traverses, and number of readings per traverse. The distress data requires much less processing than the thickness data. Distress data was entered into a provided field data survey sheet. As long as the data was entered as outlined on the survey sheet, the distress data could be directly processed by MATLAB.

3.5 Averaging Coupled Measurements

After the initial preprocessing of the data, the coupled measurements were averaged. As outlined in section 3.1.2, all survey data was collected as pairs of closely spaced measurements offset 6in. The purpose of taking couples was to provide checks for all data points. The coupled measurements were compared for consistency. If the thickness calculated for the couples differed by more than 0.25in. or 6.35mm, the couple was rejected and the data was not used. If the measurements were within 0.25in, the couples were averaged, and only the average was used in further analysis. The average was assigned a location halfway between the couples in one of the five locations outlined by FHWA (see ase the collection of MIRA data (Appendix A).

Table 5)

3.6 Spatial Relation of MIRA and Distress Data

After preprocessing and averaging couples, MIRA and distress data were spatially related within MATLAB. Spatial relation was performed by reading in the MIRA and distress data and associating data which fell with a specified proximity. As the MIRA data was taken at set intervals, and distress data was randomly distributed, it was determined that MIRA locations would serve as base points and distress would be assigned to MIRA measurements. Specifically, a distress measurement occurring within +/- 5ft of a MIRA location was assigned to that MIRA data point. If a distress was recorded at exactly 5ft from a MIRA location; that is, exactly between two measurements, it was at risk of being assigned to both or neither adjacent traverses. To avoid this, it was determined that a distress would only be associated with a MIRA measurement if the difference in longitude location d was $-5 > d \geq 5$. This prevents double assignment and failure to assign. This processing produced several outputs for distress, MIRA data, and spatial combinations of the two.

4. RESULTS

Basic descriptive statistics were also computed for MIRA and distress datasets. The average, standard deviation, various percentiles, maximum, and minimum values were determined for thickness and velocity. Basic longitudinal and traverse statistics were also calculated for MIRA data, including max change within a transverse transect, as well as maximum changes between transverse transects. Basic distress statistics calculated included total number of transverse transects affected and percent transverses affected

4.1 Basic Thickness Statistics

The basic thickness statistics were calculated for the surveys taken on HWY 60E, HWY 60W, HWY 100, and I 394. The results are given in Table 9.

Table 9: Basic Thickness Statistics

	HWY 60E	HWY 60W	HWY 100	I 394
Design Thickness	203 (8)	203 (8)	229 (9)	254 (10)
Average Thickness	196 (7.7)	200 (7.9)	220 (8.7)	258 (10.2)
Deviation from Design	-7 (-0.3)	-3 (-0.1)	-9 (-0.3)	4 (0.2)
Standard Deviation	10.0 (0.4)	10.9 (0.4)	10.9 (0.4)	10.2 (0.4)
Coefficient of Variation	0.051	0.054	0.049	0.039
25th Percentile	188 (7.4)	192 (7.6)	212 (8.3)	253 (10)
50th Percentile	195 (7.7)	199 (7.8)	220 (8.7)	259 (10.2)
75th Percentile	203 (8)	207 (8.1)	227 (8.9)	265 (10.4)
Maximum Thickness	225 (8.9)	234 (9.2)	250 (9.8)	287 (11.3)
Minimum Thickness	164 (6.5)	170 (6.7)	200 (7.9)	216 (8.5)
Thickness Range	61 (2.4)	64 (2.5)	50 (2.0)	71 (2.8)
Maximum Trans. Difference	32.6 (1.3)	35.1 (1.4)	43.5 (1.7)	30.4 (1.2)
Maximum Long. Difference	35.1 (1.4)	43.7 (1.7)	50.0 (2)	39.0 (1.5)

Table 9 presents the basic thickness statistics for the surveys performed. The main entry is mm and the entry within the () is inches. Maximum Trans. Difference is the maximum difference between

measurements within a single transverse transect and is proxy for transverse thickness gradient. Maximum Long. Difference is the maximum difference between measurements in two adjacent transverse transects and is a proxy for longitudinal thickness gradient.

The basic thickness statistics presented in Table 9 show that the pavement thickness was highly variable over the survey area. The greatest thickness variability occurred in HWY 100 and HWY 60W, which had a standard deviation of 10.9 [in]. The least variable thickness occurred in HWY 60E, which had a standard deviation of 10.0 [in]. The coefficient of variation, a metric which standardized the variability of datasets based on the mean value, suggests that HWY 60W is most variable and I 394 is the least variable. The largest range in thickness recorded was 2.8 [in] and occurred within I 394. The smallest range in thickness recorded was 2.0 [in] and was recorded within HWY 60E. The variability seen in these datasets is similar to the variability seen by Vancura in HWY1, but greater than the variability seen in HWY2 and HWY3 (Vancura, 2013). The mean and median are similar for all datasets, suggesting that thickness is approximately normally distributed for all the highways.

For the surveys performed, average thickness was less than the design thickness, contradicting the results reported by previous studies (Vancura, 2013, Selezneva, Jiang, and Mladenovic, 2002). For the surveys performed in this study, three of the four highways were deficient in thickness. The greatest deficiency occurred in HWY 100, where the average thickness reported from the survey was 8.7in, 0.3in less than the design thickness of 9in. Only I 394, with an average thickness of 10.2 in. and a design thickness of 10 in. met or exceeded the design thickness.

4.2 Basic Velocity Statistics

The basic velocity statistics were calculated for the surveys taken on HWY 60E, HWY 60W, HWY 100, and I 394. The results are given in Table 10. All velocity statistics are report in [m/ms].

Table 10: Basic Velocity Statistics

All values in [m/ms]	**HWY 60E**	**HWY 60W**	**HWY 100**	**I 394**
Average Velocity	2.58	2.55	2.65	2.74
Standard Deviation	0.119	0.099	0.106	0.122
Coefficient of Variation	0.046	0.039	0.040	0.045
25th Percentile	2.48	2.49	2.57	2.73
50th Percentile	2.53	2.53	2.66	2.76
75th Percentile	2.71	2.57	2.74	2.79
Maximum Velocity	2.84	2.88	2.91	2.91
Minimum Velocity	2.35	2.3	2.34	2.1
Velocity Range	0.49	0.58	0.57	0.81
Maximum Trans. Difference	0.226	0.200	0.298	0.673
Maximum Long. Difference	0.230	0.444	0.440	0.685

The basic velocity statistics presented in Table 10 show that pavement velocity varied between surveys but fell within the range expected for PCC pavements (Freeseman, Hoegh, and Khazanovich 2016). The highest velocity of 2.74 [m/ms] was reported on I 394 while the lowest velocity of 2.55 [m/ms] was reported on HWY 60W. The greatest velocity variability, as measured by the standard deviation, occurred in I 394 which had a standard deviation of 0.122 [m/ms]. The least variable thickness, as measured by the standard deviation, occurred in HWY 60W, which had a standard deviation of 0.99 [m/ms]. The coefficient of variation, a metric which standardized the variability of datasets based on the mean value, suggests that HWY 60E has the most variable velocity and HWY 60W has the least variable. The largest range in velocity recorded was 0.81 [m/ms] and occurred within I 394. The smallest range in velocity recorded was 0.49 [m/ms] and was recorded within HWY 60E. The mean and median values are similar, suggesting velocity is normally distributed

4.3 Basic Distress Statistics

Visual distress surveys were performed in conjunction with all MIRA surveys. Basic statistics of distress occurrence rate are presented in Table 11.

Table 11: Basic Distress Statistics

`	HWY 60E		HWY 60W		HWY 100		I 394	
Distress Type	# Trans. Affected	% Trans. Affected	# Trans. Affected	% Trans. Affected	# Trans. Affected	% Trans. Affected	# Trans. Affected	% Trans. Affected
Transverse Joint spalling	40	20.00%	30	10.00%	22	14.38%	32	16.00%
longitudinal joint spalling	25	12.50%	14	4.67%	50	32.68%	27	13.50%
faulted joint	0	0.00%	1	0.33%	0	0.00%	1	0.50%
faulted crack	0	0.00%	1	0.33%	0	0.00%	0	0.00%
cracked or broken panel	57	28.50%	95	31.67%	13	8.50%	7	3.50%
overlaid or patched panel	11	5.50%	16	5.33%	4	2.61%	29	14.50%
durability cracking	0	0.00%	0	0.00%	0	0.00%	0	0.00%
all/any distress	90	45.00%	135	45.00%	77	50.33%	89	44.50%

The visual distress surveys conducted produced many similarities and differences in the distress profiles in the datasets. All roadways surveyed continued at least 15% spalling and all surveys exhibited distress on about 50% of the transverses. Cracked and broken panels made up a large portion of the distress for HWY 60E and HWY 60W, but were only minor distresses in HWY 100 and I 394. Faulted joints, faulted cracks, and durability cracking were very rarely reported in any survey and will not be considered in further analysis. All roadways have an average overall distress rate of around 45%. The individual distress profiles of the roadways are discussed below.

The distress surveys conducted on HWY 60E and 60W revealed high rates of cracking. As a Joint Reinforced Concrete Pavement (JRCP), midpanel cracking is expected to occur (Huang,1994). It is crucial to verify that the recorded distress was not midpanel cracking, as this is a design feature of JRCP and does not indicate pavement distress. As-designed JRCP midpanel cracks are characterized by tightness. If the crack widens, it can be considered a distress. Post survey verification of the cracking as true distress cracking was done by looking at images taken of the roadway surface. The results of this investigation show that the cracking is not midpanel cracking

and is in fact distress cracking. An image of the cracking is presented in Figure 28. Thus, the cracked and broken panels recorded in the HWY 60 surveys will be considered in further analysis.

Figure 28: Cracking seen on HWY 60

HWY 60E

The distress survey taken over HWY 60E shows that cracked and broken panels and longitudinal and transverse spalling are the dominant distress. Approximately 22% of traverses exhibited transverse or longitudinal joint spalling and 28.5% of traverses exhibited cracked or broken panels. A total of 45% of traverses within the survey contained at least one distress type. Zero instances of faulted joints, faulted cracks, or durability cracking were reported within HWY 60E.

HWY 60W

Similar to HWY 60E, the distress survey taken over HWY 60W shows that cracked and broken panels and longitudinal and traverse spalling are the dominant distress. 15% of traverses exhibited either transverse or longitudinal joint spalling and 32% of traverses exhibited cracked or broken

panels. As with HWY 60E, a total of 45% of traverses within the survey contained at least one distress type. Zero instances of durability cracking were reported within HWY 60W, however one instance each of faulted joint and faulted cracked were reported.

HWY 100

The dominant distress types recorded during survey of HWY 100 were longitudinal and transverse joint spalling. 14% of traverses exhibited transverse joint spalling and 33% exhibited longitudinal joint spalling. In contrast to HWY 60E and HWY 60W, cracked and broken panels were a minor distress type and occurred in only 8.5% of traverses. At 50%, HWY 100 had a slightly higher overall distress rate than HWY 60E or HWY 60W.

I 394

The dominant distress types recorded during the survey of I 394 were longitudinal and transverse spalling. 16% of transverses exhibited transverse joint spalling and 13.5% exhibited longitudinal joint spalling. Overlaid and patched panels were a minor distress type and occurred in 14.5% of traverses. I 394 had the lowest incidence of cracked and broken panels at only 3.5%. At 44.5%, the total distress data of I 394 was consistent with HWY 60E and HWY 60W.

4.4 Visual Output of Spatially Related MIRA and Distress Data

In addition to the tabular outputs, visual representation of the spatially related MIRA data and distress was also desired. Specifically, a visual representation of the spatial variability of thickness and velocity was desired. These figures would show the longitudinal and traverse variability, as well as the type and possibly the severity of the distress as well. These figures would provide an initial, pre-statistical foundation, to explore relationships. Both two and three dimensional figures were explored. Three different figures were created to explore MIRA data variation and distress. Examples and description of the figures are presented below.

4.4.1 3D Surface Figure

First, a three dimensional surface plot was explored. This figure allowed visual analysis of the spatial aspects of the thickness and velocity variation. An example of the plot and discussion are presented below.

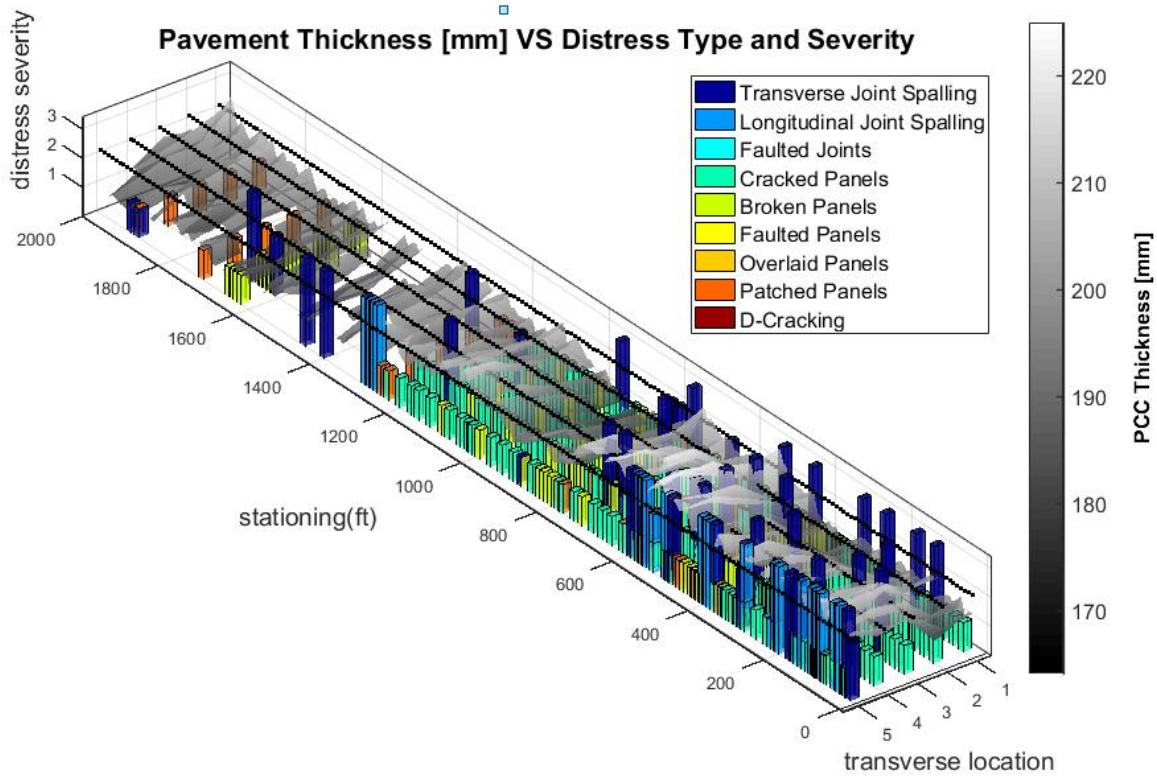

Figure 29: 3D Surface Plot

Figure 29 presents the surface plot representation of the MIRA data variability and distress. The x-axis labeled “transverse location” denotes the location of the couple measurements as defined by the FHWA. Location 1 through 5 refer to the following locations respectively: right of right wheel path, right wheel path, center of the wheel path, left wheel path, and left of left wheel path. For a typical 12ft wide truck lane (right most), these locations correspond the following approximate distance from the fog line on the right shoulder: 11.4ft, 9.5ft, 6ft, 2.5ft, and 0.6ft. The y-axis corresponds to the length of survey completed. The grey contoured surface depicts either thickness or velocity (See figure title). Blank spots in the contoured surface denote a couple error. The thickness or velocity magnitude can be inferred from the grey scale color bar on the right side of the figure. The colored bars mark locations where distress was recorded in the field survey. The

color of the bar denotes the distress type recorded (Figure 29 (see legend)), while the height of the bar denotes the severity. The severity levels of 1-3 can be interpreted from the z-axis tick levels. The small black dots depict the locations of the individual couples. For velocity data, the elevation of the black dots depicts the average velocity of the survey. For thickness data, the elevation of the black bots depicts the design thickness.

4.4.2 2D Contour Plot

A simpler 2-D contour plot was developed. An example and discussion of this plot is presented below.

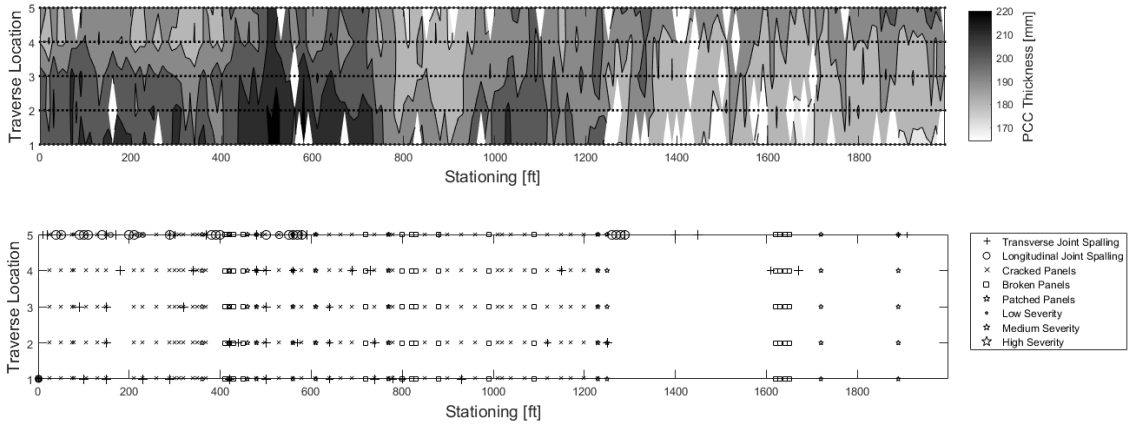

Figure 30: 2D Contour Plot

An alternate surface plot is presented in Figure 30. Figure 29 is confusing for surveys with highly variable MIRA data and high rate of distress. Therefore, Figure 30 was developed in an attempt to simplify the data presentation. As can be seen in Figure 30, two separate plots are used to display MIRA and distress data rather than overlaying the data. The top plot presents a contour of MIRA data (thickness or velocity). Lighter colors denote low values of MIRA data as well as couple errors while darker colors denote higher values. The x-axis labeled “Transverse Location” denotes the location of the couple measurements as defined by the FHWA. Location 1 through 5 refer to the following locations respectively: right of right wheel path, right wheel path, center of the wheel path, left wheel path, and left of left wheel path. For a typical 12ft wide truck lane (right most), these locations correspond the following approximate distance from the fog line on the right shoulder: 11.4ft, 9.5ft, 6ft, 2.5ft, and 0.6ft. The y-axis corresponds to the length of survey

completed. Distress data is presented in the lower figure. In the interest of potential black and white publication, unique symbols were used to represent individual distress types and symbol size was used to represent distress severity.

4.4.3 2D Line Plot

Finally, a simple line plot was created in order to simultaneously compare thickness, velocity and distress. An example and discussion of the plot are presented below.

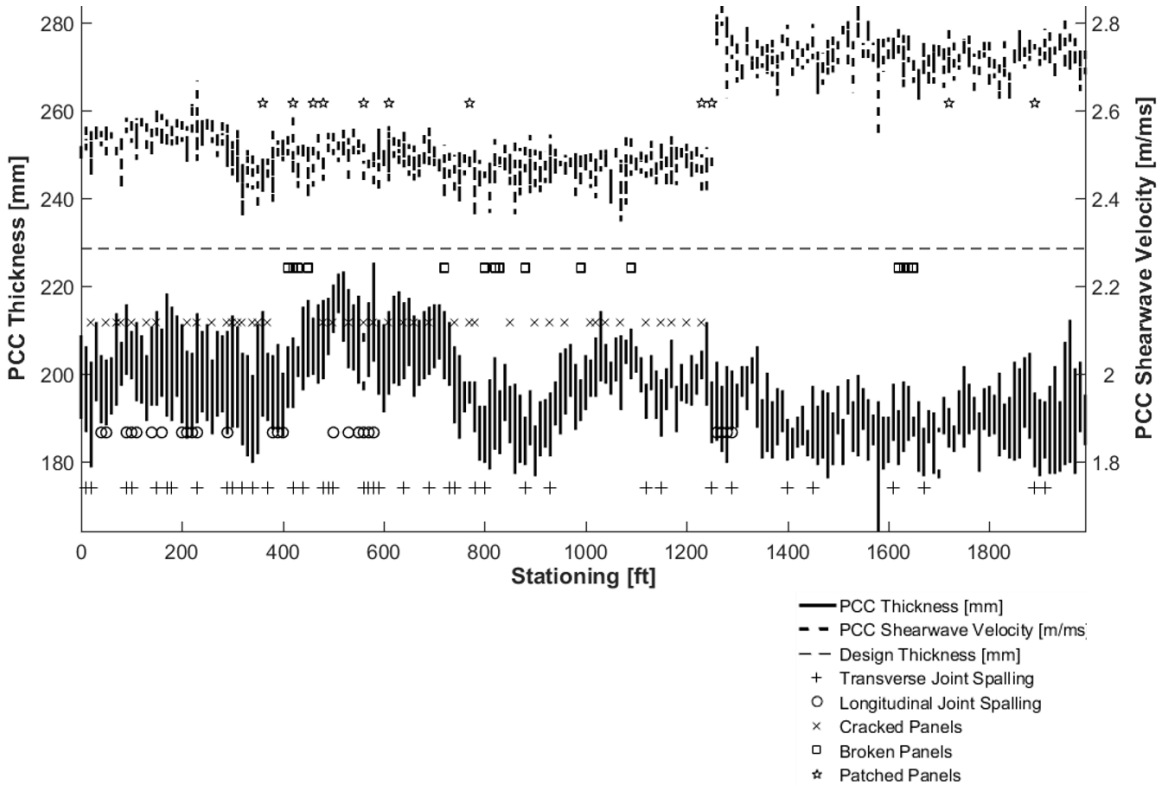

Figure 31: 2D line plot

In addition to the contour and surface plots above, a figure capable of displaying both thickness and velocity was also desired. Figure 31 was created for this purpose. This figure displays both thickness and velocity along the traverse. The x-axis denotes the length of the survey. The solid line denotes thickness while the broken lines denotes velocity. Each vertical thickness and velocity line corresponds to the measurements along a single transverse transect. The x-axis position of the vertical thickness and velocity lines corresponds the transverse stationing of the transverse transect.

The vertical limits of each individual line correspond to the maximum and minimum MIRA data values recorded within the transverse transect. The value of thickness and velocity measurements is presented on the y-axis. The straight dashed black line is the design thickness for the section. The symbol markers denote locations where distress was recorded during the field survey. The distress type can be referenced from the key in the upper right corner. The varying elevations of the markers is not significant; it was merely implemented to avoid stacking and make the plot easier to read.

5. ANALYSIS

The analysis of MIRA and distress collected on Minnesota HWY 60, HWY 100 and I 394 will now be presented. The analysis will focus on both visual and statistical results.

5.1 MIRA and Distress Analysis: Highway 60E

The analysis of MIRA and distress data collected on HWY 60E will be analyzed. The spatial relationship between PCC thickness, shear wave velocity and observed distress will be explored.

5.1.1 Highway 60E Analysis: Thickness

The survey conducted over HWY 60E suggests several interesting trends and relationships between thickness, velocity and observed distress. The overall data quality of the Highway 60E survey was quite good. There are few couple errors, which gave a very complete map of both thickness and velocity. The figures created for the data for Highway 60E show several interesting trends.

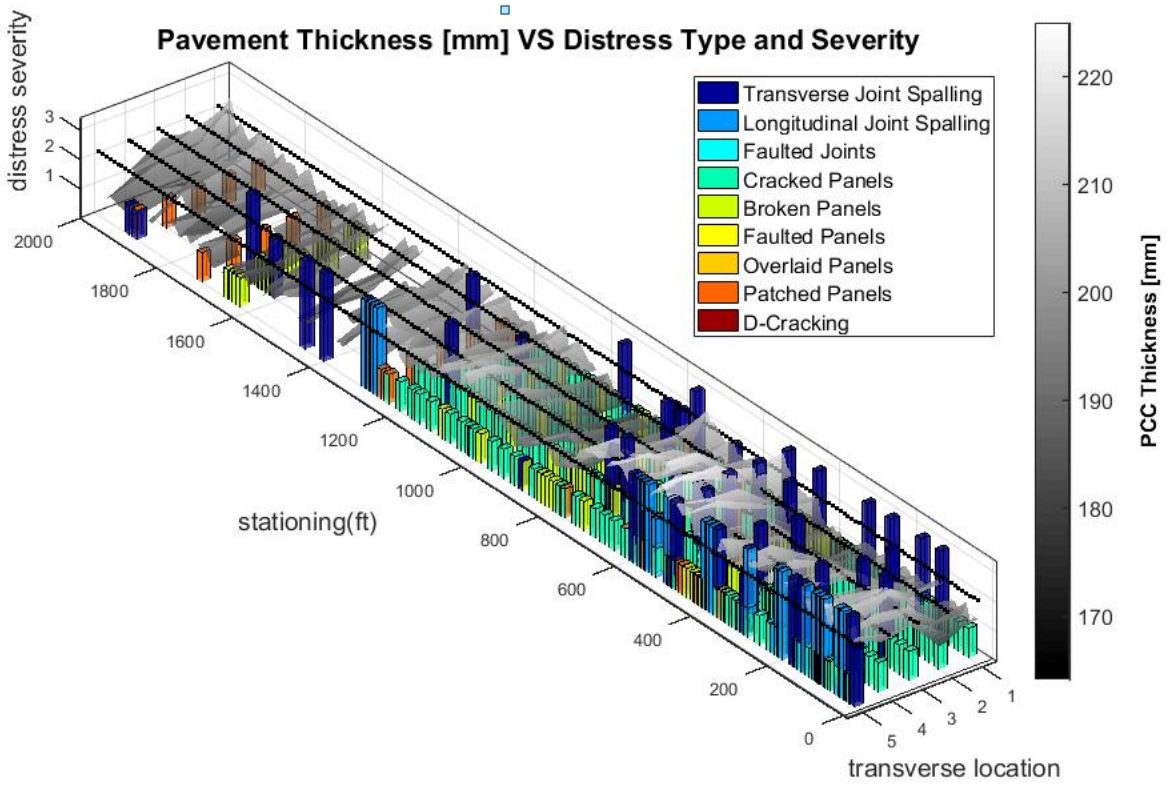

Figure 32: HWY 60E Thickness Surface Plot

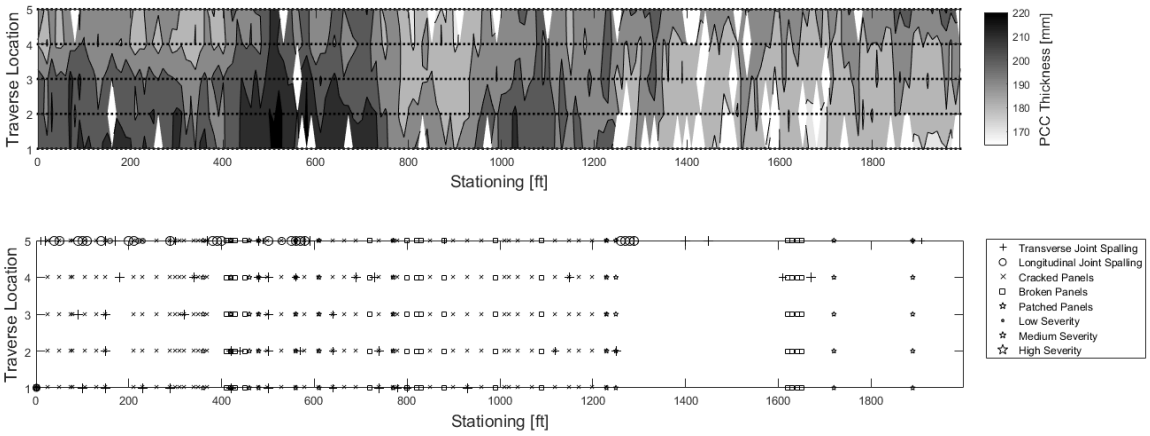

Figure 33: HWY 60E Thickness Contour Plot

Thickness over the HWY 60E survey area varies greatly. The thickness data taken over HWY 60E was found to have an average of 195 [mm], a standard deviation of 10.26 [mm], and coefficient of variation of 0.0526. The average thickness is approximately 8 [mm] below the design thickness of 203.2 [mm] (8 in). The maximum thickness encountered during the survey was 225 [mm] and the minimum was 171.5 [mm].

Thickness on the Highway 60E survey can be roughly separated into two sections (Figure 32). Section 1, which occurs from 0 to approximately 1300ft appears to have a higher thickness than Section 2, which occurs from 1300ft to the end of the survey. Additionally, section 1 appears to have decreasing thickness left to right (negative slope) while section 2 has increasing thickness left to right (positive slope). The average thickness of section 1 was found to be 199 [mm] while the average thickness of section 2 was found to be 187.8 [mm].

Visual Inspection of the 2D and 3D graphs suggest some interesting trends between thickness variation and observed distress. First, converse to expectations, Section 1, which has a higher thickness, appears to have more distress. Though the increase in distress occurrence is most dramatic with and broken panels, it can be seen in other distresses as well. Interestingly, the unexpected result that increase in thickness correlations to an increase in distress was also reported (and rejected as a false correlation) by FHWA in their logistic analysis (Miller and Bellinger, 2002).

5.1.2 Highway 60E Analysis: Velocity

Similar to thickness, velocity over the HWY 60E survey area varies greatly. The figures created for the velocity data for Highway 60E show several interesting trends.

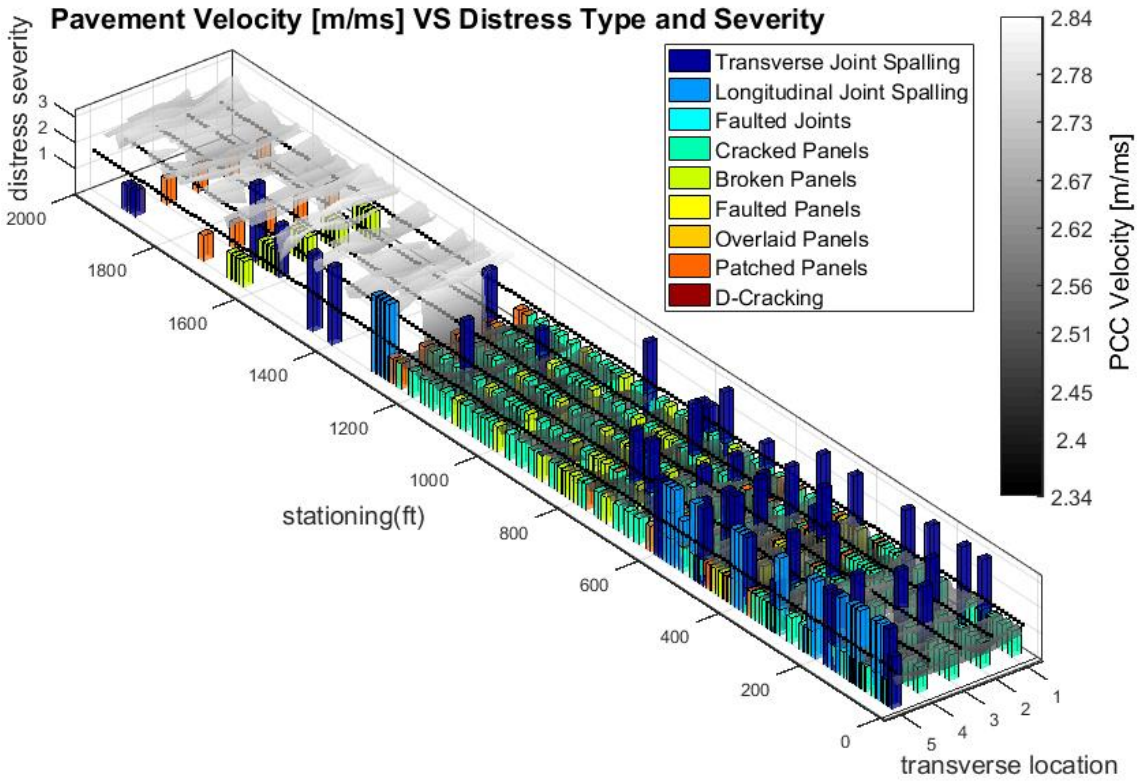

Figure 34: HWY 60E Velocity Surface Plot

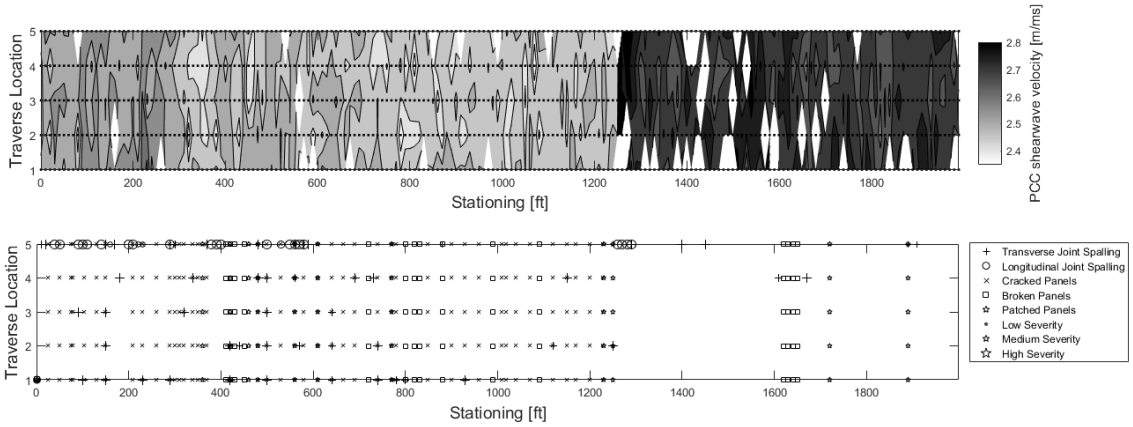

Figure 35: HWY 60E Velocity Contour Plot

The velocity data taken over HWY 60E was found to have an average of 2.58 [m/ms], a standard deviation of 0.120 [m/ms], and coefficient of variation of 0.0463. It is interesting to note that the coefficient of variation for thickness and velocity (0.0526 and 0.0463 respectively) are quite similar. The maximum velocity encountered during the survey was 2.48 [m/ms] and the minimum was 2.35 [m/ms]. The velocity standard deviation of HWY 60E was the highest standard deviation of velocity encountered in any survey.

Similar to thickness, velocity on the Highway 60E survey can be separated into two sections. This separation occurs in the same location as the thickness separation, but is much more well-defined. Section 1, which occurs from 0ft to approximately 1300ft has a lower velocity than Section 2, which occurs from 1300ft to the end of the survey. The average velocity of section 1 is 2.50 [m/ms] while the average velocity of section 2 is 2.73 [m/ms]. In the velocity dataset, it can clearly be seen that a decrease in velocity corresponds to a dramatic increase in distress. This increase can more clearly be seen in the occurrence of cracked and broken panels, but also appears to occur for spalling.

The observed relationship between velocity and distress is compelling. However, a statistical determination of significance is still needed. Additionally, an investigation of design and construction data will be required to determine additional factors which may contribute to the sudden change in observed distress.

5.1.3 Highway 60E Analysis: Combined Velocity and Thickness VS Distress

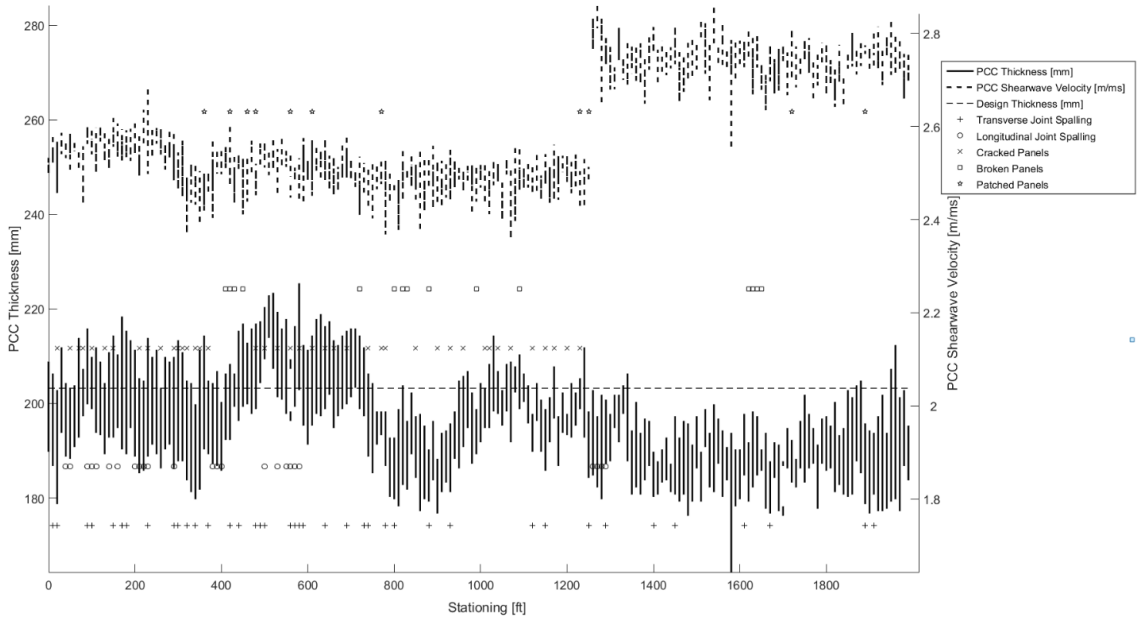

Figure 36: HWY 60E Combined Thickness and Velocity VS Distress

Figure 36 shows the combined velocity and thickness VS observed distress plot for HWY 60E This plots reveals the discrete velocity sections suggested in Figure 34 and Figure 35. Figure 36 gives more insight to thickness variation than Figure 32 and Figure 33. From Figure 36, it can be seen that the thickness within section 1 (0ft to 1300ft) is not only higher on average than the thickness sin section 2, but also more variable. This visual analysis suggests that, though average pavement thickness does not appear to correlate with distress, pavement thickness variability may. Visual comparison of pavement thickness and velocity does not suggest any relationship between the two parameters.

5.2 MIRA and Distress Analysis: Highway 60W

The analysis of MIRA and distress data collected on HWY 60W will be analyzed. The spatial relationship between PCC thickness, shear wave velocity and observed distress will be explored.

5.2.1 Highway 60W Analysis: Thickness

The survey conducted over HWY 60W suggests interesting relationships between thickness, velocity and observed distress. The overall data quality of the Highway 60W survey was quite good. There are few couple errors, which gave a very complete map of both thickness and velocity. The figures created for the data for Highway 60W show several interesting trends.

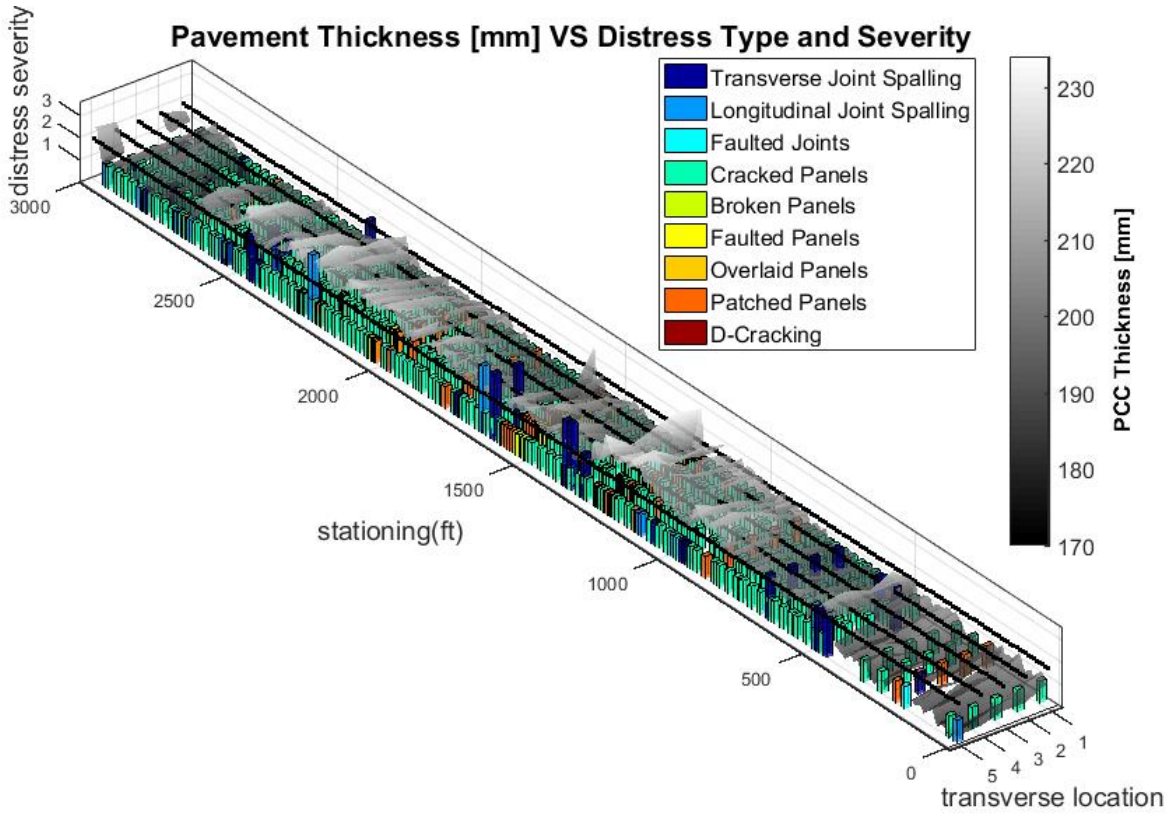

Figure 37: HWY 60W Thickness Surface Plot

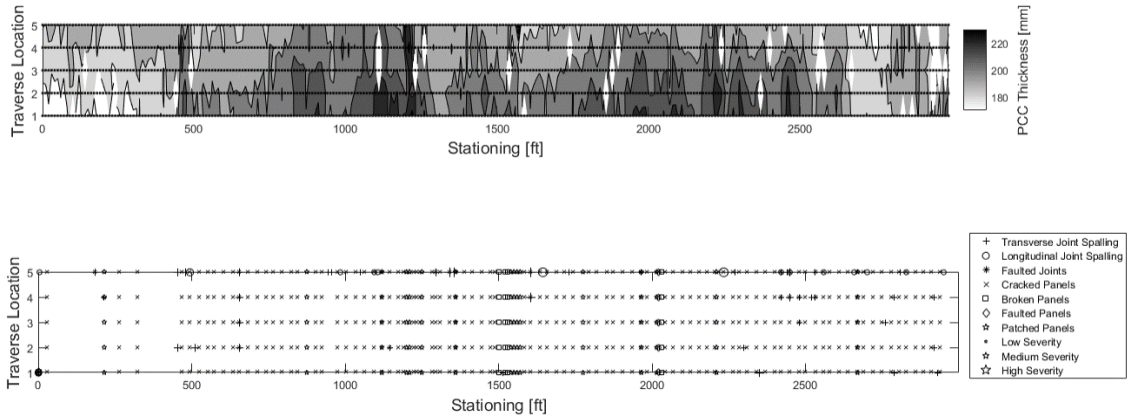

Figure 38: HWY 60W Thickness Contour Plot

Similar to HWY 60E, the distress survey taken over HWY60W shows that low severity cracked and broken panels and longitudinal and traverse spalling are the dominant distress. 15% of traverses exhibited either transverse or longitudinal joint spalling and 32% of traverses exhibited cracked or broken panels. As with HWY60E, a total of 45% of traverses within the survey contained at least one distress type.

The thickness data taken over HWY 60W was found to have an average of 199 [mm], a standard deviation of 11.00[mm], and coefficient of variation of 0.055. The average thickness is approximately 4 [mm] below the design thickness of 203.2 [mm] (8 in). The maximum thickness encountered during the survey was 234 [mm] and the minimum was 169 [mm]. The magnitude of the largest change in thickness within a traverse was found to be 35 [mm]. The magnitude of the largest change in thickness between traverses was found to be 41 [mm]. These statistics are quite similar to those determined for HWY 60E.

Similar to HWY 60E, thickness on the HWY 60W survey can be roughly separated into three sections. Section 1, which occurs from 0 to approximately 450ft appears to have a lower thickness and a more negative slope than preceding data. Section two appears from 450ft to 2600ft and has higher thickness and more positive slope. Finally, section three appears from 2600ft to the end of survey and has a decreased thickness and no apparent slope. Section one was found to have an average thickness of 185.7 [mm], section 2 was found to have an average thickness of 203 [mm], and section 3 was found to have an average thickness of 192 [mm].

Visual Inspection of the 2D and 3D graphs suggest some interesting trends between thickness and observed distress for HWY60W. As with HWY 60E, it appears that the thickest section (section 2) appears to have most distress.

5.2.2 Highway 60W Analysis: Velocity

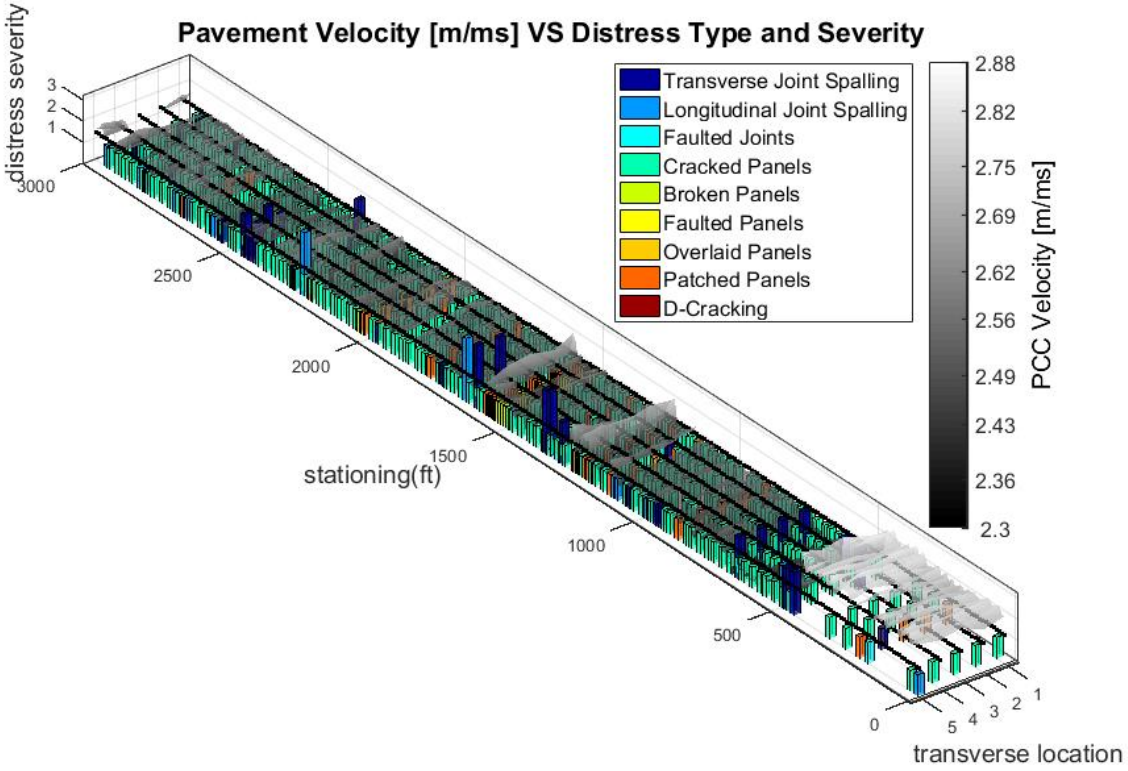

Figure 39: HWY 60W Velocity Surface Plot

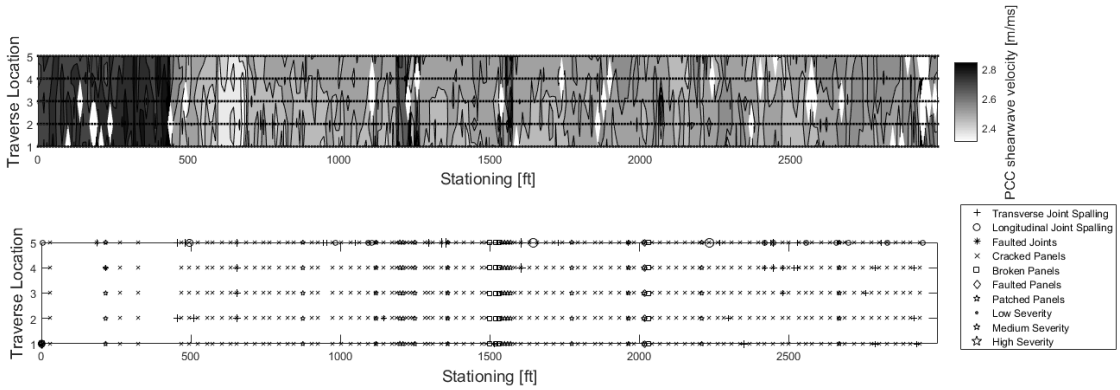

Figure 40: HWY 60W Velocity Contour Plot

The velocity data taken over HWY 60W was found to have an average of 2.55 [m/ms], a standard deviation of 0.100 [m/ms], and coefficient of variation of 0.0392. As with HWY 60E, the coefficient of variation for thickness and velocity (0.055 and 0.0392 respectively) are quite similar. The maximum velocity encountered during the survey was 2.88 [m/ms] and the minimum was 2.30 [m/ms]. The magnitude of the largest change in velocity within a traverse was found to be 0.20 [m/ms]. The magnitude of the largest change in velocity between traverses was found to be 0.44 [m/ms].

Velocity on the Highway 60W survey can be separated into two sections. It is interesting to note that while thickness section 1 and 2 determined in visual inspection of Figure 37 and Figure 38 are apparent in the velocity data, section 3 is not. Section 1, which occurs from 0 to approximately 450ft has a much higher velocity than section 2, which occurs from 450ft to the end of the survey. Section one was found to have an average velocity of 2.75 [m/ms] section 2 was found to have an average velocity of 2.52 [m/ms].

The inverse relationship between distress and velocity is same that was observed in the HWY 60E. Though compelling, a statistical determination of significance is still needed and an investigation of design and construction data will be required to determine additional factors which may contribute to the sudden change in observed distress.

5.2.3 Highway 60W Analysis: Combined Velocity and Thickness VS Distress

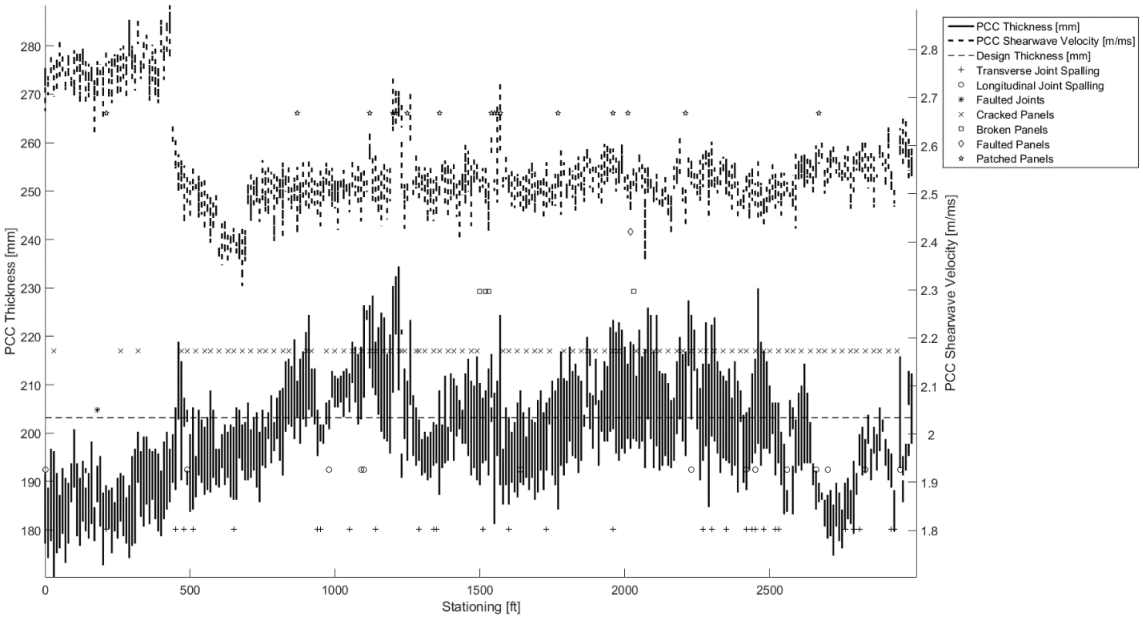

Figure 41: HWY 60W Combined Thickness and Velocity VS Distress

Figure 41 shows the combined velocity and thickness VS observed distress plot for HWY 60W This plots reveals the discrete velocity sections suggested in Figure 39 and Figure 40. The three distinct thickness sections suggested in Figure 37 and Figure 38 are not as apparent in Figure 41. However, the velocity sections suggested in Figure 39 and Figure 40 can clearly be seen. The sudden increase in distress occurrence associated with the decrease in velocity seen around 500ft can clearly been seen in Figure 41. Visual comparison of pavement thickness and velocity does not suggest any relationship between the two parameters.

5.3 MIRA and Distress Analysis: Highway 100

The analysis of MIRA and distress data collected on HWY 100 will be analyzed. The spatial relationship between PCC thickness, shear wave velocity and observed distress will be explored.

5.3.1 Highway 100 Analysis: Thickness

The data taken for HWY 100 is less intriguing than that taken for HWY 60E and HWY 60W. The data quality of the data is poor. The high rate of couple errors makes the distress and velocity surfaces highly discontinuous.

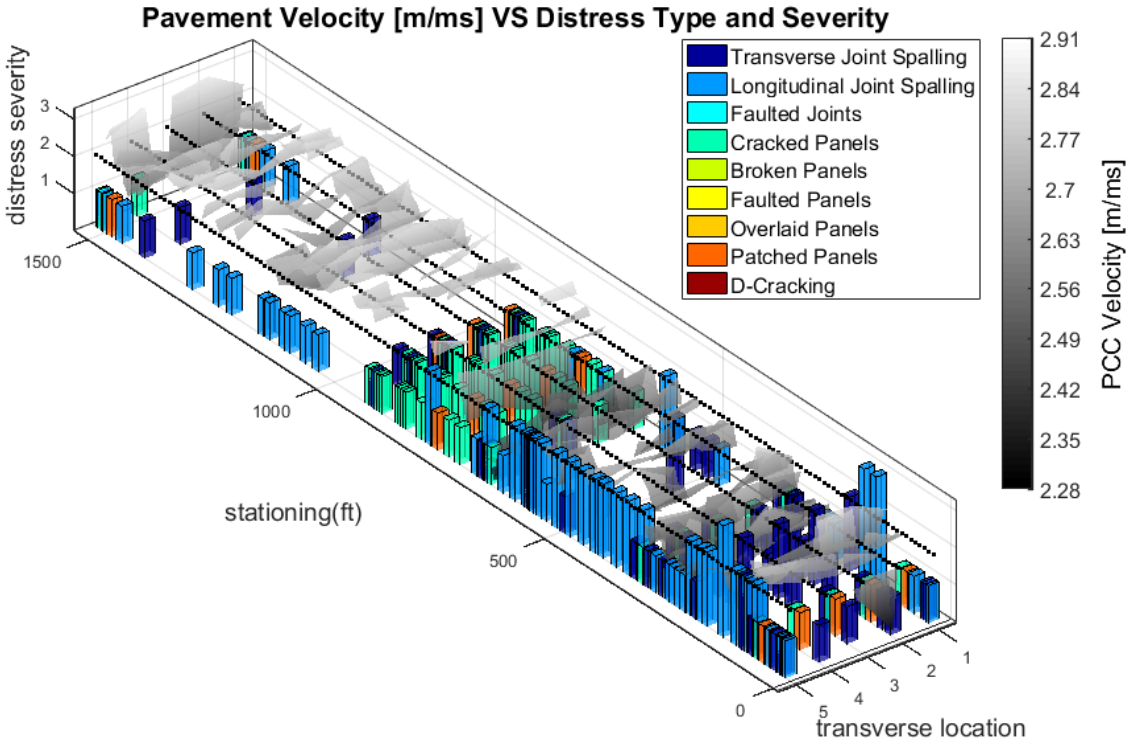

Figure 42: HWY 100 Thickness Surface Plot

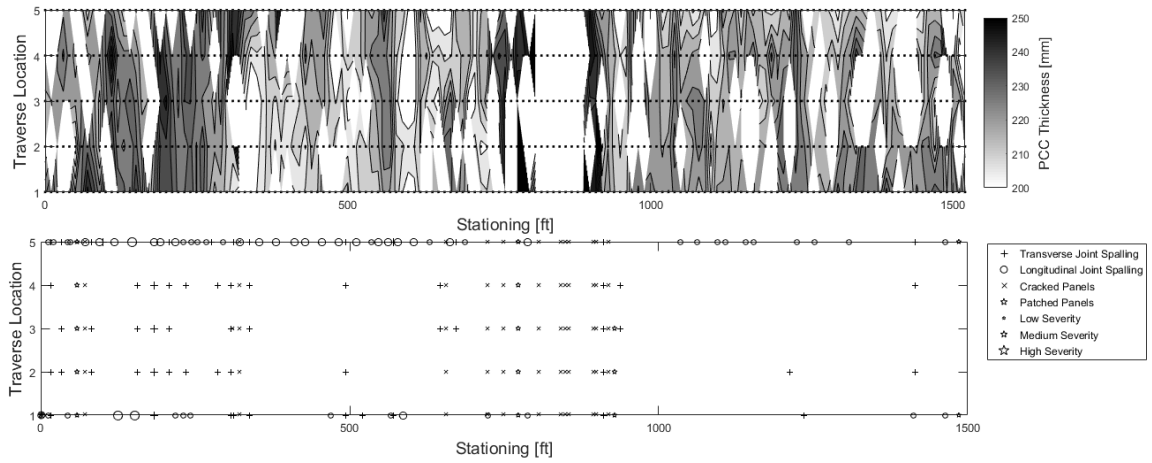

Figure 43: HWY 100 Thickness Contour Plot

The dominant distress types recorded during survey of HWY 100 was spalling. 14% of traverses exhibited transverse joint spalling and 33% exhibited longitudinal joint spalling. Cracked and broken panels were a minor distress type and occurred in only 8.5% of traverses. At 50%, HWY 100 had a slightly higher overall distress rate than HWY 60E or HWY 60W.

The thickness data taken over HWY 100 was found to have an average of 222 [mm], a standard deviation of 19.5[mm], and coefficient of variation of 0.088. The average thickness is approximately 6.5 [mm] below the design thickness of 228.6 [mm] (9 in). The maximum thickness encountered during the survey was 349 [mm]. This measurement was taken at approximately 800ft and corresponds to the large spike in on the contour image (Figure 42 and Figure 43). This would correspond to thickness of nearly 14in, and is likely an error due to the erratic data quality. The minimum thickness was 150 [mm] and was taken immediately after the spike. Like the maximum value, this is likely an error. The values reported for the largest change in thickness within a traverse and the largest change in thickness between traverses were found to be 97.5 [mm] and 162 [mm] respectively. Like the max and min thickness, these were determined from data near the 800ft and likely errors.

Thickness data on HWY 100 cannot be separated into obvious sections as it was on HWY 60E and HWY 60W. For this survey, the 2D figure is more useful in looking for trends, as the 3D figure is scaled to accommodate the erroneous thickness measurements. The only definitive feature seen in

the data is region of erratic thickness which occurs near 800ft. Unlike HWY 60E and HWY 60W, there is no clear visual relationship between thickness variation and observed distress. It appears that the cracked panels are centered near the 800ft region where the erratic thickness variation is observed.

5.3.2 Highway 100 Analysis: Velocity

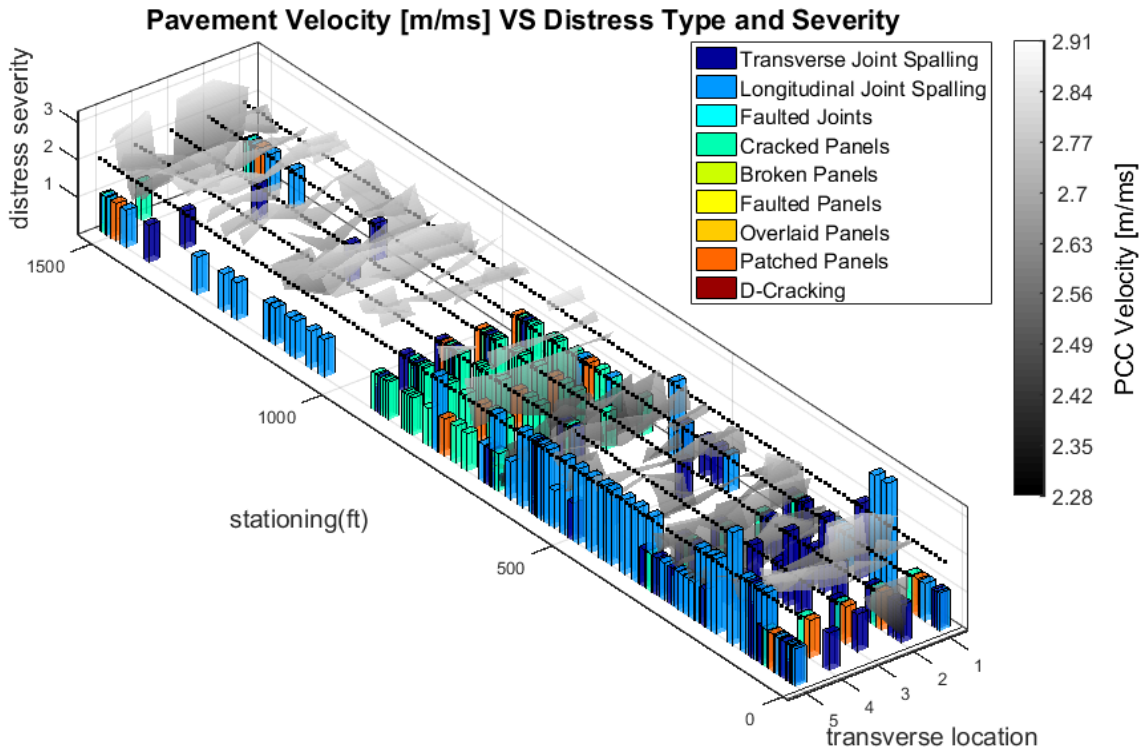

Figure 44: HWY 100 Velocity Surface Plot

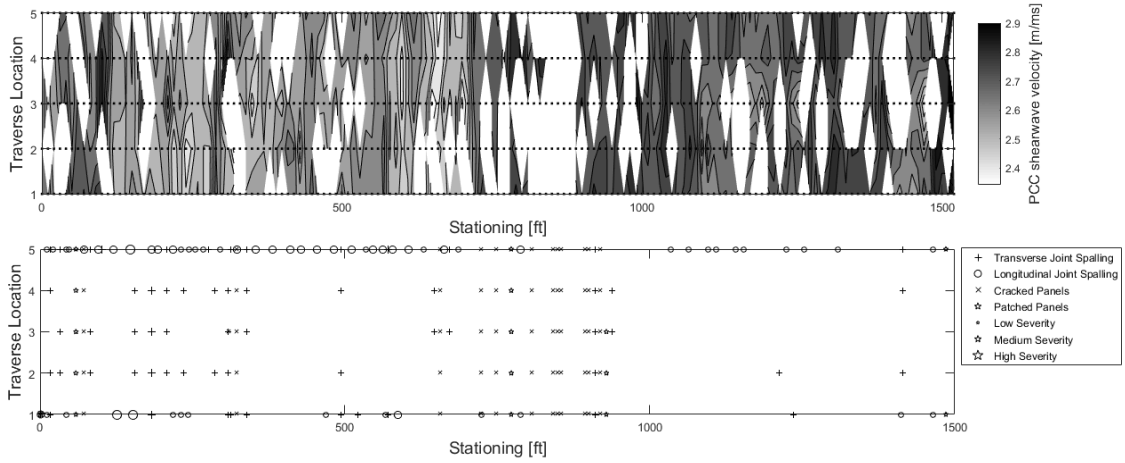

Figure 45: HWY 100 Velocity Contour Plot

The velocity data taken over HWY 100 was found to have an average of 2.65 [m/ms], a standard deviation of 0.10[m/ms], and coefficient of variation of 0.0392. The maximum velocity encountered during the survey was 2.92 [m/ms]. The minimum thickness was 2.34 [m/ms]. The magnitude of the largest change in velocity within a traverse was found to be 0.298 [m/ms]. The magnitude of the largest change in velocity between traverses was found to be 0.44 [m/ms].

Unlike thickness data, there appears to be separate sections of velocity data. Though the separation in sections is not as strong as it was in HWY 60E and HWY 60W, there appears to a region of low velocity from 0 to 950ft (section 1) and a region of higher velocity from 950ft to the end of the survey (section 2) (Figure 44 and Figure 45). The average velocity of section 1 is 2.62 [m/ms] while the average velocity of section 2 is 2.72 [m/ms]. In the velocity dataset, there appears to be an inverse relationship between velocity and distress. This relationship seems to be consistent across all distress types. Even more than strong relationship seen in the HWY 60E and HWY 60W velocity datasets, this less visually apparent dataset demands statistical analysis.

5.3.3 Highway 100 Analysis: Velocity and Thickness VS Distress

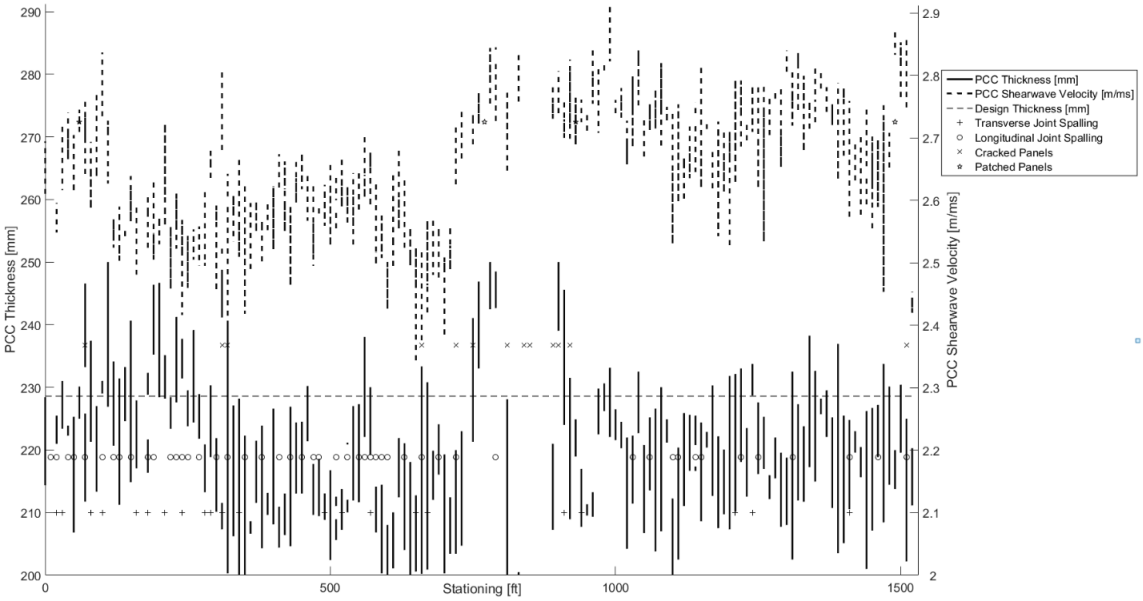

Figure 46: HWY 100 Combined Thickness and Velocity VS Distress

Figure 46 shows the combined velocity and thickness VS observed distress plot for HWY 100. This plot also suggests the velocity sections observed in (Figure 44 and Figure 45) as well as a possible increase in distress occurrence with decreased velocity. Visual comparison of pavement thickness and velocity does not suggest any relationship between the two parameters.

5.4 MIRA and Distress Analysis: Interstate 394

The analysis of MIRA and distress data collected on I 394 will be analyzed. The spatial relationship between PCC thickness, shear wave velocity and observed distress will be explored.

5.4.1 Interstate 394 Analysis: Thickness

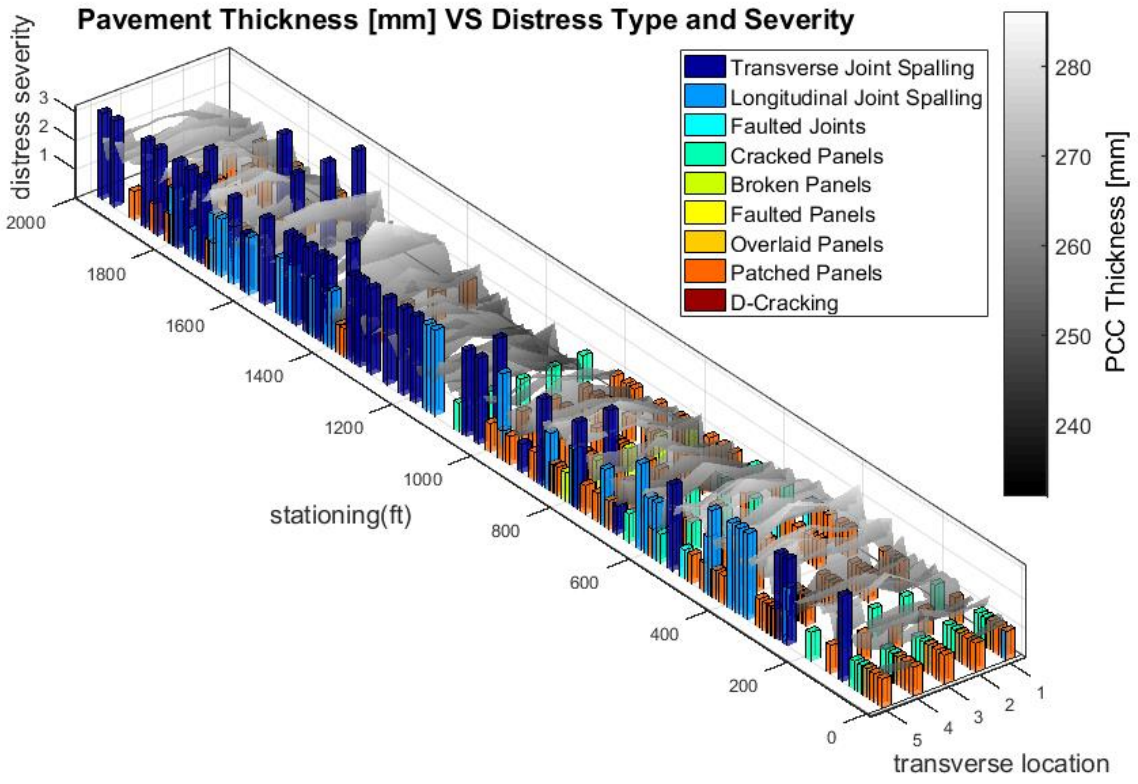

Figure 47: I-394 Thickness Surface Plot

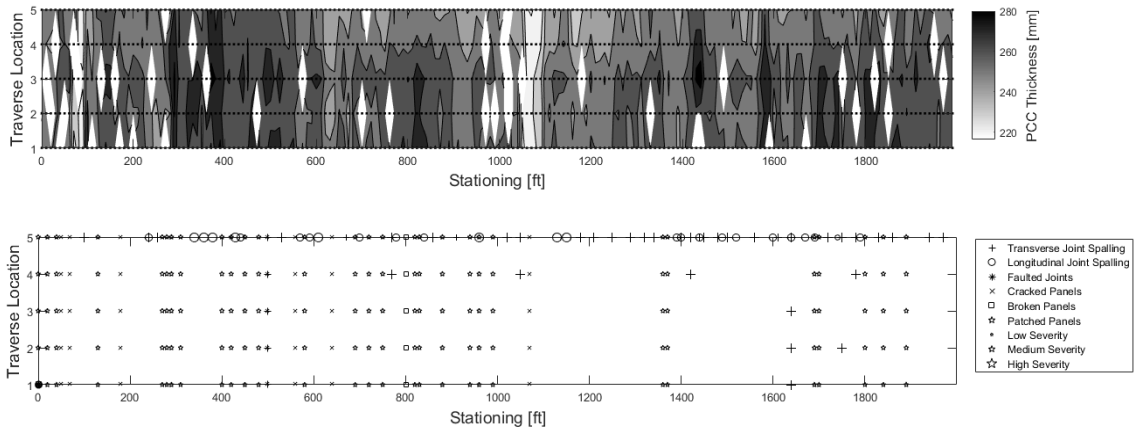

Figure 48: I 394 Thickness Contour Plot

The data taken for I 394 is of moderate quality. The dominant distress types recorded during survey of HWY 100 was spalling. 14% of traverses exhibited transverse joint spalling and 33% exhibited longitudinal joint spalling. Cracked and broken panels were a minor distress type and occurred in only 8.5% of traverses. At 50%, HWY 100 had a slightly higher overall distress rate than HWY 60E or HWY 60W.

The thickness data taken over I 394 was found to have an average of 259 [mm], a standard deviation of 11.9[mm], and coefficient of variation of 0.045. This is the lowest coefficient of variation encountered in any survey. The average thickness is approximately 5 [mm] above the design thickness of 254 [mm] (10 in). The maximum thickness encountered during the survey was 342 [mm] and the minimum was 154 [mm]. The magnitude of the largest change in thickness within a traverse was found to be 97.5[mm]. The magnitude of the largest change in thickness between traverses was found to be 152 [mm].

Similar to HWY 100, I 394 cannot be separated into obvious sections as it was on HWY 60E and HWY 60W. The only potential variation of interest which can be seen visually is the occasional erratic measurements seen from 800ft to 1450ft (Figure 47 and Figure 48). Outside of this region, I-394 appears to have the most consistent thickness of any dataset. This observation is supported by the fact that I 394 has the lowest coefficient of variation of any survey. The only visual relationship between thickness and distress is the seeming lack of distress in the erratic area from 800ft to 1450ft.

5.4.2 Interstate 394 Analysis: Velocity

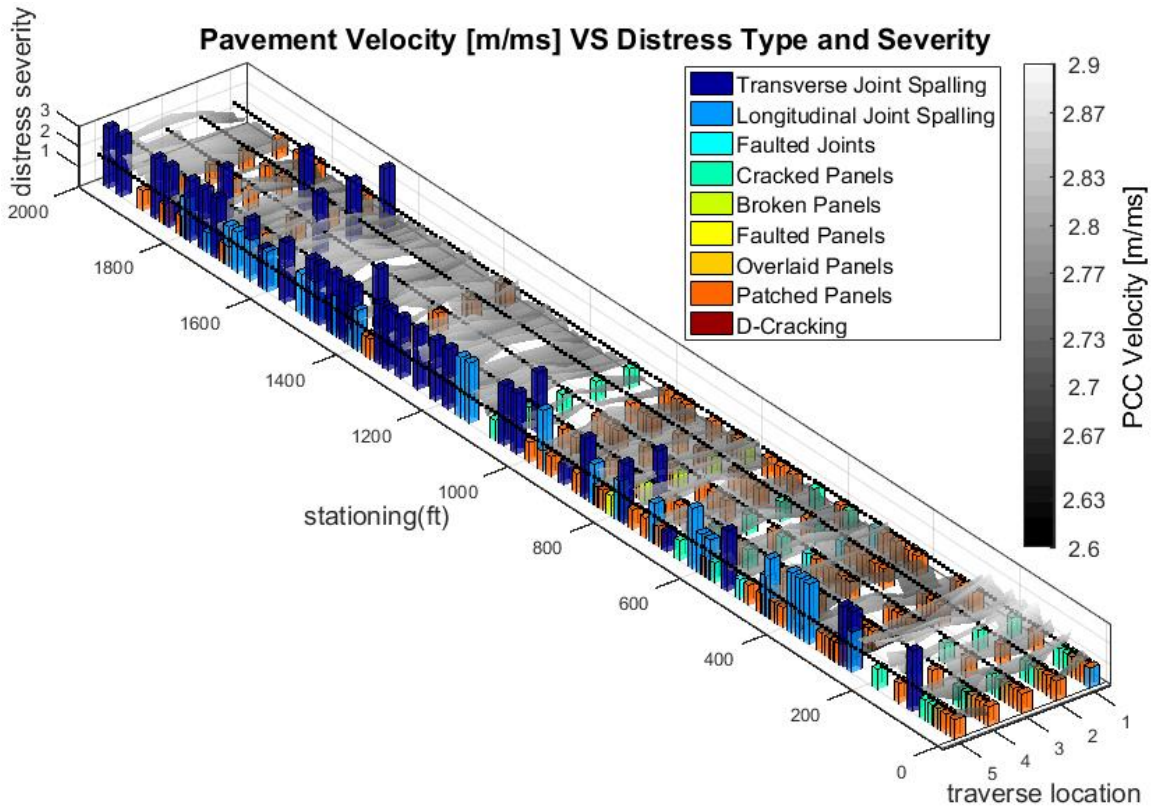

Figure 49: I-394 Velocity Surface Plot

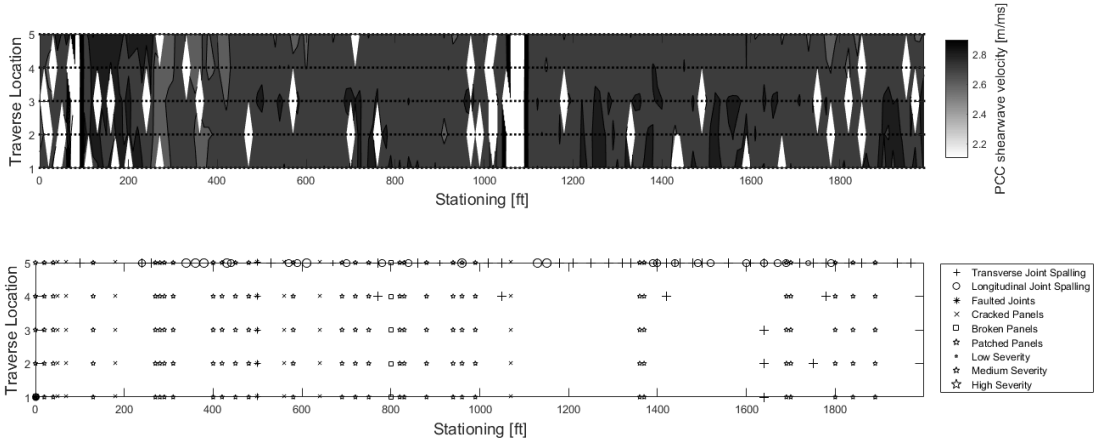

Figure 50: I-394 Velocity Contour Plot

The velocity data taken over I 394 was found to have an average of 2.75 [m/ms], a standard deviation of 0.043[m/ms], and coefficient of variation of 0.0156. This coefficient of variation was the smallest found for any velocity dataset, and the average velocity was the highest. The maximum velocity encountered during the survey was 2.91 [m/ms]. The minimum velocity was 2.52 [m/ms]. The magnitude of the largest change in velocity within a traverse was found to be 0.284 [m/ms]. The magnitude of the largest change in velocity between traverses was found to be 0.295 [m/ms].

5.4.2 Interstate 394 Analysis: Combined Velocity and Thickness VS Distress

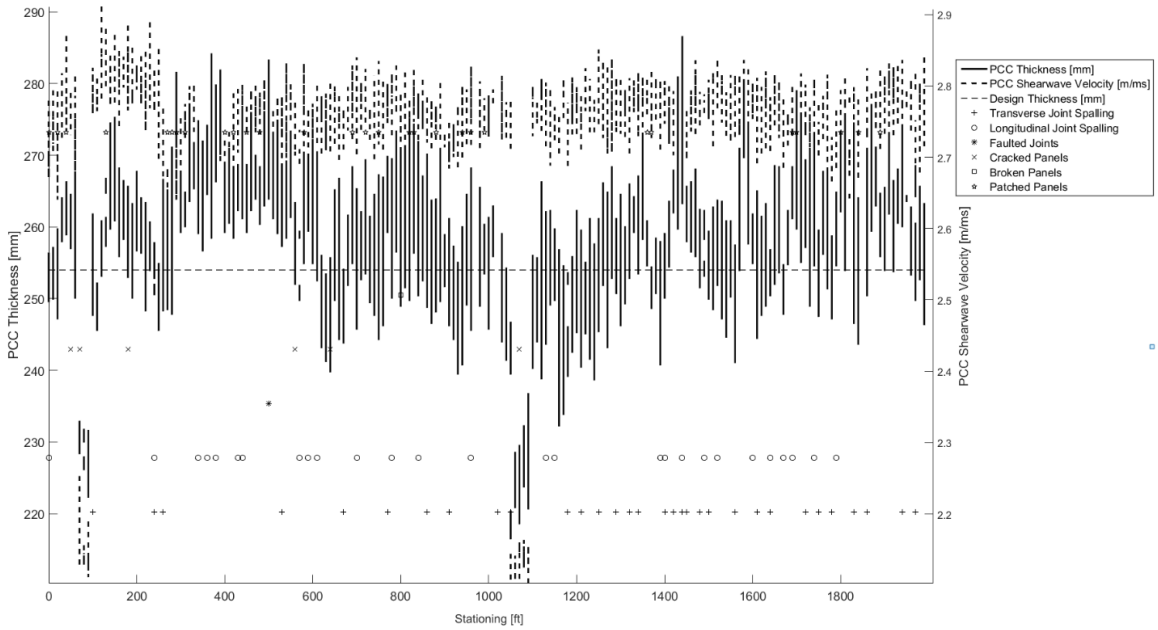

Figure 51: I 394 Combined Thickness and Velocity VS Distress

Figure 51 shows the combined velocity and thickness VS observed distress plot for I 394. This plot shows the extreme low values recorded for thickness and velocity suggested by other plots created for this survey. The extreme values are likely errors and do not reflect true pavement conditions. Visual comparison of pavement thickness and velocity does not suggest any relationship between the two parameters.

5.5 MIRA and Distress Analysis: Interstate 494

As discussed in section 4, the data quality of the surveys conducted on I 494 was very poor for both surveys conducted. Initial plotting and analysis of the data resulted in rejection of data from further analysis due to high rate of couple errors. An example data set is presented in Figure 52. Note the high rate of couple errors results in an incomplete surface plot.

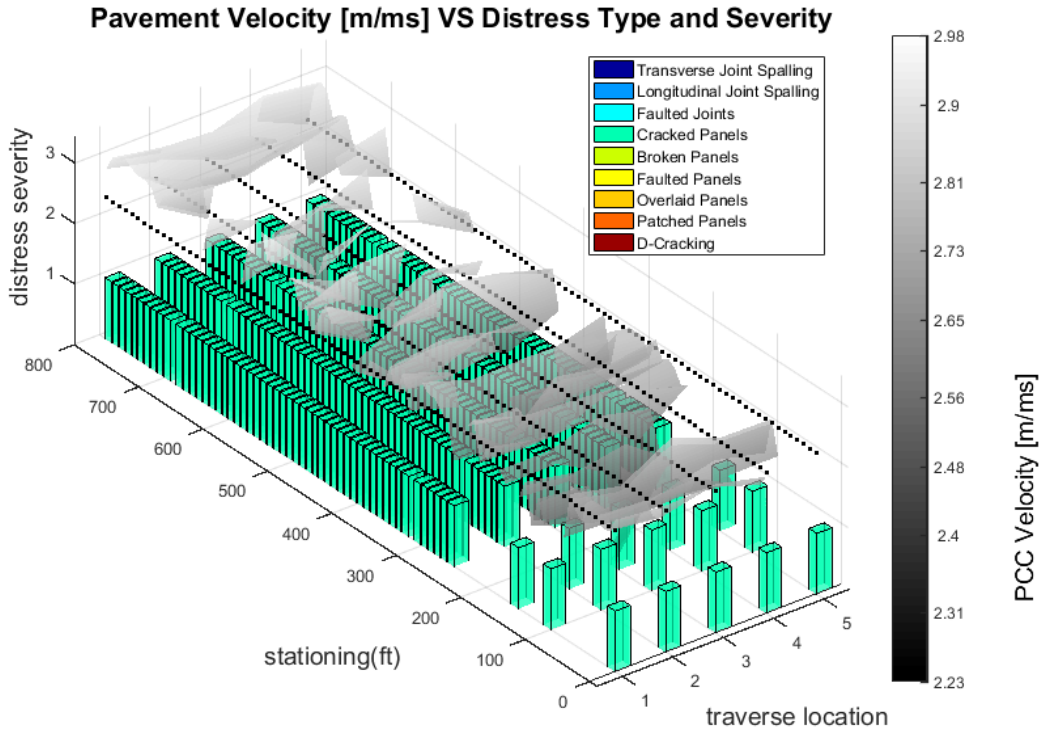

Figure 52: I 494a Example Surface Plot

5.6 Predictor Selection for Regression Analysis

In order to statistically test the relationship between PCC thickness and shear wave velocity variation and distress, predictors which described the surface variation were computed.

5.6.1 Introduction to Predictor Selection

In order to investigate the significance of thickness and velocity variation on observed distress several predictors were computed from the data collected. These predictors were designed to exhaustively test all feasible properties of thickness and velocity variation which could affect distress. As a main goal of the study was to investigate thickness and velocity variation, rather than just absolute thickness and velocity, a minimum spatial scale had to be selected to compute spatial changes in thickness and velocity. The individual transverse transects (Figure 23) were chosen as this base spatial unit over which variation would be computed. This was done for several reasons. First, previous work done by Vancura suggested that there was large variation in thickness in the transverse direction. Using individual transverse transects would allow this variation to be better quantified. Secondly, data was much denser in the transverse direction which allowed for more precise spatial relation of variation metrics and observed distress. Finally, denoting each transverse transect as a base unit would greatly simplify data processing and distress association.

The predictors investigated included average transverse thickness/velocity, transverse standard deviation, average transverse slope, average longitudinal slope, average absolute slope per transverse, absolute maximum slope per transverse, maximum absolute difference in thickness variation per transverse, max magnitude of critical point per transverse, sum of magnitudes of critical points per transverse, and average change in transverse slopes between adjacent traverses. Each one of these predictors resulted in one numeric value per traverse. Full description of the predictors is provided in section 5.6.2.

Once the predictors had been calculated for a dataset, it was necessary to spatially relate the predictors to neighboring distresses for statistical analysis. This was simply done by proximity. A transverse transect would be associated with distresses which occurred with +/- 5ft of the transect. For example, a transect taken at 100ft would be associated with any distress occurring from 95ft to 105ft. The actual association includes a less than or equal to on the upper end of the associated range to ensure that distress exactly 5ft from a transverse are assigned to only one transverse. The

result of this association is a logical array denoting the existence or non-existence of the distresses type near a transverse. This logical array can then be paired with a corresponding predictor array and statistically analyzed for a relationship.

5.6.2 Predictor Definitions

Visual analysis and application of basic mechanistic principals resulted in the selection of 10 predictors. The chosen predictors are presented (Table 12) and discussed below. Predictors were calculated for both thickness and velocity, but only the Average Transverse Velocity (X_1) was analyzed for velocity data for reasons discussed in section 5.9.

Table 12: Predictor Variables

X_1	Average Transverse Value
X_2	Traverse Standard Deviation
X_3	Average Transverse slope
X_4	Absolute Transverse Slope
X_5	Absolute Max transverse Slope
X_6	Maximum Absolute Difference
X_7	Sum of Critical Points
X_8	Largest Critical Point
X_9	Average Change in Traverse Slope
X_{10}	Average Longitudinal Slope

1. Average transverse thickness

   The average thickness/velocity per traverse is the arithmetic mean of the transverse measurements, determined by Equation 1, as follows:

$$t_{ave,i} = \frac{\sum_{j=1}^{m} t_{i,j}}{m} \quad (1)$$

   Where $t_{ave,i}$ is the calculated average thickness/velocity for the *ith* transverse, *m* is the number of measurements per transverse (usually 5), and $t_{i,j}$ is the averaged couple thickness/velocity measurement.

2. Transverse Standard deviation

   The transverse standard deviation is the sample standard deviation of the transverse measurements, determined by Equation 2, as follows:

$$std_i = \sqrt{\frac{\sum_{j=1}^{m}(t_{i,j} - t_{ave,i})^2}{m-1}} \quad (2)$$

   Where std_i is the standard deviation of the *ith* transverse and *m* is the number of measurements within the transverse.

3. Average transverse slope

   The average transverse slope is the difference in thickness between the start and end of the transverse, determined by Equation 3, as follows:

$$s_i = \frac{(t_{i,1} - t_{i,5})}{L_t} \quad (3)$$

   Where S_i is the transverse slope, $t_{i,1}$ is the first measurements in the transverse *i*, $t_{i,5}$ is the last measurements in the transverse and L_t is the length of the transverse. Note that for a survey taken from right to left across the lane, a positive slope indicates decreasing thickness from right to left, while a

negative slope indicates increasing thickness from right to left. For the data collected in this survey, a negative slope is indicative a slab which thins toward the shoulder while a positive slope is indicative a slab which thickens toward the shoulder.

4. Absolute transverse slope

   To explore the significance of overall degree of slope along a transverse, and to eliminate the influence of slope direction, the absolute slope was calculated by Equation 4 and Equation 5, as follows:

$$s_{i,k} = \frac{(t_{i,j} - t_{i,j+1})}{L_c} \tag{4}$$

   Where $s_{i,k}$ is the traverse slope between adjacent couples and L_c is the distance between the couples. The overall degree of slope is then calculated (Equation 5) by summing the absolute values of the slopes between the individual couples within the transverse:

$$sAbs_{ave,i} = \frac{\sum_{i=1}^{k} abs(s_{i,k})}{m} \tag{5}$$

   Where, $sAbs_{ave,i}$ is the average slope of the transverse.

5. Absolute max transverse slope

   To explore the effect of the high degrees of slope, the absolute maximum slope per traverse was computed. This predictor returns the largest magnitude of slope, whether positive or negative while maintaining the sign of the slope. The predictor is determined by Equation 6.

$$st_{MAX,i} = \mathrm{MAX}\big(abs(s_{i,k})\big) \tag{6}$$

   Where $st_{MAX,i}$ is the absolute max traverse slope. The sign associated with the maximum absolute value is then reassigned to the highest magnitude slope found.

6. Maximum absolute difference in thickness

   The maximum absolute difference in thickness along a transverse was computed by comparing the maximum and minimum thickness within each transverse using Equation 7, as follows:

$$maxAbsDiff_i = \text{abs}\left(\text{MAX}(t_{i,j}) - MIN(t_{i,j})\right) \quad (7)$$

   Where $maxAbsDiff_i$ is the maximum absolute difference in thickness/velocity, $\text{MAX}(t_{i,j})$ is the maximum value along the traverse, and $MIN(t_{i,j})$ is the minimum value in the traverse.

   Changes from positive to negative slopes, referred to as critical points, were assumed to have potential to create stress concentrations. To investigate the effect of critical points, two predictors were calculated. The first was the sum of the slope changes of all the critical points within each traverse. The second was the slope change of the maximum critical point.
   The presence of a critical point was determined by comparing adjacent slopes (Equation 8). If the product of the slopes is negative, the sign of the slope has changed, and a critical point exists. A maximum of three critical points could occur along one traverse.

$$Logical_{cp}, i = if(s_{i,k} * s_{i,k+1}) < 0 = TRUE \quad (8)$$

   In locations where a critical point was found, the magnitude of the critical point was determined by comparing the change in slope by Equation 9, as follows:

$$CP_i = abs(s_{i,j}) + abs(s_{i+1,j}) \quad (9)$$

   Where CP is the magnitude of the critical point, $s_{i,j}$ is the transverse slope

7. Sum of critical points

To explore the cumulative effects of multiple critical points, the magnitude of all critical points occurring on a traverse were summed using Equation 10, as follows:

$$sumCrit_i = \sum_{i=1}^{l} CP_i \tag{10}$$

Where $sumCrit_i$ is the sum of all the critical points occurring within the transverse.

8. Largest critical point

The effect of the largest magnitude of critical point was also of interest. The maximum critical point was determined using Equation 11, as follows:

$$largestCrit_i = MAX(CP_i) \tag{11}$$

Where $largestCrit$ is the largest critical point within the transverse.

9. Average change in transverse slope

To explore the effects of the change in traverse slope between adjacent traverses, the average change in traverse slope was calculated by Equation 12, as follows:

$$aveChngTrvSlope_i = s_{ave,i} - s_{ave,i+1} \tag{12}$$

Where $aveChngTrvSlope_i$ is the difference in slope between adjacent transverse.

10. Average longitudinal slope

To explore the effects of the longitudinal slope, the absolute average longitudinal slope was calculated (Equation 13) by comparing the change in the average thickness of adjacent transverses.

$$aveLongSlope_i = abs\left(\frac{(t_{ave,i} - t_{ave,i+1})}{d_l}\right) \quad (13)$$

Where $aveLongSlope_i$ is the average longitudinal slope, $t_{ave,i}$ is the average thickness of the transverse, and d_l is the longitudinal distance between transverses.

5.7 Logistic Regression Analysis

In order to further explore the visual trends noted in the previous analysis, a more thorough statistical method was desired. Logistic regression was chosen for this purpose.

5.7.1 Introduction to the Logistic Model

Several interesting trends were noted in the visual analysis of the thickness and velocity VS distress plots created (see section 5.1 5o 5.4). To statistically quantify the significance of these observations, regression analysis was performed. Logistic regression was used to determine the correlation of predictors and distress. Logistic regression is useful in modeling the probability of a binary response, in this case the occurrence or non-occurrence of distress. An example of a logistic model is shown in Figure 53 (Wikipedia, 2016).

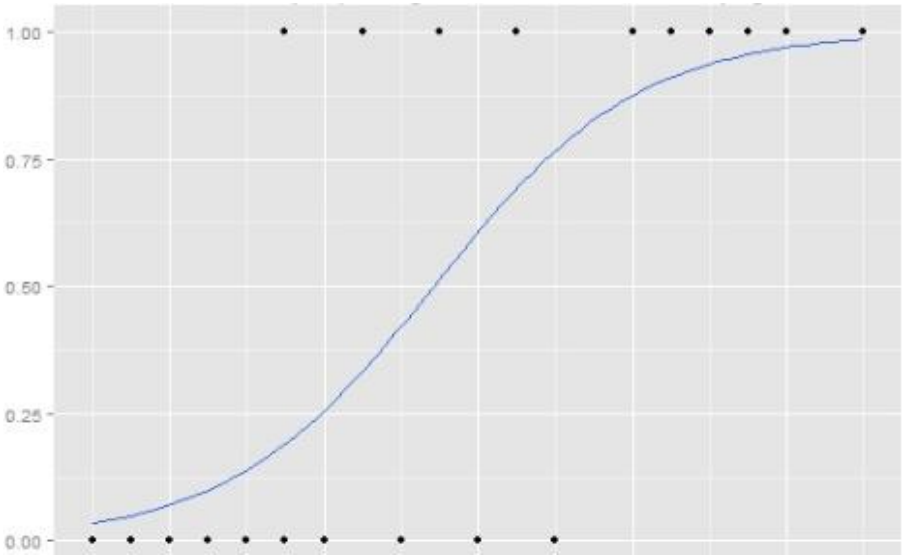

Figure 53: Example of Logistic Model

Unless otherwise noted, all implementation of the logistic regression model was taken from Hosmer, et al (2013). All analysis was performed in MATLAB. A logistic model was employed to test the significance of the proposed regressesors (Section 5.6). The logistic regression is a transform of the linear one regressor model. The linear one regressor model is given by Equation 14, as follows:

$$E(Y|x) = \pi(x) = \beta_0 + \beta_1 x \tag{14}$$

Where $E(Y|x) = \pi(x)$ is the expected value of Y given *x*, β_0 is the fit intercept term and β_1 is the fit value of the linear term.

The transformation applied for the logistic model is the logit, and is given by Equation 15 and 16, as follows:

$$logit(x) = \log\left[\frac{\pi(x)}{1 - \pi(x)}\right] = \beta_0 + \beta_1 x \tag{15}$$

Therefore, once the regression model is fit, the predicted probability can be solved for as follows:

$$\pi(x) = \frac{e^{\beta_0+\beta_1 x}}{1 + e^{\beta_0+\beta_1 x}} \tag{16}$$

The logit transformation (Equation 14) preserves many of the desirable properties of a linear regression model and the principals which guide linear regression analysis apply to logistic regression. The logit is linear in its parameters, may be continuous, and may range from –∞ to +∞. The logistic regression model is bounded by 0 and 1 and is therefore valid for estimating probabilities. Unlike the linear regression model, the errors associated with the logistic regression model are binomially rather than normally distributed.

5.7.2 Fitting the Logistic Model

The unknown parameters β_0 and β_1 of the logistic regression are estimated by maximizing the likelihood function. Maximizing the likelihood function yields the values of for the unknown parameters which maximize the probability of the binary observations as a function of the observed independent variable. The likelihood function is given by Equations 17 and 18, as follows:

$$l(\boldsymbol{\beta}) = \prod_{i=1}^{n} \pi(x_i)^{y_i}[1 - \pi(x_i)]^{1-y_i} \tag{17}$$

Where $l(\boldsymbol{\beta})$ is the liklihood given fit parameters $\boldsymbol{\beta}$, $\pi(x_i)$ is the *ith* predicted probability associated with the *ith* regressor, y_i is the *ith* response, and $\boldsymbol{\beta}$ is the fit regression terms given by equation 18, as follows:

$$\boldsymbol{\beta} = \beta_0 + \beta_1 \tag{18}$$

Mathematically, it is easier to use the log of the function, referred to as the log-likelihood function. To find the value of $\boldsymbol{\beta}$ that maximizes the likelihood function, the function is differentiated with respect to β_0 and β_1 and set equal to zero. The log likelihood is given by Equation 19, as follows:

$$L(\boldsymbol{\beta}) = log(l(\boldsymbol{\beta})) = \sum_{i=1}^{n} \{y_i \log\big(\pi(x_i)\big) + (y_i - 1)log\big(1 - \pi(x_i)\big)\} \tag{19}$$

5.7.3 Significance of the Model

The statistical significance of the relationship between the predictor and response is tested by evaluating the statistical significance of the $\boldsymbol{\beta}$ fit using the maximum likelihood function. This is performed with the likelihood ratio test. The likelihood ratio, or G statistic, is testing if the model which includes fit coefficients tells us more about the outcome variable than the model which does not include the fit coefficients, referred to as the "null model" (Figure 54). The simple one-predictor model used in this study, the null model is simply the average rate of response. The likelihood is determined by taking the log of the ratio of the likelihood of the model without the test parameter over the fit maximized likelihood of the model with the parameter. If this value is large, the fit model is much better than the model without the test parameter.

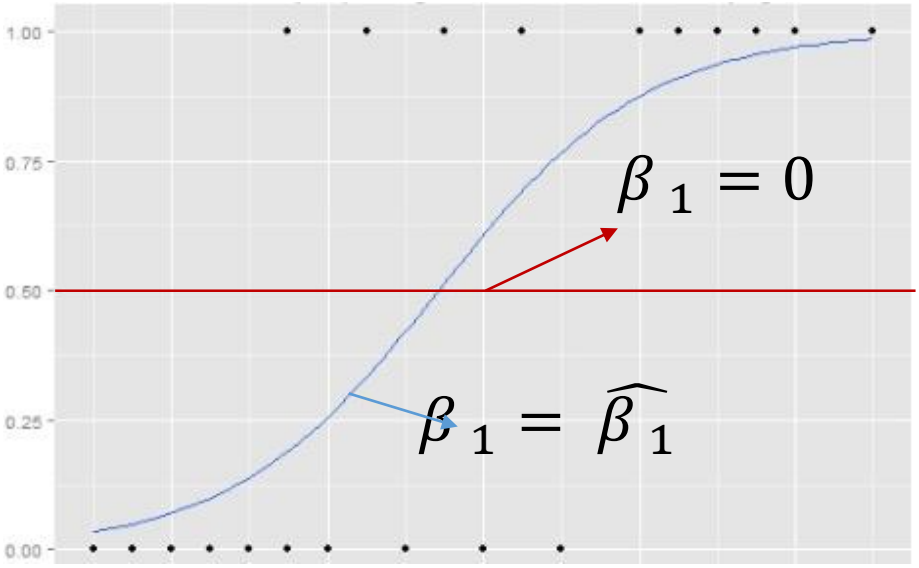

Figure 54: Fitted VS Null Model

The likelihood ratio, or G statistic is calculated to compare the models:

$$G = -2 * ln\left(\frac{likelihood\ without\ the\ variable}{likelihood\ with\ the\ variable}\right) = \quad (20)$$
$$2 * \{ln(likelihood\ with\ the\ variable) - \ln(likelihood\ without\ the\ variable)\}$$

For the simple one-predictor model used in this study, G statistic simplifies to:

$$G = -2 * ln\left[\frac{\left(\frac{n_1}{n}\right)^{n_1}\left(\frac{n_0}{n}\right)^{n_0}}{\prod_{i=1}^{n}\pi(x_i)^{y_i}[1-\pi(x_i)]^{1-y_i}}\right] \quad (21)$$

The results of this comparison can be used to formulate a hypothesis test. For the two parameter regression (β_0 and β_1) regression performed, *G* follows a chi-squared distribution with 1 degree of freedom.

To test the significance of β_1, Equations 19 and 20 are applied:

$$h_0: \hat{\beta}_1 = 0$$
$$h_1: \hat{\beta}_1 \neq 0$$

The results of the G statistic can be used to calculate a p-value as follows:

$$p - value = P(\chi^2(1)| > G) \quad (22)$$

$$\alpha = 0.05 \quad (23)$$

An $\alpha = 0.05$ denotes the probability of the rejecting the null hypothesis (that there is no correlation) when it is true. At $\alpha = 0.05$, there is only a 5% chance of claiming significant correlation when none exists.

5.8 False Positive Screening Methodology

The probability of rejecting the null hypothesis when it is true, that is of finding a significance when there is in fact none is referred to as a type I error. As hypothesis tests are designed to challenge accepted truths, a rejection is generally much more of a powerful statement than failure to reject. It is for this reason that probability of type I errors must be quantified. The probability of a Type I error is quantified by defining an alpha value below which the null hypothesis will be rejected. The p-value is calculated to determine acceptance or rejection. If an alpha value of 0.05 is chosen, a p value calculated below 0.05 gives 95% confidence that the rejection of the null hypothesis is valid. However, this means that there is 5% chance of false positive or type I error.

The probability of encountering a type 1 error when analyzing multiple datasets is a function of the alpha chosen as well as the number of regression performed. The total number of regression performed is a product of the number of predictors, the number of distress types, the number of datasets, and the investigation of both thickness and velocity. The number of regression performed is given by equation 23

$$\begin{aligned} n = number\ of\ Predictors * number\ of\ distresses * number\ of\ surveys \\ * thickness\ or\ velocty = 10 * 8 * 4 * 2 \\ = 640\ regressions \end{aligned} \quad (23)$$

The p-value is random variable drawn from the distribution of the hypothesis test. Therefore, the expected number of false positives from n regression can be calculated by equation 24.

$$\begin{aligned} E(x) = np = 640\ regression * 0.05 \\ = 32\ false\ postives\ expected \end{aligned} \quad (24)$$

Where *n* is the number of regression and *p* is the probability of a type I error.

Therefore, 32 false-positive significant correlations are expected from 640 regression using chosen $\alpha = 0.05$. To address the likely occurrence of type 1 errors, additional guidelines were determined to separate correlations of interest. First, for a correlation to be designated as significant, it should

occur across multiple surveys. It is not enough for a relationship to be significant in 1 dataset. Ideally, significance should be found in 3 or 4 of the datasets to suggest a true correlation. Additionally, the slope of the regression coefficients must be consistent. If all four surveys are found to significantly correlate with a predictor yet the two have positive correlation and two have negative correlation this is not a consistent result and will not be considered a true correlation. Finally, though $\alpha = 0.05$ will be used as cut off for investigation, p values less than 0.05 will be preferred. It is important to note that these criteria are only guidelines and the analysis procedure may deviate slightly from the process outlined above.

The steps listed above drastically reduce the probability of a type I error. Assuming that regression coefficients are random variables, the probability of a regression coefficient being positive is 0.5 as is the probability of the coefficient being negative. This probability is independent of the probability of a type I error. Additionally, the probability that a type I errors occurs across surveys for a specific predictor-distress combination is independent of the probability of a type 1 error. Therefore, the probability of all four surveys having the same regression coefficient sign and being found significant for a given predictor – distress combination is given by equation 25.

$$\begin{aligned}&\Pr(Type\ I\ error\ \cap same\ regression\ coefficient\ \cap occurs\ across\ all\ surveys)\\&\quad = (\alpha * 0.5)^{ns} = (0.05 * 0.5)^4\\&\quad = 3.91 * 10^{-7}\end{aligned} \tag{25}$$

Application of the single predictor-distress combination probability determined equation 24 to all predictor distress combinations produces an expected number of false positive occurrences well below 1. Additionally, if the p – values determined for the regressions are less than 0.05, the probability of a false positive is even more greatly reduced. Equation 26 and 27 give the expected number of false positives if three of four predictor-distress regression are fond to be consistent.

$$\begin{aligned}&E(x) = np = 160\ predictor - distress\ combinations * (0.05 * 0.5)^3\\&= 0.0025\ false\ positives\ expected\end{aligned} \tag{26}$$

$$\begin{aligned}&E(x) = np = 160\ predictor - distress\ combinations * (0.05 * 0.5)^4\\&= 0.0000625\ false\ positives\ expected\end{aligned} \tag{27}$$

Therefore, any result designated significant using the above methodology is indeed significant with a high degree of certainty.

5.9 Distress Correlation Analysis

As discussed above, an ideal significant correlation would be found between a predictor and distress for multiple surveys. Such an ideal correlation would suggest that the predictor can be correlated with a distress type in various pavement designs and trafficking environments. However, the inconsistency of distress profiles between datasets suggests that finding the same significant correlation across all four surveys is very unlikely for a particular distress type. To address this issue, only the correlation results of datasets with similar distress profiles will be compared. Additionally, correlations will be limited to distress types which were dominant (greater than 10% of total distress) in at least two surveys. This methodology will be applied in conjunction with the false positive screening methodology discussed above. Distress types which constitute at least 10% of the total distress in at least 2 surveys include traverse joint spalling, longitudinal joint spalling, cracked and broken panels, and all distress types.

Through regression models were calculated for all combinations of the distress and predictors for thickness and velocity, not all velocity predictors will be considered. This decision is based on the different physical basis of thickness and velocity variation. Many of the predictors developed were originally developed for thickness. Thickness variation is caused by construction practices and environmental factors which can be expected to have structural variation on a small scale. Therefore, parameters like slope and critical points are expected and may provide valuable information. However, velocity is a material property and its variation is related to mix design. Discussing critical points and slopes does not make mechanistic sense when applied to velocity variability. Therefore, only the average transverse velocity will be investigated.

5.9.1 Joint Spalling Correlations

Longitudinal and Transverse joint spalling usually result from excessive stress at the joint. The excess stress generally occurs when incompressible materials, such as aggregate, infiltrates into the joint and prevents expansion of the slab. This produces large compressive stress on the slab near the joint. Joint spalling can also be caused by insufficient concrete strength or poorly designed load transfer mechanisms between joints (Huang,1994). The spalling model within the MEPDG predicts spalling occurrence as a function of age, air content, sealant application, compressive strength, annual number of freeze thaw cycles, PCC slab thickness, and PCC water content ratio (AASHTO, 2008).

The structural causes of spalling discussed above suggest that PCC thickness should only play a minor role with greater impact caused by joint construction and concrete strength. However, the empirical curve fitting performed as part of the MEPDG analysis include the variable PCC thickness, suggesting that PCC thickness may be deterministic in the occurrence of joint spalling, however, much stronger influence was found between pavement age. Therefore, the MEPDG models suggest that there may be a weak correlation between joint spalling and thickness variation. The structural causes of spalling and the MEPDG model suggest spalling occurrence may be significantly correlated with shear wave velocity, as concrete strength is included in the spalling model (AASHTO, 2008). However, the design and construction of the joint is the primary factor in joint spalling, thus it is hypothesized that the correlation may be weak.

5.9.1.1 Joint Spalling VS Thickness Variation

The logistic regression analysis performed did not find any consistent significant correlation between longitudinal or transverse joint spalling and thickness variation. Though several correlations were found, especially within the HWY 60E datasets, the correlations differed in sign and were not found across multiple surveys. The lack of significance is in agreement with structural causes of spalling as well as the findings used to calibrate the MEPDG (AASHTO, 2008), all of which suggest that thickness should play very little if any role in the occurrence spalling. The full results of the regression analysis are presented in Appendix D.

5.9.1.2 Joint Spalling VS Shear Wave Velocity Variation

The structural causes of joint spalling and findings of the MEPDG calibration performed for spalling discussed above suggest that a deficiency in pavement strength (as correlated with shear wave velocity) will likely lead to increased occurrence of spalling (AASHTO, 2008). The velocity regression results for transverse joint spalling show a weak ($p<0.05$), but significant negative correlation with average shear wave velocity (Table 13). It can be seen that the slope matches for all four surveys. This negative correlation suggests that as velocity decreases, the occurrence of transverse joint spalling increases, a result consistent with the hypothesis stated above. Only I-394 does not show this correlation as significant.

Table 13: Transverse Spalling VS SW Velocity

	HWY 60E		HWY 60W		HWY 100		I 394	
	Coeff	Sig	Coeff	Sig	Coeff	Sig	Coeff	Sig
ave vel	-3.922	0.016	-4.716	0.047	-4.516	0.046	-5.305	0.420

Investigation of the regression models shows that fit significant models (Figure 55, Figure 56, Figure 57) agree that a decrease in shear wave velocity is correlated with an increase in probability of transverse joint spalling. The decrease in shear wave velocity correlates with approximately a 300% increase in the occurrence spalling, with spalling rates increasing from 5-10% to 20-30%. See appendix F for full results of the velocity regression analysis for transverse joint spalling.

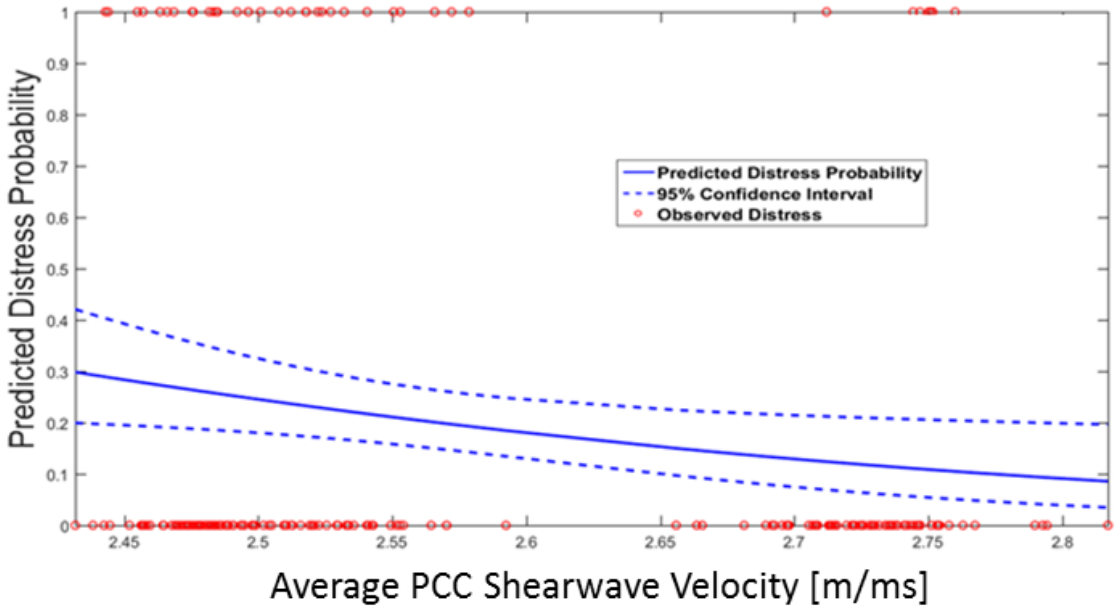

Figure 55: HWY 60E SWV versus Transverse Joint Spalling

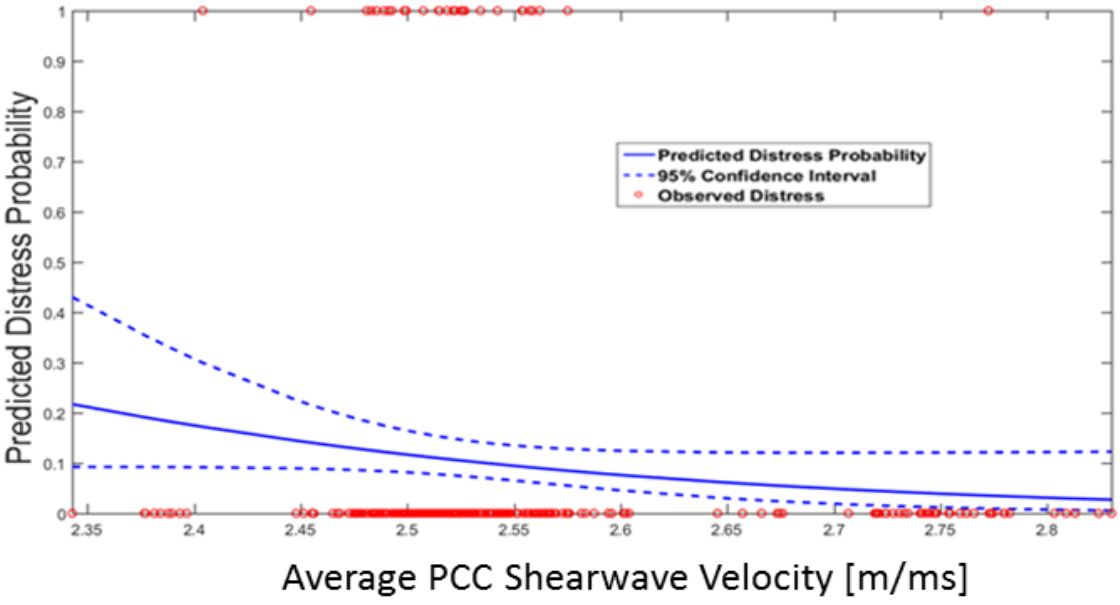

Figure 56:HWY 60W SWV versus Transverse Joint Spalling

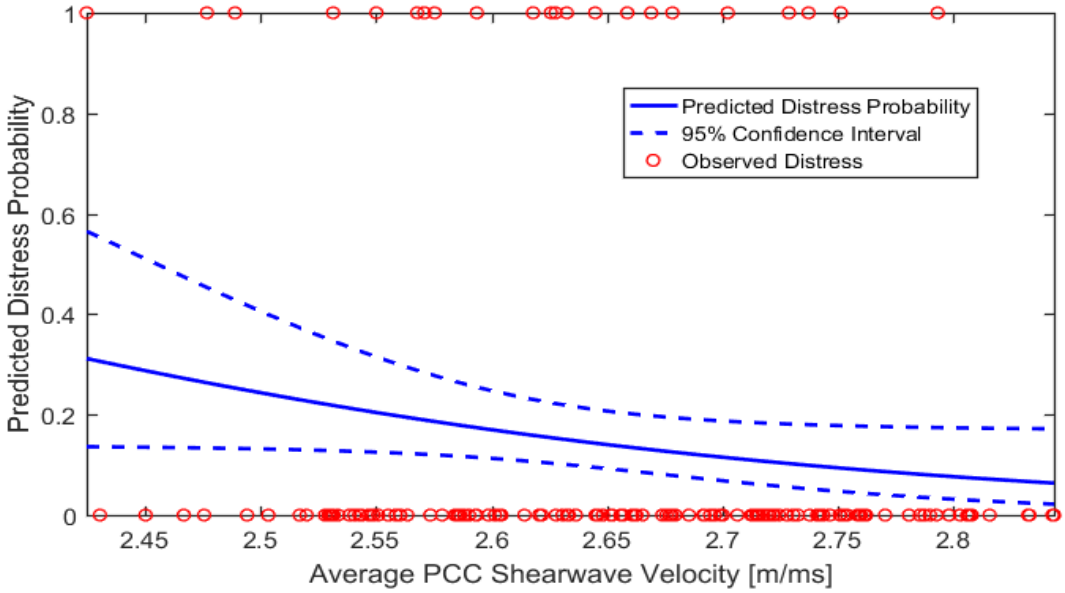

Figure 57: HWY 100 SWV versus Transverse Joint Spalling

The correlation between longitudinal joint spalling and velocity was only found to be significant only in HWY 100. However, the slopes of all four model agree that a decreasing in shear wave velocity is correlated with an increase in the probability of transverse joint spalling. Due to the lack significance, it is concluded that the correlation between shear wave velocity and longitudinal joint spalling is inconclusive. See appendix E for full results of the velocity regression analysis for longitudinal joint spalling.

5.9.2 Faulted Cracks and Joints

Faulting of cracks and joints is identified by a difference in surface elevation of pavement either side a crack or joint. Faulting is much more prevalent in pavements that lack load transfer mechanisms (Huang,1994). Faulting generally occurs with the depressed the surface uplifted in the direction of traffic, as traffic loading pumps material from beneath the leading slab and deposits it beneath the trailing slab. Pavement Warping or curling of the slab can also effect the degree of faulting. In JRCP, faulting is often caused erosion of the concrete around the dowels. Generally, damage around the dowels is caused by excessive bearing stress and damage can be avoided by limited bearing stress to less than 1500 psi. Faulting is directly considered by the MEPDG.

According to the faulting model developed in the MEPDG, faulting is function of load, maximum bearing stress, traverse joint spacing, and the estimated modulus of the subgrade.

The structural causes and findings of the MEPDG calibration performed for crack and joint faulting above suggest that PCC thickness should not play a role in the occurrence of crack and joint faulting. Rather, the construction, design and spacing of the joints and the properties of the subgrade are the primary predictors of faulting.

5.9.3.1 Faulted Cracks and Joints VS Thickness and Velocity Variation

The logistic regression analysis performed for faulted cracked and joints VS thickness and velocity variation is inconclusive, as an insufficient number of faulted cracks and joints were recorded. Only 3 instances of the faulted cracks and joints were observed in all four surveys, providing insufficient data for regression analysis.

5.9.3 Cracked and Broken Panels Correlation

Longitudinal cracks are cracks within a slab that occur parallel to the centerline of the pavement. Many factors can contribute to longitudinal cracking. The primary causes of longitudinal cracking are repetitive heavy load application, loss of foundation support, curling and warping stresses and improper design or construction of longitudinal joints (Huang,1994). Transverse or diagonal cracks are generally caused by excessive stresses resulting from heavy load repetition, temperature gradients, moisture gradient, and drying shrinkage (Huang,1994). Corner breaks are a special case of cracked or broken panels and are generally caused by loss of slab support, poor load transfer, or curling or warping (Huang,1994).

The MEPDG guide provides equations for the prediction of cracked and broken panels. According to the guide, cracked and broken panel occurrence is a function of applied load, age, month, axel type, temperature gradient, and the PCC modulus of rupture (AASHTO, 2008). The geometry and strength of the concrete, including thickness, is incorporated into the modulus of rupture, a value which is generally determined using a flexural strength test (IDOT, 2009).

5.9.3.1 Cracked and Broken Panels VS Thickness Variation

The structural causes and findings of the MEPDG calibration performed for panel cracking discussed above suggest that PCC thickness variation should play a role in the occurrence of panel cracking. The logistic regression analysis performed found consistent significant correlation between panel cracking and thickness variation (Table 14). Specially, significant correlation was found between panel cracking and Average Transverse Slope as well as between panel cracking and Absolute Maximum Traverse Slope. This relationship was found both in the HWY 60E (Figure 58 and Figure 59 and HWY 60W (Figure 60 and Figure 61) datasets. Though the consistent significant correlation only occurred in two of the four datasets, the p-values of the correlations were highly significant (Table 14). It should be noted that the lack of correlation in HWY 100 and I 394 is likely due to the fact both HWY 100 and I 394 contain very little cracking. Logistic regression does not perform well with sparse datasets (Hosmer, Lemeshow, and Sturdivant, 2013), and therefore the correlations between cracking and thickness in HWY 100 and I 394 should not be considered.

Table 14: Thickness Variation Predictors VS Cracked and Broken Panels

	HWY 60E		HWY 60W	
Significant Predictors	**Coeff.**	**Sig.**	**Coeff.**	**Sig.**
Average Traverse Slope	-0.188	0.000	-0.093	0.001
Absolute Maximum Traverse Slope	-0.063	0.000	-0.034	0.004

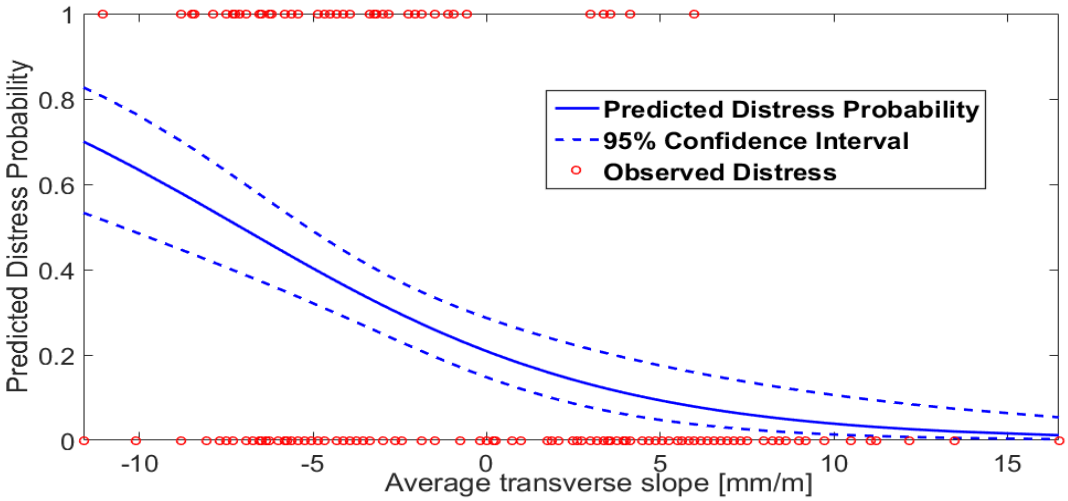

Figure 58: HWY 60 East (Thickness): Average Traverse Slope *versus* Cracked and Broken Panels.

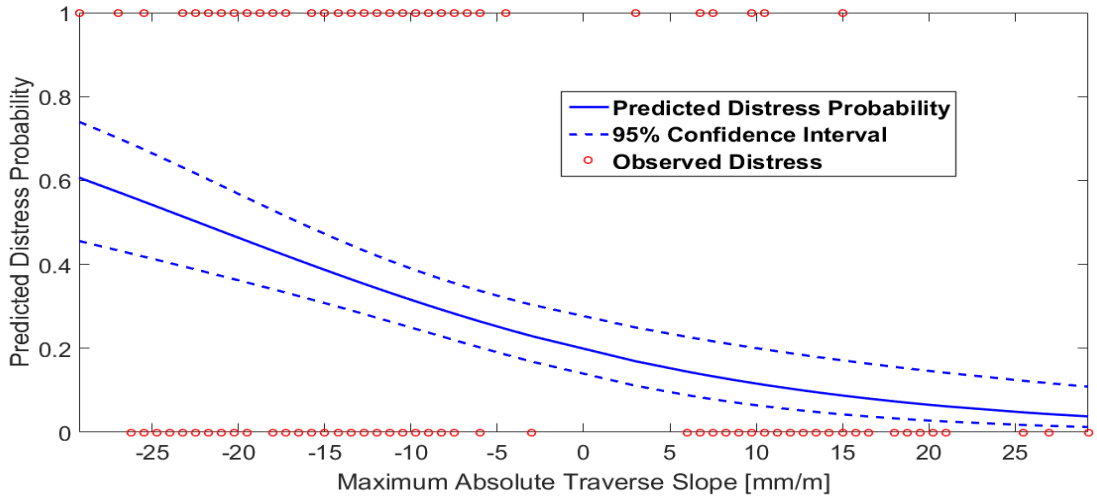

Figure 59: HWY 60 East (Thickness): Absolute Maximum Traverse Slope *versus* Cracked and Broken Panels.

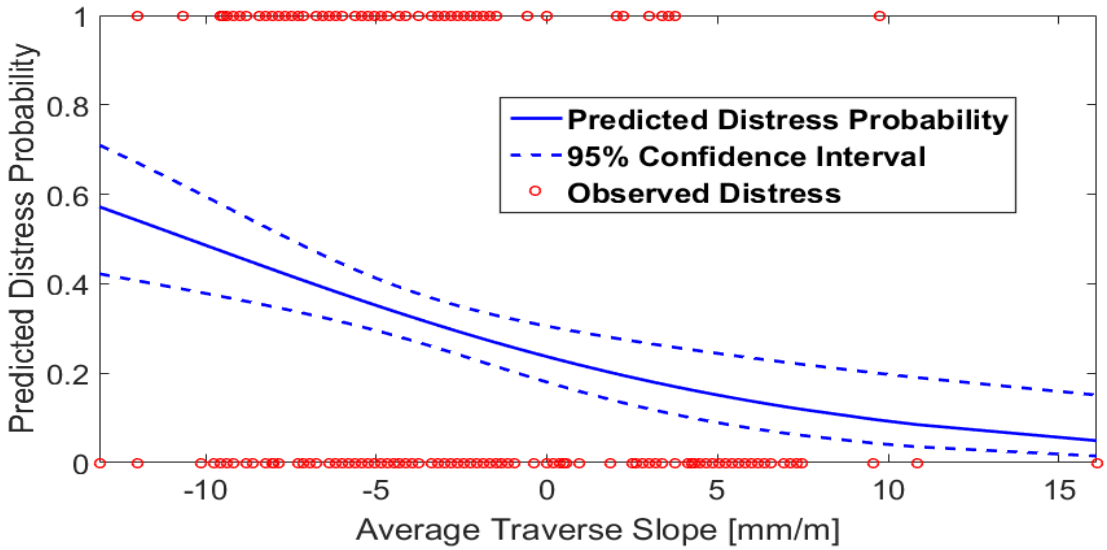

Figure 60: HWY 60 West (Thickness): Average Traverse Slope *versus* Cracked and Broken Panel.

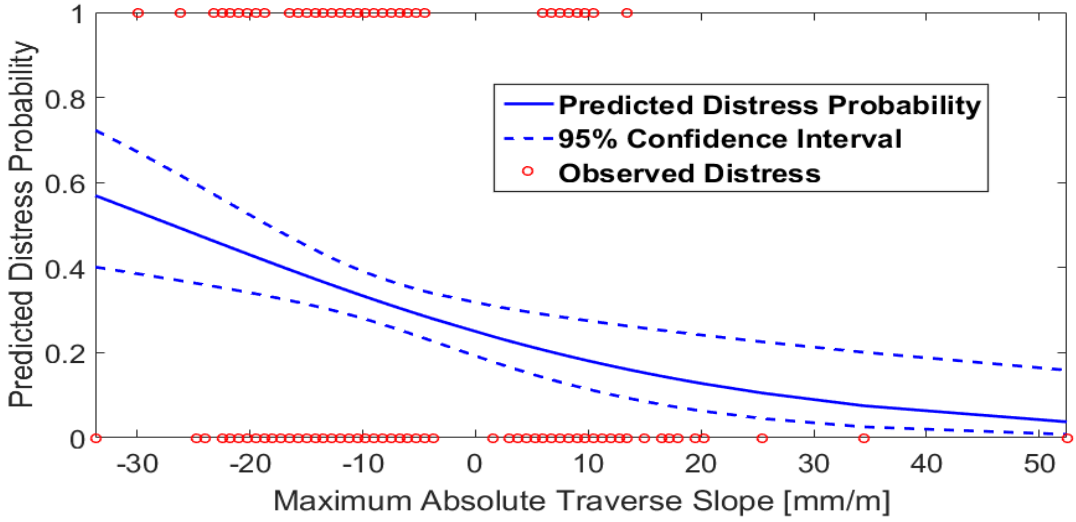

Figure 61 - HWY 60 West (Thickness): Absolute Maximum Traverse Slope *versus* Cracked and Broken panels.

The significant correlations were found between cracked and broken panel occurrence and average traverse slope and absolute maximum traverse slope (See section 5.6). Both of these correlations suggest that pavement slabs with a negative slope (thickness increases from right to left) exhibit higher rates of distress. As the surveys were conducted within the inner lanes, a slab with a negative slope will be thinner near the edge of lane than near the center. These results can clearly be seen in the surface plots created for HWY 60 (Figure 62) and HWY 60W (Figure 63).

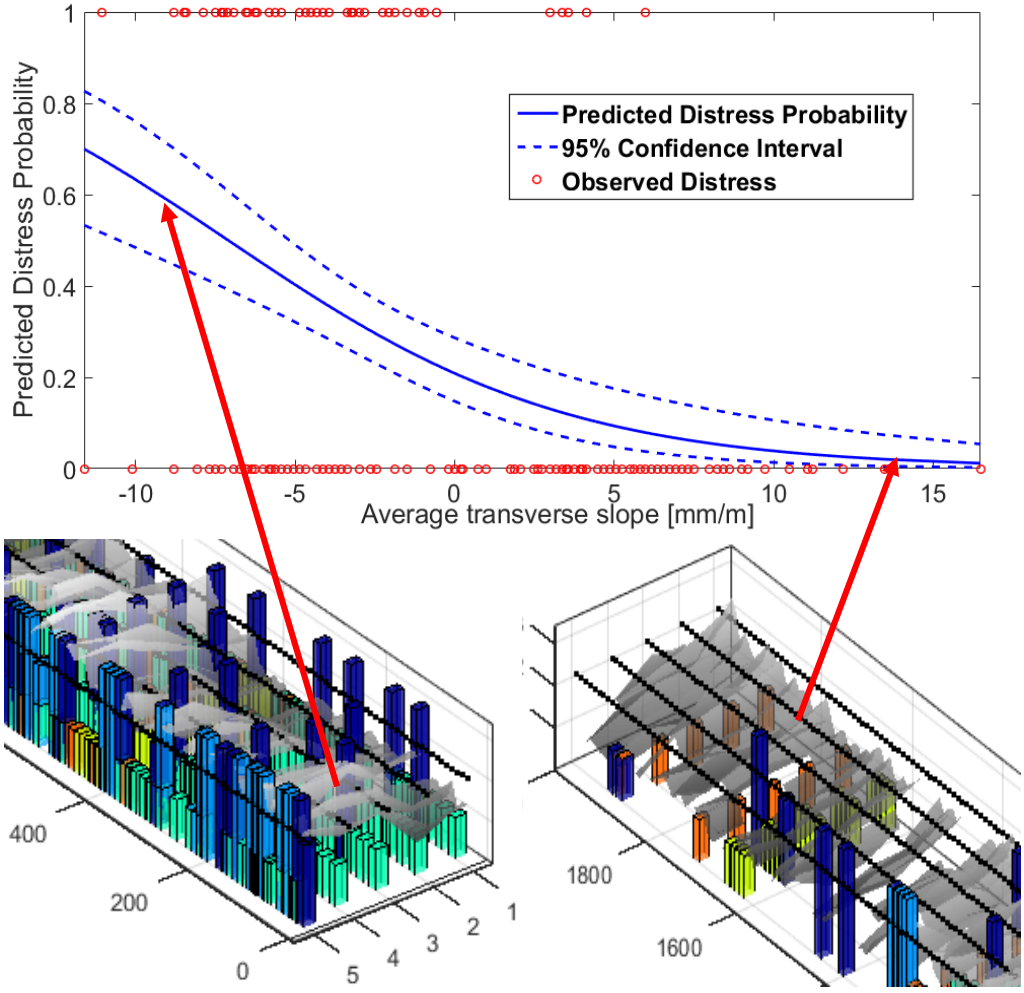

Figure 62: HWY 60E: Cracked Panels vs Thickness Slope

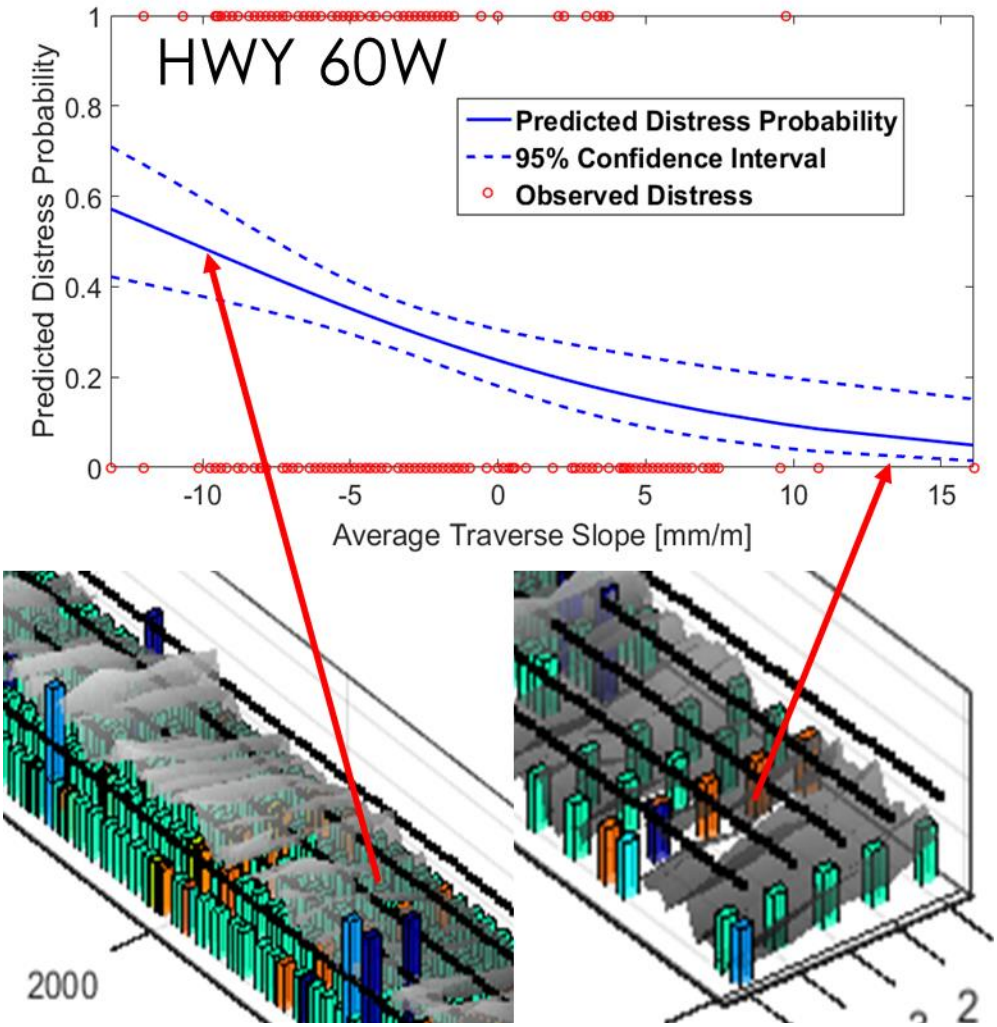

Figure 63: HWY 60W: Cracked Panels vs Thickness Slope

This relationship could have a mechanistic foundation. It is well known that edge loadings produce the critic loadings in concrete slabs. Using Westergaard's solution and its implementation in ISLAB2000, it can be seen that edge loading produces higher stresses than equivalent loads placed in the center or corner of a slab (Figure 65) (Khazanovich, 2016). When edge loads are applied, the highest stress concentration occurs under the load (Figure 66), that is, at the edge of the slab. (Khazanovich, 2016). It can be seen that the thickness slopes result in significantly differences in thickness across the slabs (Figure 64). A slab which is significantly thinner at the edge can be expected to experience more cracking than a slab which is thicker.

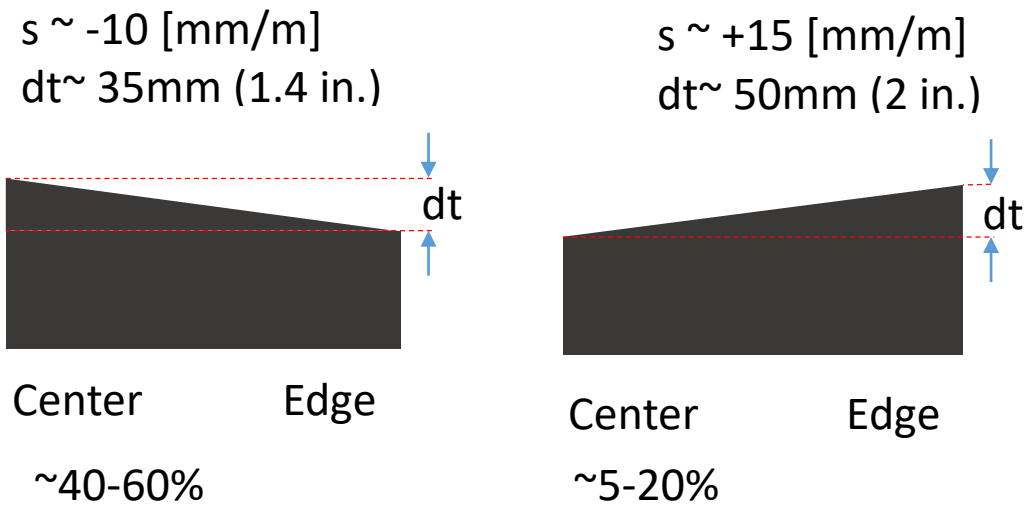

Figure 64: Effect of Thickness Slope seen in HWY 60

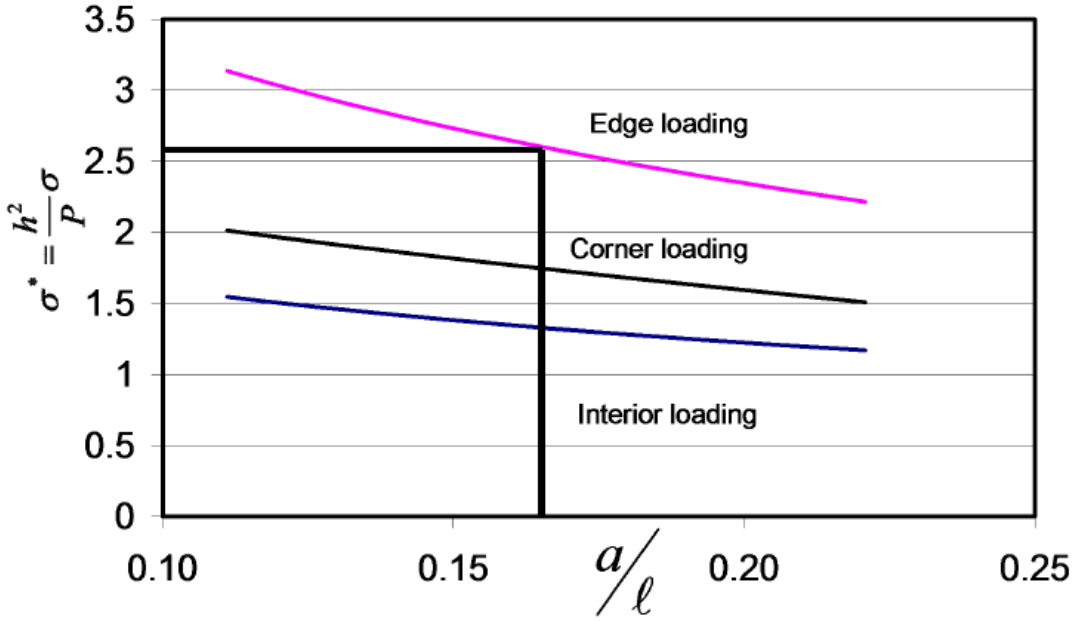

Figure 65: Stress Resultant From Edge Loading

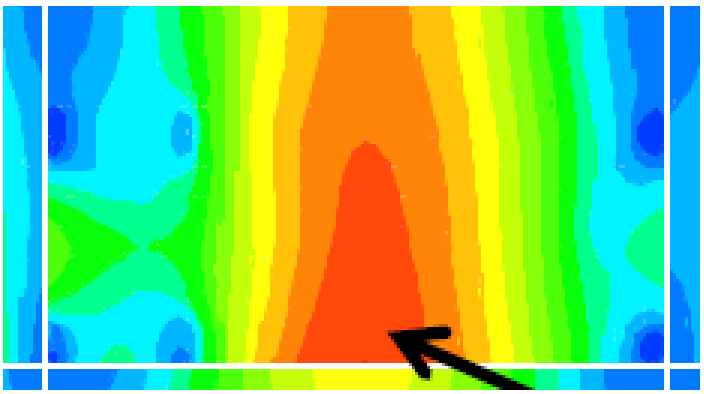

Figure 66: ISLAB2000 Model of Edge Loading

5.9.3.2 Cracked and Broken Panels VS Velocity Variation

The MEPDG guide provides equations for the prediction of cracked and broken panels. According to the guide, cracked and broken panel occurrence is a function of applied load, PCC modulus of rupture, age, month, axel type, temperature gradient, and the PCC modulus of rupture (AASHTO, 2008). The geometry of the concrete, including thickness, is incorporated into the modulus of rupture (IDOT, 2009).

The structural causes and findings of the MEPDG calibration, particularly the correlation between cracking and modulus of rupture, suggest that PCC velocity, as correlated with SWV, should play a role in the occurrence of panel cracking. As with the thickness correlations, HWY 60 East and HWY 60 West datasets are of primary interest when investigating cracked and broken panels. There was a very strong negative correlation ($p < 0.0001$) (Table 15) found between average traverse velocity and cracked and broken panels (Figure 67 and Figure 68). These results can clearly be seen surface plots create for velocity (Figure 69 and Figure 70) in the HWY 60E and HWY 60W.

Both of these correlations suggest that pavements with a lower velocity are more likely to exhibit cracked or broken panels, a conclusion which agrees with the MEPGD model. As with the thickness correlations, it should be noted that the lack of correlation in HWY 100 and I 394 is likely due to the fact both HWY 100 and I 394 contain very little cracking and logistic regression is not effective for sparse datasets (Hosmer, Lemeshow, and Sturdivant, 2013).

Table 15: Average Velocity VS Cracked or Broken Panels

	HWY 60E		**HWY 60W**	
	Coeff.	Sig.	Coeff.	Sig.
Cracked or Broken Panels	**-10.579**	**0.000**	**-5.714**	**0.000**

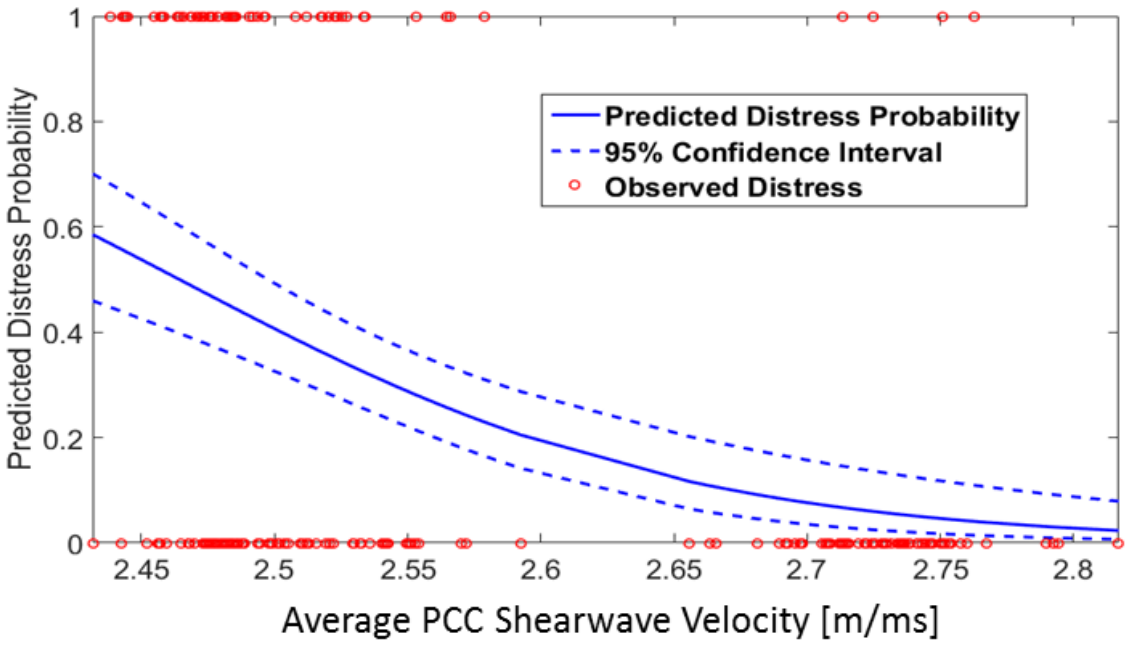

Figure 67: HWY 60E (Velocity): Average Traverse Velocity *versus* Cracked and Broken Panel.

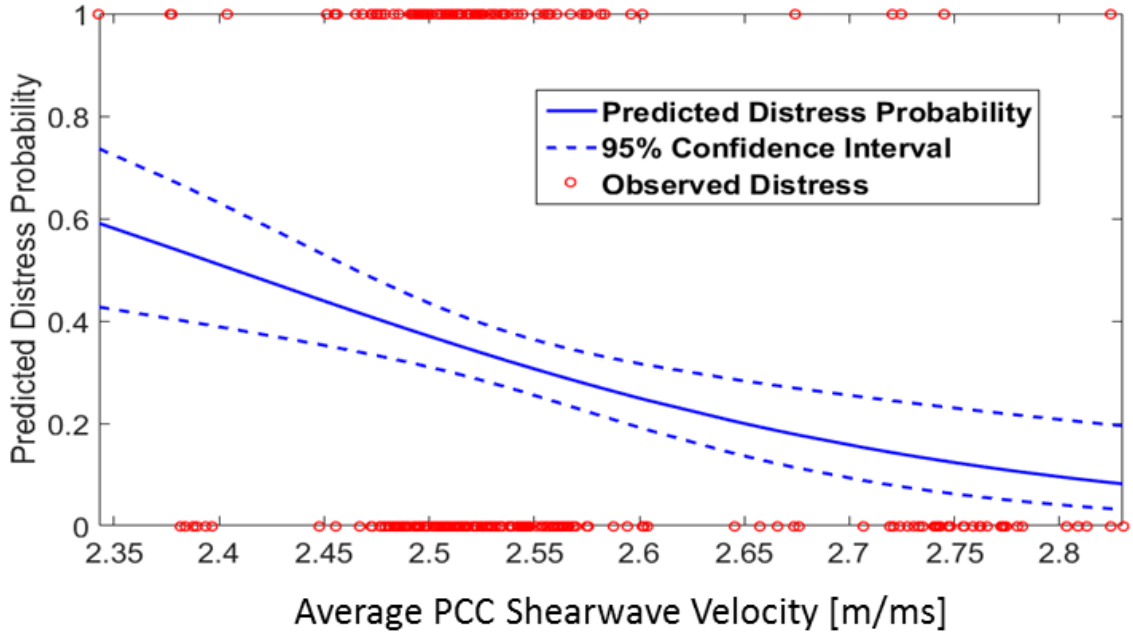

Figure 68: HWY 60W (Velocity): Average Traverse Velocity *versus* Cracked and Broken.

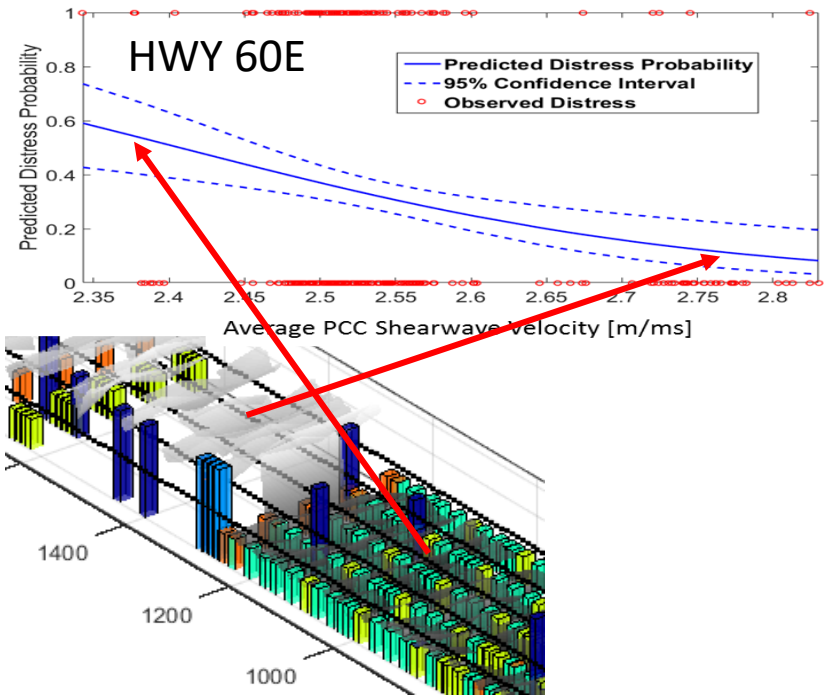

Figure 69: HWY 60E: Cracked Panels VS Velocity

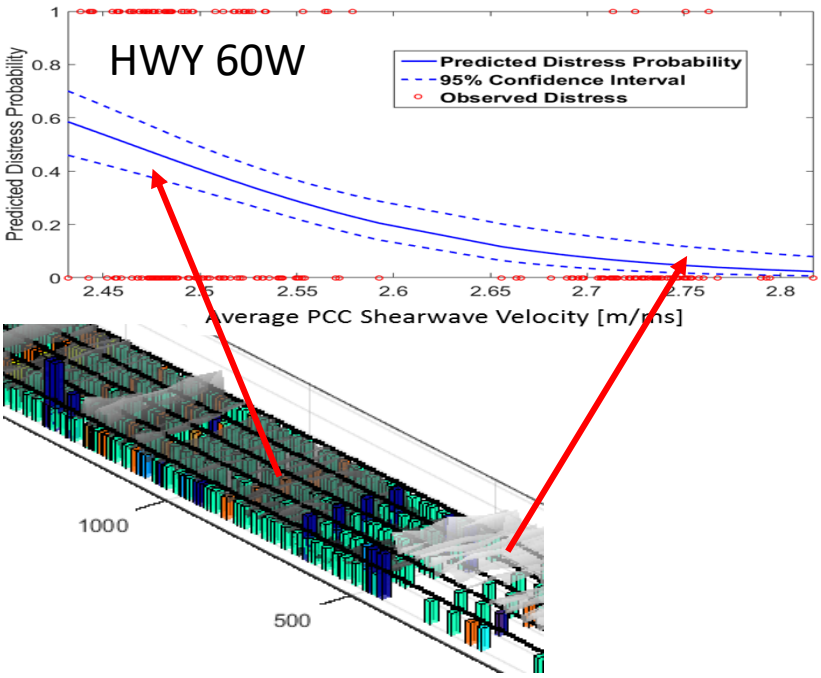

Figure 70: HWY 60W: Cracked Panels VS Velocity

5.9.4 Overlaid or patched panels

Overlaid and patched panels are not a primary distress. Rather, they are a maintenance response to distress which has already occurred. For this reason, overlaid and patched panels will not be discussed in this section.

5.9.5 Durability Cracking

Durability cracking, also referred to as 'D' cracking, often appears as closely spaced, crescent shaped surface cracks which appear parallel to cracks and joints. D cracking is generally caused by freeze thaw expansion of certain types of coarse aggregate (Huang,1994). The MEPDG model determines D cracking is a function of the age of pavement, the load, the mean air freezing index, the transverse joint spacing, and the Thornthwaite summer concentration of thermal energy (AASHTO, 2008).

5.9.5.1 Durability Cracking VS Thickness and Velocity Variation

The logistic regression analysis performed for durability cracking VS thickness variation is inclusive, as an insufficient number of durability cracking distresses were recorded.

5.9.6 All Distress

Though the MEPDG does not discuss damage in terms of "All distress", the empirical findings of the MEPDG calibration models as well as the underlining structural theories of distress occurrence suggest pavement thickness and shear wave velocity variation may manifest multiple distress types. Engineered roadways generally consider thickness and strength when incorporating a factor of safety into construction, therefore deficiencies in thickness and strength are likely only secondary causes of failure. Primary causes of failure vary greatly based on distress type (See discussion of mechanistic and MEPDG causes of distress outlined above). Combining all distress may reveal universal patterns in distress occurrence that are individually dominated by other primary failure mechanism but are all contributed to by thickness or velocity variation. This idea led to the adoption of the "All distress" indicator. All distress allows datasets with different distress profiles to be compared. This helps adjust for various design and construction differences and potential human

bias in recording. All distress may allow the detection of correlations that may not be significant in a single distress type, but are relevant for overall pavement quality.

5.9.6.1 All Distress VS Thickness Variation

The logistic regression analysis of all distress vs thickness variation revealed no new correlations. The strong negative correlations between traverse slope and cracked and broken panels dominates the HWY 60 datasets, while other datasets provide no consistently significant correlations (Appendix D).

5.9.6.2 All Distress VS Velocity Variation

A strong negative correlation ($p < 0.005$) (Table 16) was found between average SWV and all distress in all four surveys (Figure 71, Figure 72, Figure 73, Figure 74). This is not particularly surprising for HWY 60 East, HWY 60 West, or HWY 100, as all three were found to have strong significant negative correlations for particular distress-velocity combinations. However, for I-394, all distress is the only highly significant correlation, suggesting the weaker correlations of other distress are all consistent and add to create a highly significant result. The full regression results support this conclusion.

Table 16: Average Velocity VS Any/All distress

	HWY 60E		**HWY 60W**		**HWY 100**		**I 394**	
	Coeff.	Sig.	Coeff.	Sig.	Coeff.	Sig.	Coeff.	Sig.
All/Any Distress	**-5.986**	**0.000**	**-4.537**	**0.000**	**-6.128**	**0.000**	**-16.757**	**0.001**

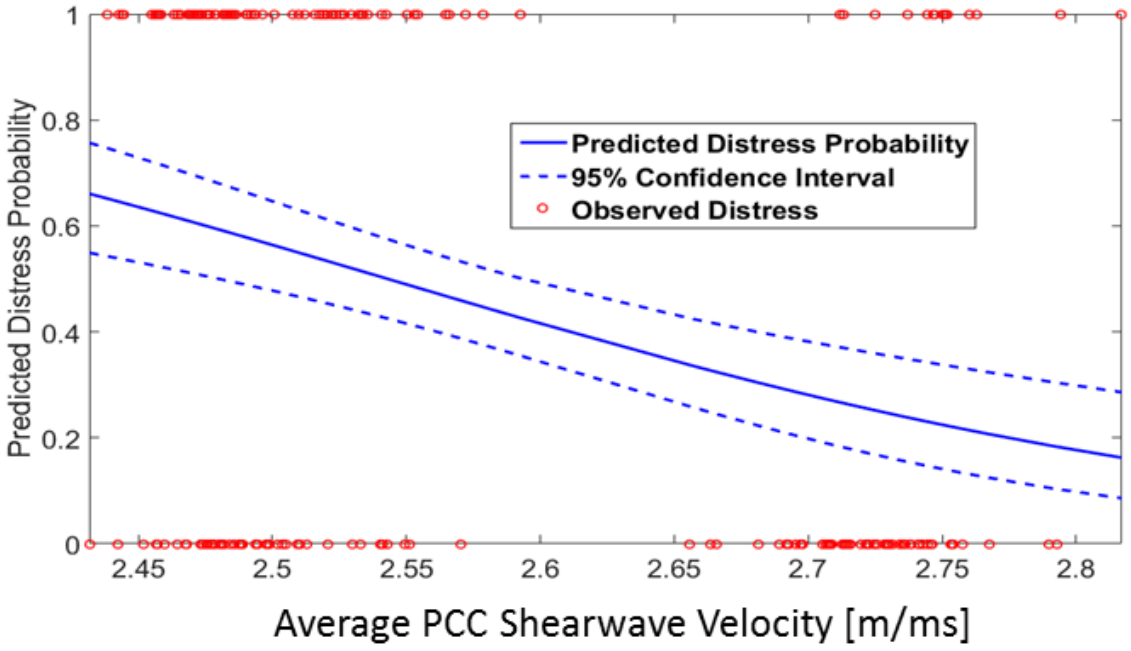

Figure 71: HWY 60 E (Velocity): Average Traverse Velocity *versus* all Distress.

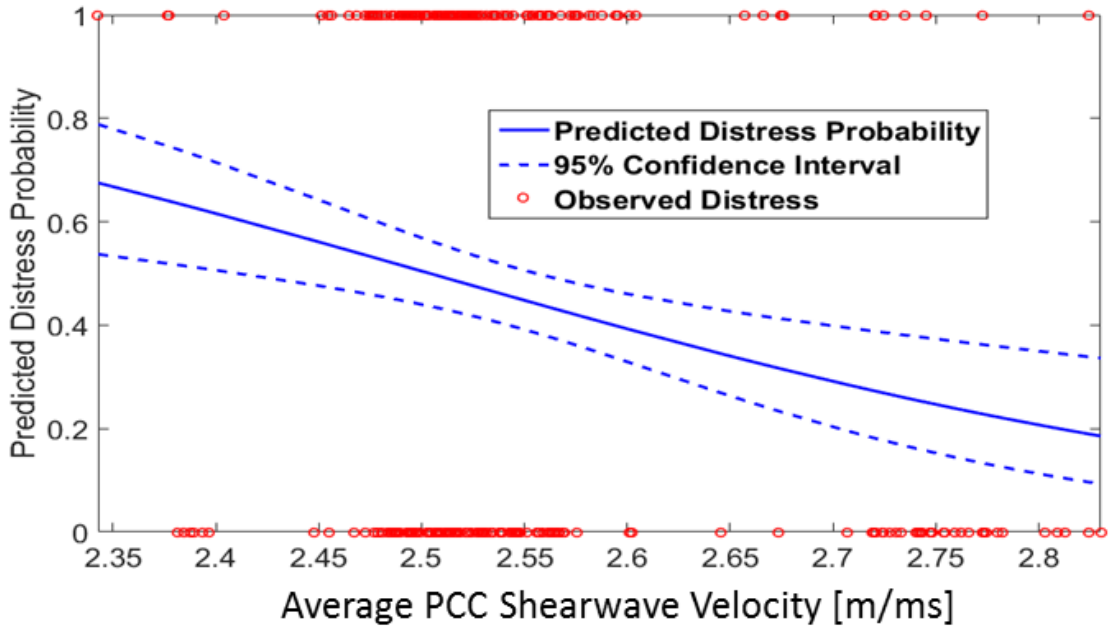

Figure 72: HWY 60W (Velocity): Average Traverse Velocity *versus* all Distress.

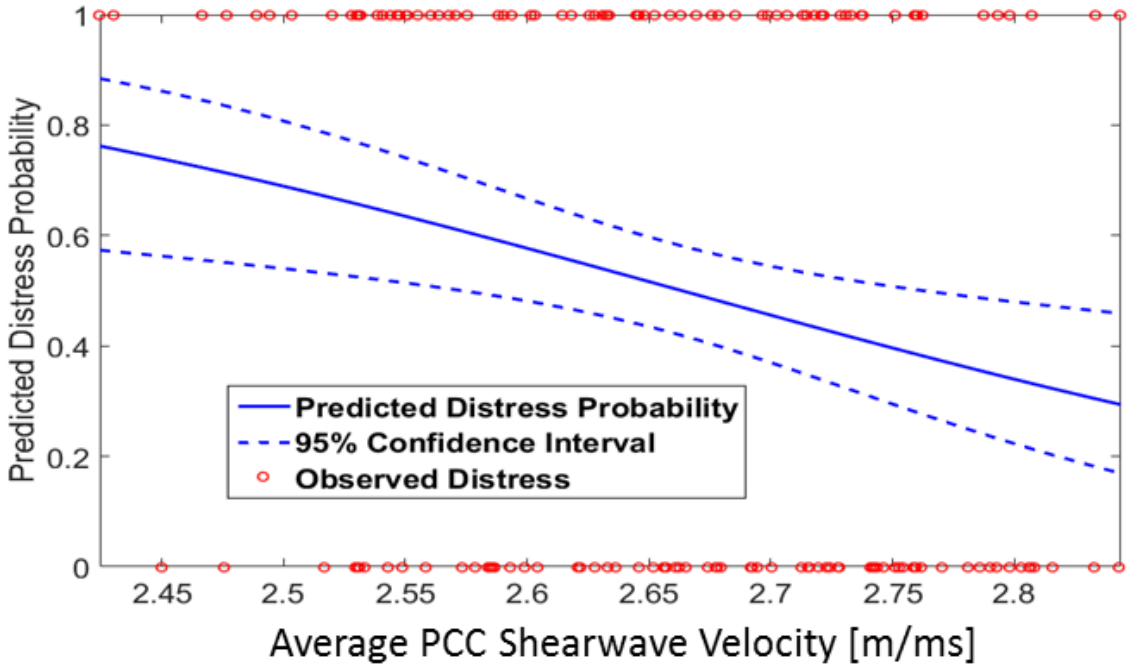

Figure 73: HWY 100 (Velocity): Average Traverse Velocity *versus* all Distress.

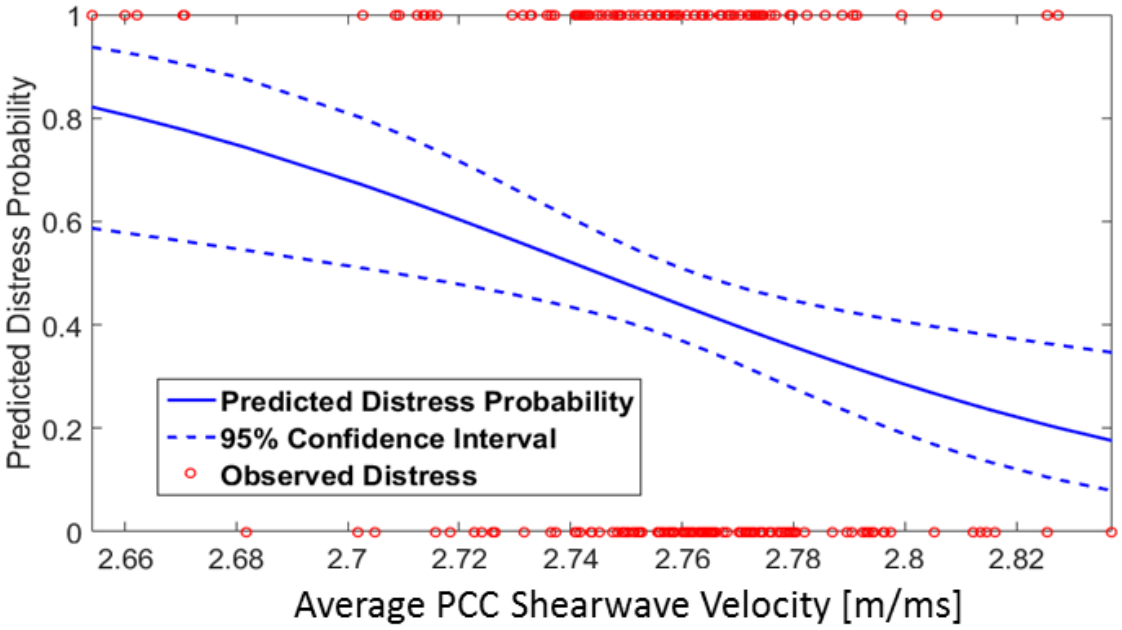

Figure 74: I-394 (Velocity): Average Traverse Velocity *versus* all Distress.

5.10 Pavement Design Data Analysis

To better understand the results of the visual and regression analysis, design data for survey sections was analyzed. Design data was taken from MnDOT COPES electronic records and is presented below (MnDOT, 2016). Construction records were unable to be located for any projects. It should be noted that the design data may be incomplete, and without the construction records the exact features of the roadways cannot be known.

5.10.1 HWY 60 Design Data

The design data for HWY 60 gives insight to the discrete thickness and velocity sections seen in the data. Both surveys of HWY 60 were unknowingly conducted over pavements constructed at two different times with different designs. The different design sections are outlined in Figure 75 and Figure 76. It can be seen that segment 1 defines the low velocity section with decreased performance while segment 2 defines the higher velocity increased performance sections.

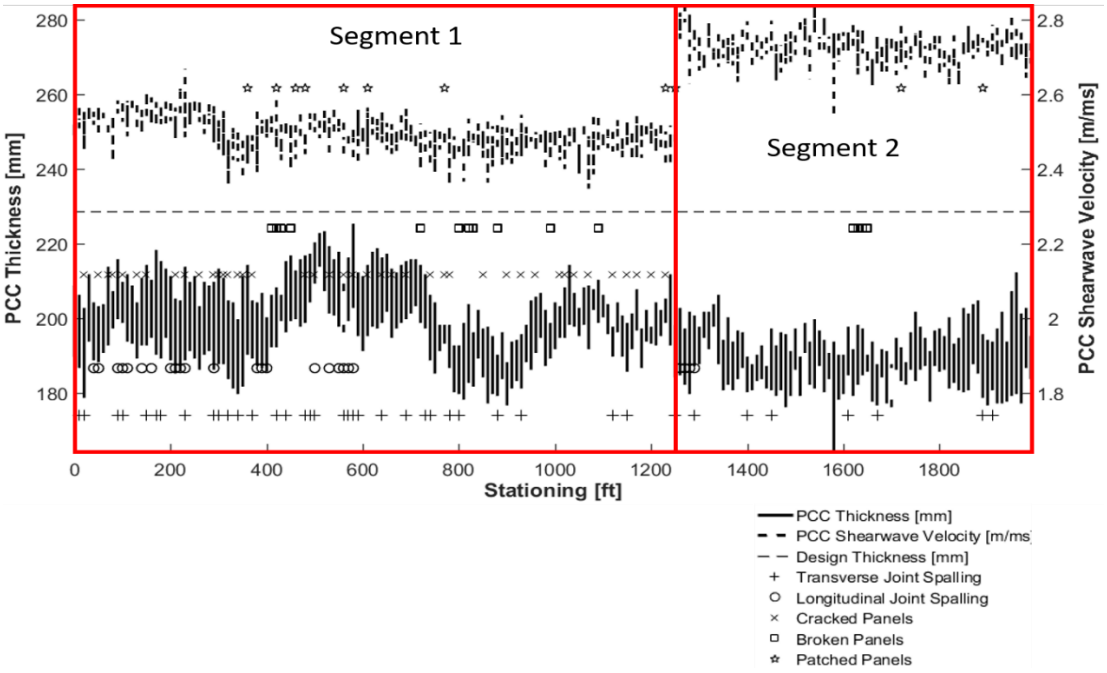

Figure 75: HWY 60E Discrete Segments

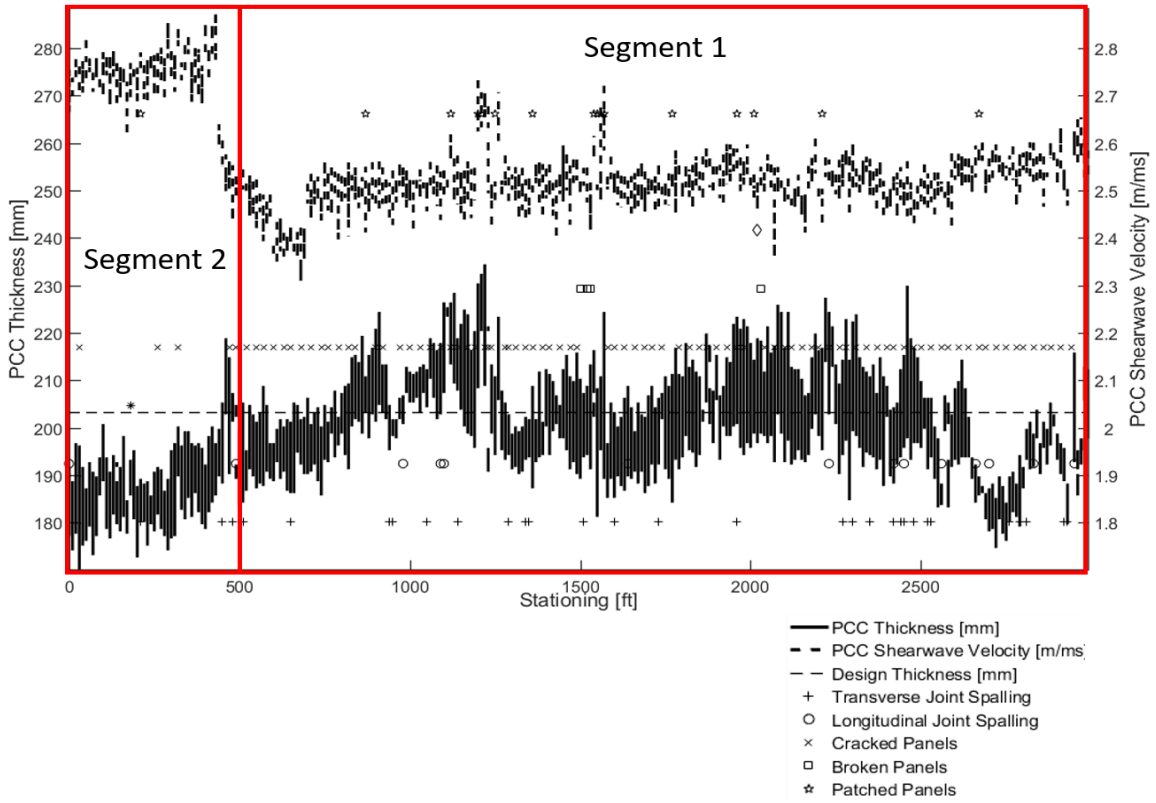

Figure 76: HWY 60W Discrete Segments

Key design changes are listed in Table 17 and concrete mix data is presented in Table 18 for the two sections is presented below. The two segments are separated within HWY 60E and HWY 60W as shown in Figure 75 and Figure 76 .

Table 17: HWY 60 Design data

	Begin. MP - End MP	Date Completed	Joint Sealant	Base Type	Base Thick. mm (in.)	Drainage	Core Compressive Strength (psi)	Design Thick. (in.)
Segment 1	49.91 - 53.27	1-Oct-88	Neoprene	NA	NA	Long. Drains	5161	8
Segment 2	53.27 - 54.17	1-Jun-87	No Sealant	Crushed Gravel	76 (3)	None	5053	8

NA = data not available

Review of the design data shows that segment 1 was constructed in October of 1988, contains the joint sealant neoprene, and has longitudinal drainage while segment 2 was constructed in June of 1987 and claims to contain no sealant or drainage. Without the construction records, these findings cannot be verified, so they will be assumed to represent the true roadway conditions. Based on the design data alone it would be expected that segment 1, which is 1.5 years younger, contains joint sealant, and contains longitude drainage would perform better than segment 2. However, this is clearly not the case. This suggests that the mix design may play a role in the difference in performance. The mix data is presented in Table 18.

Table 18: HWY 60 Mix Design Data

	Mix design (lb/yd$^{3)}$	
	Segments 1	Segments 2
Coarse Agg.	1791	1858
Fine Agg.	1200	1200
Cement	472	451
Water	260	240
W/C	0.55	0.53
Flyash	83	79
Coarse Aggregate Source - Type	Northern ConAgg (167001) - Gravel/crushed New Ulm Quartz (152003) – Gravel	New Ulm Quartz (152003) - Crushed - Quartzite/ Granit

Table 18**Error! Reference source not found.** shows that segment 1 and 2 have very similar volumetric. Segment 1 has slightly more cement content while having less coarse aggregate, however the ratio of water to cement is similar both highways. A higher level of cement content may imply higher shrinkage stress, explaining the greater number of cracks in segment 1. The coarse aggregate source also provides clues to the diverse performance. It can be seen that segment 1 contains the coarse aggregate Northern ConAgg (167001). A review of MnDOT procedures revealed that this aggregate is no longer used due to issues with spalling and cracking. It is believed that the high levels of carbonate (41.32 to 55.8 %) found in this aggregate play a key role in the poor performance (Koubaa, Snyder, and Peterson, 1997). As Stage 1 had a 50/50 mix of coarse aggregates including Northern ConAgg (167001), the poor performance indicates that mixing good quality aggregate with bad quality aggregate does not mask the latter's performance.

The extent to which the coarse aggregate Northern ConAgg (167001) effected the performance of HWY 60 is not known. Additionally, the effect of the aggregate on the shear wave velocity is not known. It is, however, possible that this aggregate accounted for the decrease in shear wave velocity. The surface shear wave velocity is calculated by producing a best-fit estimation using the 45 sensor pairs of the MIRA device. Though the effective depth of the surface shear wave velocity is minimal, aggregates occur on the surface at approximately the same concentrations as they do in the overall volume of the concrete. A typical coarse aggregate concentration by volume is 25-35% (Koubaa, Snyder, and Peterson, 1997). Therefore, the surface shear wave is impacted by the properties of the coarse aggregates, as they account for a significant proportion of the volume and surface area of the pavement used to compute the shear wave velocity.

Coarse aggregates used in Minnesota come from a variety of sources and contain many different mineral and rock types. Typical components of coarse aggregate include carbonates mixed with siliceous secondary minerals which can be sedimentary, metamorphic, or igneous in origin (Koubaa, Snyder, and Peterson, 1997). The shear wave velocity of carbonates is lower than that of other rock types expected in a coarse aggregate (Mavko,2005). Therefore, an aggregate which contains high carbonate content, such as Northern ConAgg (167001) should be expected to produce lower shear wave velocities than aggregates which contain less carbonate. In conclusion, more research is needed on the relationship between surface shear wave velocity, concrete mix components, and pavement performance, but the known relationships between mineral types, shear wave velocity, and strength properties make it possible that change in shear wave velocity and performance seen were a direct result of the change in aggregate.

5.10.2 HWY 100 Design Data

Unlike HWY 60, the surveyed section of HWY 100 was of a consistent design. The design data (Table 19) and concrete mix data (Table 20) are presented below.

Table 19: HWY 100 Design Data

Begin. MP - End MP	Date Completed	Joint Sealant	Base Type	Base Thickness mm (in.)	Drainage	Core Compressive Strength (psi)
49.91 - 53.27	1-Oct-73	Neoprene	Crushed Gravel	13	Long. Drains	5775

From Table 19 it can be seen that HWY 100 is over 10 years older than HWY 60. Age is a primary factor in spalling occurrence (Huang,1994) (AASHTO, 2008), thus the age of roadway likely explains the high rate of spalling. The increased compressive strength and increased design thickness may play a role in the decreased occurrence of cracked and broken panels as compared to HWY 60.

Table 20: HWY 100 Concrete Mix Data

	Mix design ($lb/yd^{3)}$
	Segment 1
Coarse Agg.	2323
Fine Agg.	906
Cement	530
Water	225
Flyash	0
Coarse Agg. Size (in.)	1.5

5.10.3 I 394 Design Data

Like HWY 100, the surveys taken on I 394 were conducted over areas of consistent design. The design (Table 21) and mix data (Table 22) are presented below.

Table 21: I 394 Design Data

Beginning MP - End MP	Date Completed	Joint Sealant	Base Type	Base Thickness mm (in.)	Drainage	Core Compressive Strength (psi)	Design Thickness (in.)
49.91 - 53.27	1-Oct-90	No sealant	Uncrushed Gravel	NA	Long. Drains	5080	10

From Table 21 it can be seen that I 394 is the youngest pavement section surveyed. Interestingly, I 394 exhibits spalling rates similar to that seen in HWY 60, a significantly older roadway. This is likely due to the lack of sealant used on the roadway. Sealant prevents the infiltration of incompressible aggregates into the joint, which is a primary driver of spalling (Huang,1994). The higher traffic loads experienced by I 394 may also help explain the high rates of spalling. At 10 in, I 394 is the thickest pavement investigated. This thickness and the moderate compressive strength likely plays a factor in the low level of cracked and broken panel occurrence (Table 11).

Table 22: I 394 Concrete Mix Data

	Mix design ($lb/yd^{3)}$
	Segment 1
Coarse Agg.	3124
Fine Agg.	1052
Cement	460
Water	250
Flyash	81
Coarse Agg. Size (in.)	NA

6. RECOMMENDATIONS

Though the results of this study are based on limited data and exact causal relationship between pavement performance and shear wave velocity is unknown, recommendations can still be made about material QA/QC and potential surveying procedure.

6.1 Material QA/QC Procedures

First, this study also demonstrated the importance of material QA/QC. Though the exact causal relationship between shear wave velocity and pavement performance is not known, shear wave velocity is controlled by material properties. The correlations seen in every data set can, therefore, be seen as correlations between material properties and performance.

Based on these results, it can be recommended that material QA/QC remains a focus of pavement design and research. The importance of material was clearly seen in HWY 60, where a change in coarse aggregate seems to be a primary factor in an observed change in pavement performance. The importance of material QA/QC is well known and current efforts being extended in improving QA/QC are well justified. A successful example of this process can be seen in the removal from service of coarse aggregate Northern ConAgg (167001), the aggregate which appears to contribute to the poor performance of HWY 60.

6.2 Conceptual Model for Detection of Potentially Deficient Pavements

Based on the findings of this study, an analysis methodology is proposed to identify construction changes which may lead to adverse pavement performance. The methodology is based on the observation from the HWY 60 datasets that a velocity survey conducted over a uniformly designed and constructed section of pavement will have a much lower standard deviation than a survey conducted over pavements with discrete changes in construction or design (Figure 77, Table 23). Therefore, a standard deviation above a certain threshold may be indicative of a design or construction change capable of producing adverse pavement performance.

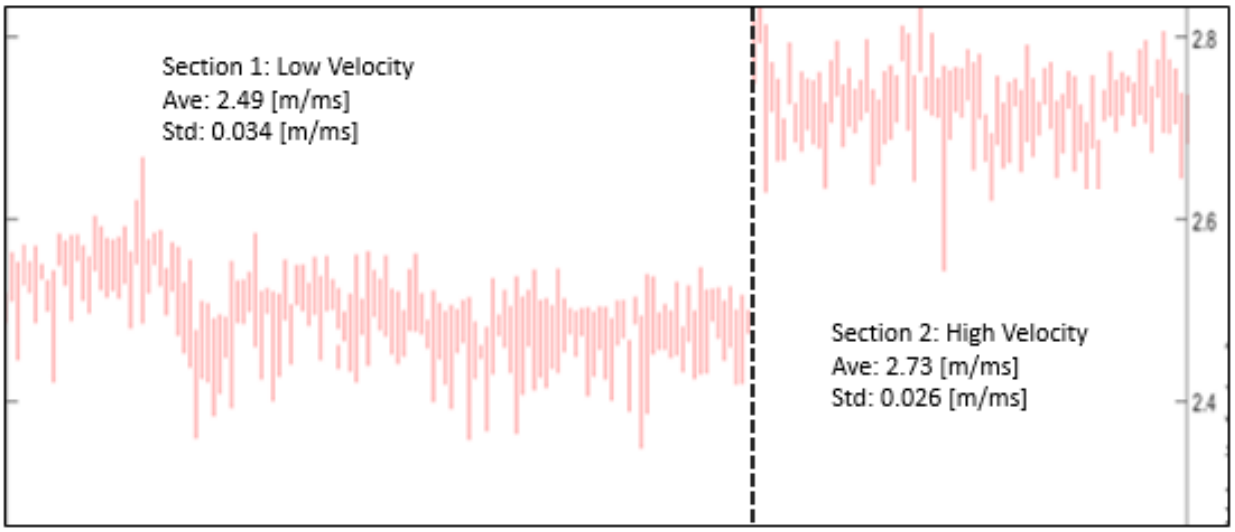

Figure 77: Variability of discrete velocity sections

Table 23: Shear Wave Velocity Variability for Velocity Sections from HWY 60

	HWY 60E			HWY 60W		
Section	Avg. Vel. (m/ms)	Std. dev. (m/ms)	Var. $(m/ms)^2$	Avg. Vel. (m/ms)	Std. dev. (m/ms)	Var. $(m/ms)^2$
High velocity	2.728	0.0261	0.0007	2.754	0.0334	0.0011
Low velocity	2.498	0.0344	0.0012	2.513	0.0447	0.0020
Combined	2.565	0.1099	0.0121	2.547	0.0939	0.0088

6.3 Surface Shear Wave Velocity Proposed Survey Methodology

The following methodology is proposed to identify a design or construction change capable of producing adverse pavement performance.

1. Surveys must be conducted a minimum of 28 days after concrete was poured to eliminate variation due to degree of curing (Freeseman, Hoegh, and Khazanovich 2016).

2. Surveys should consider both transverse and longitudinal variation. Therefore, a survey pattern of three traverse measurements per slab are suggested. The measurements should be taken in the middle of the slab. The traverse locations proposed are as follows (Figure 78):

Location 1: Right Wheel Path

Location 2: Center of Wheel Path

Location 3: Left Wheel Path

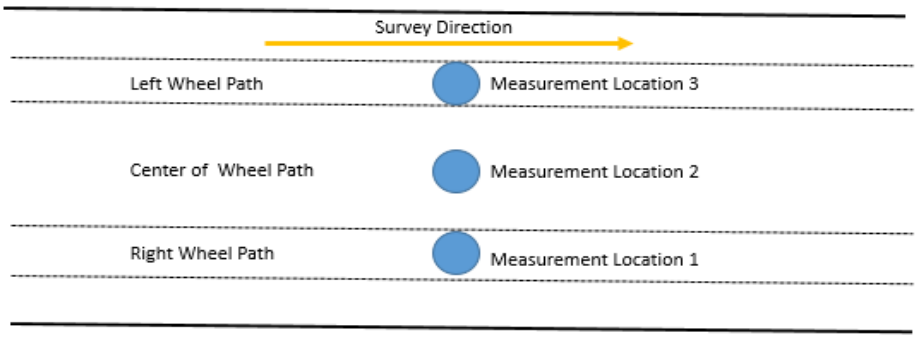

Figure 78: Shear wave velocity measurement locations per slab

3. All measurements should be taken in repeated couples. To conduct a repeat measurement, the first measurement is taken, the device is lifted and replaced in the sample location, and another measurement is taken. In the final analysis, the couples will be compared to test for error.

4. To produce statically sound results, the survey should be conducted for a minimum of 20 slabs, for a total of 60 couples or 120 total measurements on each side of the suspected design/construction change. Such a survey may be expected to take 1-2 hrs.

5. Special attention should be given to sections which are known to have experienced changes in mix design, construction interruption, or other unusual circumstances.

6. Once data collection is complete, compute the population standard deviation of the dataset.

7. If the computed population standard deviation is above 0.1 m/ms, there may be a potential significant change in material properties and further analysis must be completed. If the computed population standard deviation is less than 0.1 m/ms, the variability of the shear wave velocity within the survey section is not of concern.

8. If the population standard deviation was found to be greater than 0.1 m/ms, visually plot the velocity data along the survey. If a jump in the surface shear wave velocity can be visually determined, further analysis is required. If no visual jump is apparent, the variability may be due to intrinsic material variability or variation due to degree of curing and is not of concern.

9. If a visual jump is apparent, separate the visually distinct sections and compute the arithmetic mean and standard deviation for each section.

10. Using the mean and standard deviation computed for each section, perform a two-sampled t-test for equal variance. This statistical test will determine if the mean values of the two sections are statistically different. The two-sample t-test for equal variance is given by:

The null hypothesis is given by Equation 28:

$$H_0: \mu_1 - \mu_2 = 0 \tag{28}$$

Whereas, alternative hypothesis is given by Equation 29:

$$H_1: \mu_1 - \mu_2 \neq 0 \tag{29}$$

Where μ_1 is the shear wave velocity mean value of the first section and μ_2 is the mean value of the second section.

The null hypothesis will be rejected at a 95% confidence (Equation 30):

$$\alpha = 1 - 0.95 = 0.05 \tag{30}$$

The statistic can be calculated by Equation 31:

$$t = \frac{(\overline{x_1} - \overline{x_2})}{s_p \left[\left(\frac{1}{n_1}\right)^2 - \left(\frac{1}{n_2}\right)^2 \right]} \tag{31}$$

Where t is the computed value for t-statistic; $\overline{x_1}$ is the arithmetic average of the first section; $\overline{x_2}$ is the arithmetic average of the second section; n_1 is the number of measurements within the first section; n_2 is the number of measurements within the second section; and s_p is the pooled variance.

The pooled variance given by Equation 32:

$$s_p = \sqrt{\frac{(n_1 - 1) * {s_1}^2 + (n_2 - 1) * {s_2}^2}{n_1 + n_2 - 2}} \quad (32)$$

Where s_1 is the population standard deviation of section 1 and s_2 is the population standard deviation of section 2.

The degrees of freedom associated with the statistical test are calculated by Equation 33:

$$\delta = n_1 + n_2 - 2 \quad (33)$$

Where δ is the degrees of freedom for the t-test.

The t-statistic can now be used to determine the p-value for the hypothesis test (Equation 34).

$$p - value = \Pr(T \geq t | df = \delta) \quad (34)$$

If the computed $p - value$ is less than the previously defined α, the null hypothesis is rejected and the difference in the pavement sections are determine to be statistically significant. A t-test is easily implemented in Microsoft Excel, MATLAB, and other commonly available analytical applications.

11. If the results of the t-test determined statistical significance for the visual jump, follow up investigation is suggested. Validation of mix design, coring, additional surveying, and review of construction records is advised to find anything which may explain the change in material properties suggested by the analysis.

7 CONCLUSION

In order to investigate possible correlations between Portland cement concrete (PCC) thickness and velocity variations and observed surface distresses, a combination of non-destructive ultrasonic tests and visual distress surveys were performed on four existing highway projects in the state of Minnesota.

Average thickness results show that for three of the four surveys conducted (HWY 60E, HWY 60W and HWY 100), the concrete slabs were slightly thinner than the designed thickness. Only I 394 had an average slab thickness greater than the design thickness. Closely spaced PCC thickness measurements reveal that slab thickness is highly variable in both longitudinal and transverse directions. The overall standard deviation in slab thickness varied between 10 [in] and 10.9 [in] resulting in coefficients of variation between 0.039 [] and 0.054[]. Maximum differences in thickness within roadways varied by 2.0 [in] to 2.8 [in]. On average, thickness over a varied transversely across the lane by 0.31 [in], with maximum variations in excess of 1 [in]. Longitudinal variability was found to be slightly greater than transverse variability. The average longitudinal variability was 0.54 [in]. between consecutive traverses (10 ft. spacing). The maximum variations for this case were also in excess of 1 [in].

The velocity survey results show that pavement velocity varied between surveys but fell within the range expected for PCC pavements. Average velocities ranged from 2.55 [m/ms] to 2.74 [m/ms]. Standard deviations for velocity measurements ranged from of 0.99 [m/ms] to 0.122 [m/ms]. The coefficient of variation for velocity varied between 0.039 [] to0.046[], values which are very similar to those reported for thickness.

The visual distress surveys conducted produced many similarities and differences in the distress profiles in the datasets. All roadways surveyed contained at least 15% spalling and all surveys exhibited distress on about 50% of the transverses. Cracked and broken panels made up a large portion of the distress for HWY 60E and HWY 60W, but were only minor distresses in HWY 100 and I 394. Faulted joints, faulted cracks, and durability cracking were very rarely reported in any survey and were not considered in the full analysis.

Visual and regression analysis of the observed distress and thickness and velocity variability found several interesting trends. The most interesting results is the seeming lack of correlation between thickness variation and distress. This may result from the key role thickness plays in design. As a primary design parameter, design thickness is carefully controlled to fulfill reliability requirements and generally conservative designs with excess thickness are favored. Therefore, it is unlikely distress will be caused by thickness deficiencies, as pavement are specifically designed to not be insufficiently thick and have been historically overdesigned with respect to thickness.

A more significant and consistent correlation was found between observed distress and concrete shear wave velocity. This relationship was most dramatic in the HWY 60 surveys, where two sections with discrete velocity and distress profiles were visually apparent. The first section presented high velocity and low rates of distress occurrence and the section presented a lower velocity and higher rates of distress occurrence. This same relationship was found to occur in all other datasets as well. All data sets found a significant negative correlation between surface shear wave velocity and distress occurrence, suggesting that as shear wave velocity decreases, the probability of distress occurrence increases. As shear wave velocity correlates with flexural and compressive strength (Freeseman, Hoegh, and Khazanovich 2016) (Heisey, Stokoe and Meyer, 1982), these results agree with structural causes of distress and the MEPDG models (AASHTO, 2008) (Huang,1994).

To evaluate the potential influences of design and mix parameters on the observed correlations between shear wave velocity and distress, the discrete case of HWY 60 was investigated. Investigation of the design data for HWY 60 shows that the significant correlations between observed distress and shear wave velocity result from changes in pavement design. The first segment presented a lower velocity and high rates of distress and was constructed using an aggregate known to have reliability issues while the second segment was constructed with quality aggregates and presented high velocity and lower rates of distress.

Though this study is based on limited data and casual relationship between shear wave velocity and performance is not fully understood, several conclusions can still be drawn from these results. First, it is clear that, at least for data collected in this study, that the surface shear wave velocity measured using MIRA ultrasonic testing is correlated with pavement performance. Surveys such as the one

conducted in this study may be employed in the future to provide information on potential future performance of in-service pavements.

This study also produced crucial information on the effect of project-scale deviations from design thickness on pavement performance. All the pavements surveyed in this study had regions of pavement thickness in excess of design thickness as well as regions which were thickness deficient. Both visual and regression analysis suggested that was no correlation between deviations from design thickness and pavement performance. Pavements which were over-built did not perform any better than pavements which were under-built. This speaks to the success of the current design methodology, which tends to produce conservative pavements which are slightly over designed with respect to thickness. These conservative designs are intended to prevent the typical thickness deviations in expected in as-built pavements from producing failure. According to these results, these designs have performed as intended, as regions which are thickness deficient to produce higher distress rates. As pavement designs become thinner and more optimal, thickness variation will likely play an important role in pavement performance.

This study also demonstrated the importance of material QA/QC. Though the exact causal relationship between shear wave velocity and pavement performance is not known, shear wave velocity is controlled by material properties. The correlations seen in every data set can, therefore, be seen as correlations between material properties and performance. This was clearly seen in HWY 60, where a change in coarse aggregate seems to be a primary factor in an observed change in pavement performance. The importance of material QA/QC is well known. Road agencies are constantly working to improve the quality of concrete mixes. A successful example of this process can be seen in the removal from service of coarse aggregate Northern ConAgg (167001), the aggregate which appears to contribute to the poor performance of HWY 60.

Finally, this study clearly showed the benefits of nondestructive methods over traditional methods for pavement testing. The speed, coverage and data density offered by MIRA provides information on thickness and velocity variation that would be possible using traditional methods. The type of analysis done in this study could not have been conducted using core data and the application of nondestructive testing data to QA/QC protocols would provide a great reduction in the uncertainty associated with the QA/QC estimates currently used. Specially, a simplified version of the shear

wave velocity survey conducted in this study is recommended for use for surveying in service pavements. A survey could be conducted over changes in design to determine changes which have the potential to significantly influence pavement performance.

8 FUTURE STUDY

The surface shear wave velocity surveys performed on HWY 60 produced strong correlations between pavement velocity and pavement performance and showed that shear wave velocity could be a valuable nondestructive tool to determine changes in pavement properties. These results, though promising, need to be further studied at additional sites. Increasing the database of PCC thickness and velocity vs distress will allow for a better understanding of the project scale effects of these important pavement parameters.

Additionally, laboratory investigation of the relationship between shear wave velocity, pavement materials and performance for in-service pavement is required. A better understanding of these relationships will allow for a more thorough interpretation of the shear wave velocity survey results.

Finally, the current exploration of non-destructive testing technology must be continued. The benefits of these technologies are clear, but more work is needed to make them applicable for agency design, QA/QC, and maintenance. The optimal, performance driven pavements of the future can only be designed using extensive data collection and analysis which can only be achieved using nondestructive methods.

BIBLIOGRAPHY

American Association of State Highway and Transportation Officials (AASHTO) (2008). Mechanistic-Empirical Pavement Design Guide: A Manual of Practice. Washington, D.C: AASHTO.

An, J., Nam, J., Kwon, S., and Joh, S. (2009) Estimation of the Compressive Strength of Concrete Using Shear Wave Velocity. New Technologies in Construction and Rehabilitation of Portland Cement Concrete Pavement and Bridge Deck Pavement: pp. 154-164. doi.

Carvalho, R., Stubstad, R., Briggs, R., Selezneva, O., Mustafa, E., and Ramachandran, A. Simplified techniques for evaluation and interpretation of pavement deflections for network-level analysis. No. FHWA-HRT-12-023. 2012.

Cho, M. R., Joh, S. H., Kwon, S. A., and Kang, T. H. (2007). Nondestructive In-Place Strength Profiling of Concrete Pavements by Resonance Search Technique. Proc. of 86th Annual Meeting of the Transportation Research Board, Washington, D.C.

Darter, Michael, Lev Khazanovich, Tom Yu, and Jag Mallela. "Reliability Analysis of Cracking and Faulting Prediction in the New Mechanistic-Empirical Pavement Design Procedure." Transportation Research Record: Journal of the Transportation Research Board .

Freeseman, K., Hoegh, K., and Khazanovich, L. (2016b). Concrete Strength Required to Open to Traffic. Report No. MN/RC 2016-01, Minnesota Department of Transportation. St. Paul, MN.

Freeseman, K., Hoegh, K., and Khazanovich, L. (2016) Characterization of concrete at various freeze-thaw damage conditions using SH-waves. AIP Conference Proceedings 1706, 020017 doi: 10.1063/1.4940463.

Heisey, J., Stokoe, I., Meyer, A. Moduli of pavement systems from spectral analysis of surface waves. Transportation Research Record: Journal of the Transportation Research Board, no. 852, 1982.

Hoegh, K. E. (2013) Ultrasonic Linear Array Evauluation of Concrete Pavements. Thesis. University Of Minnesota.

Hoegh, Kyle, Lev Khazanovich, and H. Yu. "Concrete Pavement Joint Diagnostics with Ultrasonic Tomography." Transportation Research Record: Journal of the Transportation Research Board 2305 (2012): 54-61. Web.

Hoegh, Kyle, Lev Khazanovich, Kenneth Maser, and Nam Tran. "Evaluation of Ultrasonic Technique for Detecting Delamination in Asphalt Pavements." Transportation Research Record: Journal of the Transportation Research Board 2306 (2012): 105-10. Web.

Hoegh, K., Khazanovich, L., and Yu, H. (2011) Ultrasonic Tomography for Evaluation of Concrete Pavements. Transportation Research Record: Journal of the Transportation Research Board 2232 85-94.

Hosmer, D. W., Lemeshow, S., and Sturdivant, R. X. (2013). Wiley Series in Probability and Statistics : Applied Logistic Regression (3rd Edition). New York, NY, USA: John Wiley & Sons.

Huang, Yang H. Pavement Analysis and Design. Upper Saddle River, NJ: Pearson/Prentice Hall, 2004. Print.

Iowa Department of Transportation. "Flexural Strength of Concrete." (2009): n. pag. 20 Oct. 2009. Web. 22 June 2016. <http://www.iowadot.gov/erl/archiveoct2011/IM/content/316.pdf>.

Jiang, Y., Selezneva, O., Mladenovic, G., Aref, S., and Darter, M. (2003) Estimation of Pavement Layer Thickness Variability for Reliability-Based Design. Transportation Research Record: Journal of the Transportation Research Board 1849 156-65.

Amador-Jiménez, Luis Esteban, and Donath Mrawira. "Reliability-based Initial Pavement Performance Deterioration Modelling." International Journal of Pavement Engineering 12.2 (2011): 177-86. Web.

Khazanovich, Lev. *"Introduction to the Westergaard Model."* CEGE 4251. University of Minnesota, Minnesota. 22 Feb. 2016. Class notes.

Kim, S. M., McCullough, B. F. (2002) Reconsideration of Thickness Tolerance for Concrete Pavements Report No. 4382-1, Federal Highway Administration, Washington, DC.

Koubaa, Amir, Mark B. Snyder, and Karl R. Peterson. Mitigating Concrete Aggregate Problems in Minnesota. Minnesota Department of Transportation, Research Services Section, 1997.

Mavko, Gary. "Conceptual overview of rock and fluid factors that impact seismic velocity and impedance." Retrieved 11.11 (2005): 2016 <https://pangea.stanford.edu/courses/gp262/Notes/8.SeismicVelocity.pdf>

Miller, J. Bellinger, W. Y. (2002) Distress identification manual for the Long-Term Pavement Performance Program, Report No. FHWA-RD-03-031, Federal Highway Administration, Washington, DC.

Miller, John S., and William Y. Bellinger. Distress identification manual for the long-term pavement performance program. No. FHWA-RD-03-031. 2003.

Minnesota Department of Transportation. (2003). Mn/DOT Distress Identification Manual. Ed. St. Paul, MN: Minnesota Department of Transportation.

Minnesota Department of Transportation. (2005). Standard Specifications for Construction, 2005 Ed. St. Paul, MN: Minnesota Department of Transportation.

Minnesota Department of Transportation. (2016). Projects on Minnesota highways, updated March 24, 2016. Available in: http://www.dot.state.mn.us/roadwork/current.html. Ed. St. Paul, MN: Minnesota Department of Transportation.

Privitera, G. J. (2012) Chapter 8: Introduction to Hypothesis Testing. Statistics for the Behavioral Sciences. Thousand Oaks: SAGE.

Selezneva, O. I., Jiang, Y. J., and Mladenovic, G. (2002) Evaluation and Analysis of LTPP Pavement Later Thickness Data, Report No. FHWA-HRT-12-041, Federal Highway Administration, Washington, DC.

Stubstad, R. N., Tayabji, S. D., Lukanen, E. O. (2002) LTPP Data Analysis: Variations in Pavement Design Inputs, Report No. Project 20-50[5]), National Cooperative Highway Research Program Transportation Research Board National Research Council, Washington.

Thom, Nick. Principles of Pavement Engineering. N.p.: ICE, 2014. Print.

Vancura, M. E. (2013) Evaluation of In-Situ Variability of Concrete Pavement Characteristics and Their Effect on Performance. Thesis. University Of Minnesota.

Wikipedia. Wikimedia Foundation, n.d. Web. 15 Dec. 2016.

Appendix A: MIRA and Distress Survey Datasheets

1. MIRA Survey Sheet

Survey Location	
Data start time	
Long Starting Point (stationing(ft))	
Long Ending Point(stationing(ft))	

traverse	meas. ct	Long. Dist	Verify	TRAVERSE NOTES
1	10			
2	20			
3	30			
4	40			
5	50			
6	60			
7	70			
8	80			
9	90			
10	100			
11	110			
12	120			
13	130			
14	140			
15	150			
16	160			
17	170			
18	180			
19	190			
20	200			
21	210			
22	220			
23	230			
24	240			
25	250			
26	260			
27	270			
28	280			
29	290			
30	300			
31	310			
32	320			
33	330			

2. Distress Survey Sheet

	enter data!
Survey location	
Image survey date	
Performed by	
lane(# from right shoulder)	
direction(N,S,E,W,ect)	

	enter data!
step size(ft)	10
starting stationing(ft)	
ending stationing(ft)	

location #	**Description**	**d from fogline(ft)**
location 1	**left edge**	11.4
location 2	**left wheel**	9.5
location 3	**center**	6.0
location 4	**right wheel**	2.5
location 5	**right edge**	0.6

		Location 1		**Location 2**		**Location 3**		**Location 4**		**Location 5**	
section	**stationing**	**type**	**severity**	**type**	**severity**	**type**	**severity**	**type**	**severity**	**type**	**severity**

Appendix B: MIRA Survey Best Practices

At the start of the field study conducted for this project, no methodology was available for the implementation of MIRA survey as a pavement management technique. Therefore, methodology was refined by trial and error during the surveys. At the conclusion of the invitation, the following best practices are suggested.

1. Survey patterns should be tailored to the type of data collected. For this project, thickness and velocity measurements were desired, so the survey pattern was skewed away from for features which may interfere with thickness or velocity data such as joints or large surface distresses. For surveys interested in subsurface condition, it makes more sense to focus measurements on regions most likely to have failures, such as traverse joints.
2. It is necessary to take repeat measurements. Though MIRA is highly accurate in ideal conditions, it is sensitive to heterogeneities, and errors may be introduced during analysis. Taking couples guards against this. If two repeated measurements taken very close together are found to differ, that data should be discarded.
3. The level of spatial accuracy required should also be considered. If very high levels of spatial accuracy are required over a small area, a tape measurer and chalk line are required. For moderate levels of spatial accuracy, a measuring wheel is sufficient. If available, laser range finders are also quite useful and fast.
4. Data organization is crucial. Surveys can have thousands of measurements. One missed measurement can throw off all the data, and post processing the error back out of data is extremely difficult and often impossible. Therefore, it is recommended that instead of creating one data file for the wheel survey, small sections (approximately 100 measurements) should be saved individually. Also, data files must be named to reflect location and also time stamped.
5. It is necessary to balance data needs with time to implement. In general, 500 to 2000 couples can be taken in a day depending on the survey complexity. If time is insufficient, adjustments to the pattern may be required.
6. Determine supplementary field data requirements before the survey. For example, if a thickness vs distress study is being conducted, a method to record distress must be considered.
7. Prepare datasheets for MIRA survey and supplementary field data before performing the survey. This will ensure all the necessary data is collected.

8. While conducting the survey, record all details and unexpected deviations. Take pictures of roadway features. All recorded observations should have time, date, location, and associated file references. Also record thought and initial ideas.
9. Once a survey is started, the pattern should not be changed. Any changes in the pattern need to be exactly recorded.
10. The stationing, GPS, or some other absolute location must be recorded for the start and end of the survey.

Appendix C: MnDOT Design Data for Roadways Investigated

A. Hwy 60E Design Data: Survey From MP50+3600 to MP53+3600

COPES Data From Route: 60 9/21/2015

Route:	60	**ControlSection:**		**IDNO:**	10602502
BeginMP:	50.69	**District:**	MANKATO	**County:**	COTTONWOOD
EndMP:	53.69	**Area:**	WINDOM	**Lanes:**	2
Current Surface:	JRCP			**Divided:**	YES
Previous Surface:	ON GRADE				
Date Completed:	01-Oct-1988				

SP:	1703-49				
Direction:	DECREASING				
Slab Thickness:	8.00				
Lane Width:	12				

Joints

Trans Joint Load System:	DOWELS	**Dowel Diameter:**	1.00		
Transverse Joint Spacing:	27.00	**Dowel Coating:**	EPOXY	**Dowel Spacing:**	12.00
Skew:	2	**Dowel Method:**	PREPLACED/BASKETS	**Dowel Length:**	15.00
Random Joints:	NO				
Method to Form Trans:	DOWELS	**Rt Shld Joint Type:**			
Method to Form Long:	SAWED WEAKENED PLANE				

Tie Bar Diameter:	.5	**Joint Sealant:**	NEOPRENE	**Rt Shld Tiebar Diam:**	
Tie Bar Length:	30	**Joint Width:**	.38	**Rt Shld Tiebar Len:**	
Tie Bar Space:	36	**Joint Depth:**	1.1	**Rt Shld Tiebar Spacing:**	

Reinforcing

Type of Rebar:	WELDED WIRE MESH	**Trans Type:**	SMOOTH	**Trans Diameter:**	0.23
Rebar Method:	MECHANICALLY INSTALLI			**Trans Spacing:**	12.00
Yield Strength:	65.00	**Long Type:**	SMOOTH	**Long Diameter:**	0.27
				Long Spacing:	12.00

Concrete

Mix Design				
Coarse Size:	0			
Coarse:	1,791.00	**L Coarse I:**	167001	Northern ConAgg GRAVEL/CRUSHED
Fine:	1,200.00	**L Coarse II:**	152003	New Ulm Quartz GRAVEL
Cement:	462.00	**S Coarse I:**	167001	Northern ConAgg GRAVEL/CRUSHED
Water:	260.00	**S Coarse II:**		GRAVEL
Flyash:	83.00	**Fine I:**	117003	Windom Agg NATURAL SAND
		Fine II:		

Paver Method:	SLIP FORM
Cure Method:	MEMBRANE CURING COMPOUND
Finish Method:	ASTROTURF AND TINE

Additive:		
	Range	
(Core) Compressive Strength:	5,161.00	3,140.00
(Beam) Flexural Strenght:		

Base/Subgrade

ML Base Type:	
Soil Classification:	0.00
Design R Value:	0.00
Stabilized Base Thick:	
Unstabilized Base Thick:	

Shoulder

Surface:	
Width:	0
Thick:	0
Base Thick:	

Drainage

Type:	LONGITUDINAL DRAINS
Location:	

B. Hwy 60E Design Data: Survey From MP53+230f to MP53+2220

COPES Data From Route: 60 9/21/2015

Route:	60	**ControlSection:**		**IDNO:**	10600702	**SP:**	1703-50
BeginMP:	53.27	**District:**	MANKATO	**County:**	COTTONWOOD	**Direction:**	DECREASING
EndMP:	54.17	**Area:**	WINDOM	**Lanes:**	2	**Slab Thickness:**	8.00
Current Surface:	JRCP			**Divided:**	YES	**Lane Width:**	12
Previous Surface:	ON GRADE						
Date Completed:	01-Jun-1987						

Joints

Transverse Joint Spacing:	27.00	**Trans Joint Load System:**	DOWELS	**Dowel Diameter:**	1.00
Skew:	2	**Dowel Coating:**	EPOXY	**Dowel Spacing:**	12.00
Random Joints:	NO	**Dowel Method:**	PREPLACED/BASKETS	**Dowel Length:**	15.00
Method to Form Trans:	DOWELS	**Rt Shld Joint Type:**	BUTT		
Method to Form Long:					

Tie Bar Diameter:	0	**Joint Sealant:**	NO SEALANT	**Rt Shld Tiebar Diam:**	
Tie Bar Length:	0	**Joint Width:**	0	**Rt Shld Tiebar Len:**	
Tie Bar Space:	0	**Joint Depth:**	0	**Rt Shld Tiebar Spacing:**	

Reinforcing

Type of Rebar:	WELDED WIRE MESH	**Trans Type:**	SMOOTH	**Trans Diameter:**	0.23
Rebar Method:	MECHANICALLY INSTALL			**Trans Spacing:**	12.00
Yield Strength:	70.00	**Long Type:**	DEFORMED	**Long Diameter:**	0.27
				Long Spacing:	12.00

Concrete

Mix Design	**L Coarse I:**	152003	New Ulm Quartz	CRUSHED QUARTZITE/GRANITE
Coarse Size: 2	**L Coarse II:**			
Coarse: 1,858.00	**S Coarse I:**	152003	New Ulm Quartz	CRUSHED QUARTZITE/GRANITE
Fine: 1,200.00	**S Coarse II:**			
Cement: 451.00	**Fine I:**	117003	Windom Agg	NATURAL SAND
Water: 240.00	**Fine II:**			
Flyash: 79.00				

Paver Method: SLIP FORM
Cure Method: MEMBRANE CURING COMPOUND
Finish Method: ASTROTURF AND TINE

Additive:

Range

(Core) Compressive Strength: 5,053.00 — 2,500.00

(Beam) Flexural Strenght:

Base/Subgrade

ML Base Type: CRUSHED GRAVEL

Soil Classification: 0.00

Design R Value: 0.00

Stabilized Base Thick: 3

Unstabilized Base Thick:

Shoulder

Surface: ASPHALT CONCRETE
Width: 8
Thick: 2
Base Thick: 3

Drainage

Type: NO SUBSURFACE DRAINAGE

Location: CONTINUOUS ALONG PROJECT

C. Hwy 60E Design Data: Survey From MP53+2230ft to MP52+4250ft

COPES Data From Route: 60 9/21/2015

Route: 60 ControlSection:
BeginMP: 49.91 District: MANKATO
EndMP: 53.27 Area: WINDOM
Current Surface: JRCP
Previous Surface: ON GRADE
Date Completed: 01-Oct-1988

IDNO: 10602501
County: COTTONWOOD
Lanes: 2
Divided: YES

SP: 1703-49
Direction: INCREASING
Slab Thickness: 8.00
Lane Width: 12

Joints

Transverse Joint Spacing: 27.00
Skew: 2
Random Joints: NO
Method to Form Trans: DOWELS
Method to Form Long: SAWED WEAKENED PLANE

Trans Joint Load System: DOWELS
Dowel Coating: EPOXY
Dowel Method: PREPLACED/BASKETS
Rt Shld Joint Type:

Dowel Diameter: 1.00
Dowel Spacing: 12.00
Dowel Length: 15.00

Tie Bar Diameter: .5
Tie Bar Length: 30
Tie Bar Space: 36

Joint Sealant: NEOPRENE
Joint Width: .38
Joint Depth: 1.1

Rt Shld Tiebar Diam:
Rt Shld Tiebar Len:
Rt Shld Tiebar Spacing:

Reinforcing

Type of Rebar: WELDED WIRE MESH
Rebar Method: MECHANICALLY INSTALL
Yield Strength: 65.00

Trans Type: SMOOTH
Long Type: SMOOTH

Trans Diameter: 0.23
Trans Spacing: 12.00
Long Diameter: 0.27
Long Spacing: 12.00

Concrete

Mix Design
Coarse Size: 0
Coarse: 1,791.00
Fine: 1,200.00
Cement: 472.00
Water: 260.00
Flyash: 83.00
Additive:
(Core) Compressive Strength: 5,161.00
(Beam) Flexural Strenght:

L Coarse I:	167001	Northern ConAgg	GRAVEL/CRUSHED
L Coarse II:	152003	New Ulm Quartz	GRAVEL
S Coarse I:	167001	Northern ConAgg	GRAVEL/CRUSHED
S Coarse II:			GRAVEL
Fine I:	117003	Windom Agg	NATURAL SAND
Fine II:			

Range 3,140.00

Paver Method: SLIP FORM
Cure Method: MEMBRANE CURING COMPOUND
Finish Method: ASTROTURF AND TINE

Base/Subgrade

ML Base Type:
Soil Classification: 0.00
Design R Value: 0.00
Stabilized Base Thick:
Unstabilized Base Thick:

Shoulder

Surface:
Width: 0
Thick: 0
Base Thick:

Drainage

Type: LONGITUDINAL DRAINS
Location:

D. HWY 100 Design Data Survey From MP3 + 4380ft to MP4 +620ft

COPES Data From Route: 100 9/21/2015

Route:	100	**ControlSection:**		**IDNO:**	11000601	**SP:**	2734-18
BeginMP:	3.90	**District:**	GOLDEN VALLEY	**County:**	HENNEPIN	**Direction:**	INCREASING
EndMP:	4.64	**Area:**	GOLDEN VALLEY	**Lanes:**	3	**Slab Thickness:**	9.00
Current Surface:	JRCP			**Divided:**	YES	**Lane Width:**	12
Previous Surface:	ON GRADE						
Date Completed:	01-Oct-1973						

Joints

Transverse Joint Spacing:	27.00	**Trans Joint Load System:**	DOWELS	**Dowel Diameter:**	1.00
Skew:	0	**Dowel Coating:**	PAINT AND/OR GREASE	**Dowel Spacing:**	12.00
Random Joints:	NO	**Dowel Method:**	PREPLACED/BASKETS	**Dowel Length:**	18.00
Method to Form Trans:	DOWELS	**Rt Shld Joint Type:**			
Method to Form Long:					

Tie Bar Diameter:	.62	**Joint Sealant:**	NEOPRENE	**Rt Shld Tiebar Diam:**	
Tie Bar Length:	30	**Joint Width:**	.63	**Rt Shld Tiebar Len:**	
Tie Bar Space:	36	**Joint Depth:**	2	**Rt Shld Tiebar Spacing:**	

Reinforcing

Type of Rebar:	WELDED WIRE MESH	**Trans Type:**	NONE	**Trans Diameter:**	0.22
Rebar Method:	BETWEEN LAYERS			**Trans Spacing:**	12.00
Yield Strength:	65.00	**Long Type:**	NONE	**Long Diameter:**	0.25
				Long Spacing:	6.00

Concrete

Mix Design	**L Coarse I:**	127003	Barton	GRAVEL/CRUSHED
Coarse Size: 1.5	**L Coarse II:**			GRAVEL
Coarse: 2,323.00	**S Coarse I:**	127003	Barton	GRAVEL/CRUSHED
Fine: 906.00	**S Coarse II:**			GRAVEL
Cement: 503.00	**Fine I:**	127003	Barton	NATURAL SAND
Water: 226.00	**Fine II:**			
Flyash: 0.00				

Paver Method: SLIP FORM
Cure Method: MEMBRANE CURING COMPOUND
Finish Method: BURLAP DRAG

Additive:

	Range
(Core) Compressive Strength: 5,775.00	3,400.00
(Beam) Flexural Strenght:	

Base/Subgrade

ML Base Type: CRUSHED GRAVEL
Soil Classification: 6.00
Design R Value: 0.00
Stabilized Base Thick: 13
Unstabilized Base Thick: 6

Shoulder

Surface: ASPHALT CONCRETE
Width: 10
Thick: 2
Base Thick: 13

Drainage

Type: LONGITUDINAL DRAINS
Location:

E. I 394 Design Data: Survey From MP6 + 4285F to MP7 + 995ft

COPES Data From Route: 394 9/21/2015

Route:	394	**ControlSection:**		**IDNO:**	13940202
BeginMP:	6.52	**District:**	GOLDEN VALLEY	**County:**	HENNEPIN
EndMP:	7.64	**Area:**	GOLDEN VALLEY	**Lanes:**	3
Current Surface:	JRCP			**Divided:**	YES
Previous Surface:	ON GRADE				
Date Completed:	01-Aug-1989				

SP:	2789-20				
Direction:	INCREASING				
Slab Thickness:	10.00				
Lane Width:	12				

Joints

Trans Joint Load System:	DOWELS	**Dowel Diameter:**	1.25		
Transverse Joint Spacing:	27.00	**Dowel Coating:**	EPOXY	**Dowel Spacing:**	12.00
Skew:	2	**Dowel Method:**	PREPLACED/BASKETS	**Dowel Length:**	15.00
Random Joints:	NO				
Method to Form Trans:	DOWELS	**Rt Shld Joint Type:**			
Method to Form Long:	SAWED WEAKENED PLANE				

Tie Bar Diameter:	.63	**Joint Sealant:**	NO SEALANT	**Rt Shld Tiebar Diam:**	
Tie Bar Length:	36	**Joint Width:**	.38	**Rt Shld Tiebar Len:**	
Tie Bar Space:	36	**Joint Depth:**	1.3	**Rt Shld Tiebar Spacing:**	

Reinforcing

Type of Rebar:	WELDED WIRE MESH	**Trans Type:**	SMOOTH	**Trans Diameter:**	0.23
Rebar Method:	MECHANICALLY INSTALLI			**Trans Spacing:**	12.00
Yield Strength:	75.00	**Long Type:**	DEFORMED	**Long Diameter:**	0.30
				Long Spacing:	12.00

Concrete

Mix Design

Coarse Size:	2	**L Coarse I:**	127003	Barton	GRAVEL/CRUSHED
		L Coarse II:			GRAVEL
Coarse:	1,967.00	**S Coarse I:**	127003	Barton	GRAVEL/CRUSHED
Fine:	1,200.00	**S Coarse II:**			GRAVEL
Cement:	451.00	**Fine I:**	127003	Barton	NATURAL SAND
Water:	240.00	**Fine II:**			
Flyash:	79.00				

Paver Method:	SLIP FORM
Cure Method:	MEMBRANE CURING COMPOUND
Finish Method:	ASTROTURF AND TINE

Additive:

		Range
(Core) Compressive Strength:	4,406.00	2,230.00
(Beam) Flexural Strenght:	724.00	142.00

Base/Subgrade

ML Base Type:	GRAVEL (UNCRUSHED)
Soil Classification:	0.00
Design R Value:	0.00
Stabilized Base Thick:	
Unstabilized Base Thick:	

Shoulder

Surface:	GRANULAR
Width:	8
Thick:	7
Base Thick:	

Drainage

Type:	LONGITUDINAL DRAINS
Location:	CONTINUOUS ALONG PROJECT

COPES Data From Route: 394

9/21/2015

Route:	394	**ControlSection:**		**IDNO:**	13940301
BeginMP:	7.64	**District:**	GOLDEN VALLEY	**County:**	HENNEPIN
EndMP:	8.67	**Area:**	GOLDEN VALLEY	**Lanes:**	3
Current Surface:	JRCP			**Divided:**	YES
Previous Surface:	ON GRADE				
Date Completed:	01-Dec-1990				

SP:	2789-48				
Direction:	INCREASING				
Slab Thickness:	10.00				
Lane Width:	12				

Joints

Trans Joint Load System:	DOWELS	**Dowel Diameter:**	1.25		
Transverse Joint Spacing:	27.00	**Dowel Coating:**	EPOXY	**Dowel Spacing:**	12.00
Skew:	2.1	**Dowel Method:**	PREPLACED/BASKETS	**Dowel Length:**	15.00
Random Joints:	NO				
Method to Form Trans:	DOWELS	**Rt Shld Joint Type:**			
Method to Form Long:	SAWED WEAKENED PLANE				

Tie Bar Diameter:	.62	**Joint Sealant:**	PREFORMED ELASTOMERIC	**Rt Shld Tiebar Diam:**	
Tie Bar Length:	36	**Joint Width:**	.38	**Rt Shld Tiebar Len:**	
Tie Bar Space:	36	**Joint Depth:**	2.6	**Rt Shld Tiebar Spacing:**	

Reinforcing

Type of Rebar:	WELDED WIRE MESH	**Trans Type:**	DEFORMED	**Trans Diameter:**	0.23
Rebar Method:				**Trans Spacing:**	12.00
Yield Strength:		**Long Type:**	DEFORMED	**Long Diameter:**	0.23
				Long Spacing:	12.00

Concrete

Mix Design		**L Coarse I:**			NONE
Coarse Size:	0	**L Coarse II:**			
		S Coarse I:			
Coarse:	0.00	**S Coarse II:**			
Fine:	0.00	**Fine I:**			
Cement:	0.00	**Fine II:**			
Water:	0.00				
Flyash:	0.00			**Paver Method:**	SLIP FORM
				Cure Method:	MEMBRANE CURING COMPOUND
Additive:				**Finish Method:**	ASTROTURF
		Range			
(Core) Compressive Strength:					
(Beam) Flexural Strenght:					

Base/Subgrade

ML Base Type:	CRUSHED GRAVEL
Soil Classification:	10.00
Design R Value:	20.00
Stabilized Base Thick:	
Unstabilized Base Thick:	3

Shoulder

Surface:	OTHER
Width:	7
Thick:	7
Base Thick:	

Drainage

Type:	LONGITUDINAL DRAINS
Location:	CONTINUOUS ALONG PROJECT

Appendix D: Observed Distress VS Thickness Variation Regression Results

		HWY 60E		HWY 60W		HWY 100		I 394	
		Coeff[a]	Sig[b]	Coeff[a]	Sig[b]	Coeff[a]	Sig[b]	Coeff[a]	Sig[b]
Transverse Joint Spalling	X_1	0.0430	0.0489	-0.0011	0.9575	0.0234	0.3591	-0.0160	0.4615
	X_2	0.1911	0.0168	-0.0816	0.2999	-0.0239	0.6509	0.1281	0.1045
	X_3	-0.1051	0.0021	-0.0402	0.3407	0.0107	0.7150	-0.0089	0.8712
	X_4	0.1043	0.1081	-0.0421	0.5834	-0.0151	0.7038	-0.0327	0.5795
	X_5	-0.0333	0.0110	-0.0319	0.0930	-0.0139	0.3207	0.0001	0.9970
	X_6	0.0726	0.0275	-0.0438	0.1890	-0.0134	0.6239	0.0418	0.2550
	X_7	0.0174	0.2046	0.0118	0.4959	-0.0167	0.3247	-0.0439	0.0030
	X_8	0.0411	0.1000	0.0039	0.8927	0.0065	0.8089	-0.0294	0.2770
	X_9	0.0213	0.7987	-0.0773	0.4339	0.0311	0.3282	0.0491	0.4876
	X_{10}	0.1430	0.6298	-0.0609	0.8037	0.0969	0.4515	0.2586	0.0728
Longitudinal Joint Spalling	X_1	0.0898	0.0008	0.0034	0.9097	0.0190	0.3276	0.0291	0.2712
	X_2	0.3372	0.0006	0.1057	0.3212	-0.0239	0.5354	-0.1271	0.1837
	X_3	-0.1038	0.0132	0.0009	0.9871	0.0779	0.0022	0.0140	0.8068
	X_4	0.1986	0.0093	-0.1341	0.2541	-0.0007	0.9802	-0.0016	0.9795
	X_5	-0.0596	0.0007	0.0009	0.9696	0.0190	0.0685	0.0148	0.3642
	X_6	0.1071	0.0065	0.0163	0.7207	-0.0003	0.9896	-0.0382	0.3593
	X_7	0.0364	0.0198	-0.0256	0.3881	0.0035	0.7595	-0.0232	0.1196
	X_8	0.0808	0.0081	0.0645	0.0585	-0.0179	0.4003	-0.0167	0.5445
	X_9	0.0824	0.3779	0.1043	0.3119	-0.0332	0.2493	0.0864	0.2334
	X_{10}	0.2402	0.4945	-0.1148	0.7488	-0.1355	0.2382	-0.3005	0.1911
Cracked and Broken Panels	X_1	0.0532	0.0067	0.0245	0.0755	0.0199	0.5343	-0.0755	0.0259
	X_2	0.0551	0.4346	0.0453	0.3606	0.0883	0.0771	0.0912	0.5578
	X_3	**-0.1877**	**0.0000**	**-0.0931**	**0.0009**	0.0393	0.2829	0.0454	0.6608
	X_4	-0.0380	0.5252	0.0255	0.5924	-0.0393	0.4766	-0.0393	0.7383
	X_5	**-0.0628**	**0.0000**	**-0.0339**	**0.0042**	0.0101	0.5605	-0.0137	0.6867
	X_6	0.0100	0.7334	0.0142	0.4965	0.0667	0.0224	0.0649	0.3598
	X_7	0.0152	0.2217	0.0009	0.9383	-0.0162	0.4514	-0.0062	0.8168
	X_8	0.0520	0.0200	0.0340	0.0654	0.0176	0.5818	0.1078	0.0354
	X_9	-0.2215	0.0186	-0.0334	0.5668	0.0051	0.9116	0.0059	0.9668
	X_{10}	-0.1196	0.6610	-0.1889	0.2409	0.2481	0.1050	0.2727	0.2617
All/Any Distress	X_1	0.0625	0.0006	0.0257	0.0454	0.0216	0.2424	0.0125	0.4582
	X_2	0.1896	0.0039	0.0450	0.3329	-0.0428	0.2327	0.0418	0.4942
	X_3	-0.1582	0.0000	-0.0660	0.0082	0.0594	0.0105	0.0267	0.5042
	X_4	0.0873	0.1055	0.0657	0.1448	-0.0406	0.1501	0.0063	0.8819
	X_5	-0.0575	0.0000	-0.0248	0.0186	0.0136	0.1723	0.0134	0.2599
	X_6	0.0572	0.0351	0.0154	0.4309	-0.0130	0.4872	0.0116	0.6758
	X_7	0.0301	0.0112	0.0149	0.1787	-0.0043	0.6920	-0.0349	0.0006
	X_8	0.0508	0.0134	0.0348	0.0509	0.0009	0.9662	-0.0423	0.0332
	X_9	-0.0975	0.1757	0.0689	0.1969	0.0034	0.8955	0.0532	0.3245
	X_{10}	0.1267	0.6021	0.1148	0.4270	0.0347	0.7288	0.2087	0.0991

0.0625 *Blue text denotes positive relationship*

-0.1038 *Red text denotes negative relationship*

0.0200 *Green text and fill denotes significant correlation at $\alpha = 0.05$*

X_3 *Bold highlighted denotes significant correlation and consistent across multiple datasets*

[a] *Coeff = The coefficient fit to the linear term in the regression by maximum likelihood estimation*

[b] *Sig = p value determined from the likelihood ratio ($\alpha = 0.05$).*

Appendix E: Observed Distress VS Velocity Variation Regression Results

	HWY 60E		HWY 60W		HWY 100		I 394	
	Coeff[a]	Sig[b]	Coeff[a]	Sig[b]	Coeff[a]	Sig[b]	Coeff[a]	Sig[b]
Transverse Joint Spalling	**-3.9223**	**0.0162**	**-4.7162**	**0.0472**	**-4.5160**	**0.0463**	-5.3055	0.4203
Longitudinal Joint Spalling	-1.3729	0.4658	-1.5168	0.6159	-8.0306	0.0000	-11.6995	0.0889
Cracked and Broken Panels	**-10.5786**	**0.0000**	**-5.7138**	**0.0001**	0.6179	0.8307	7.2970	0.6018
All/Any Distress	**-5.9865**	**0.0000**	**-4.5366**	**0.0004**	**-6.1279**	**0.0003**	**-16.7573**	**0.0014**

0.0625 *Blue text denotes positive relationship*

-0.1038 *Red text denotes negative relationship*

0.0200 *Green text and fill denotes significant correlation at α = 0.05*

X_1 *Bold highlighted denoted significant correlation and consistent across multiple datasets*

[a] *Coeff = The coefficient fit to the linear term in the regression by maximum likelihood estimation*

[b] *Sig = p value determined from the likelihood ratio (α = 0.05).*